3. SITE 462[1]

Shipboard Scientific Party[2]

HOLE 462A[3]

Date occupied: 5 November 1982

Date departed: 16 November 1982

Time on hole: 10 days, 22 hr., 22 min.

Position: 7°14.50′N; 165°01.90′E

Water depth (sea level; corrected m, echo-sounding): 5177

Water depth (rig floor; corrected m, echo-sounding): 5187

Bottom felt (m, drill pipe): Reentry into cone set in 1978 (Leg 61)

Penetration (m): 1209.0

Number of cores: 17

Total length of cored section (m): 137.3

Total core recovered (m): 74.43

Core recovery (%): 54.2

Oldest sediment cored:
Depth sub-bottom (m): 1123
Nature: Volcaniclastic, zeolitic mudstone
Age: early Aptian or older
Measured velocity (km/s): Not determined

Deepest rock cored:
Depth sub-bottom (m): 1209.0
Nature: Basalt sheet flows
Velocity range (km/s): 5.6 to 5.7

Principal results: Hole 462A is a multiple reentry in the Nauru Basin, drilled for the purpose of penetrating and sampling mid-Cretaceous igneous rocks encountered in Hole 462 in order to sample Lower Cretaceous and Jurassic strata and their underlying Jurassic crust at Magnetic Anomaly M-26. Leg 61 cored 462A to 1068.5 m. Leg 89 reentered and cleaned out the hole without difficulty to 1071.7 m; the depth discrepancy results from differences in pipe measurements between the two legs or from a temporary change of sea level. Samples of 12 extrusive igneous units and a small amount of volcanogenic sedimentary rock were recovered from the 137.3 m cored. Most of the rock is aphyric to sparsely aphyric basalt in sheet flows. Basalt locally has quench texture and may have phenocrysts of olivine (altered), clinopyroxene, and plagioclase. A pillowed sequence probably exists near 1162 m. Local occurrences of veins of smectite, pyrite, and other alteration products are common in the basalt. A few centimeters of hyaloclastite with sparse radiolarians and fish debris is near 1123 m and was recovered in chilled contact with basalt. Its age range cannot be narrowed down further than Late Jurassic to early Aptian. Reevaluation of the radiolarian faunas reported during Leg 61 in Cores 46 and 80 indicates that the intrabasalt sediments with those fossils are Aptian rather than older. The presence of the older reworked species, however, indicates that pre-Aptian sediments existed nearby. All paleomagnetic determinations show that the basalt was erupted during normal polarity. A temperature log—obtained as the hole was reentered after 4 yr.—is best interpreted as indicating that cold seawater has been flowing into the hole and out into the sediment at between 400 and 500 m sub-bottom depth.

BACKGROUND AND OBJECTIVES

Site 462, Hole 462A, was reoccupied on Leg 89 because the previous drilling campaign carried out during May, June, and July of 1978 on Leg 61 failed to reach Jurassic strata. Instead of penetrating a normal sedimentary section, presumed to overlie the lithospheric Pacific Plate that is approximately 150 m.y. old, we encountered a section of basalt sills and flows at a sub-bottom depth of 563 m (Figs. 1 and 2). These basalt units did, however, contain beds of fossiliferous sediment of Aptian and, it was thought at the time, possibly Barremian age. Drilling at 462A on Leg 61 was terminated at a total depth of 1068.5 m while still in basalt. Details of the original background, objectives, and results of Leg 61, discussed later, are from Chapter 2 of Volume 61 of the *Initial Reports of the Deep Sea Drilling Project*, Larson, Schlanger, et al. (1981). The presence of the sedimentary layers within the sill and flow complex, dated as Aptian, led to the conclusion that true plate basement had not been reached during Leg 61 drilling. Therefore, by 1981 it was still a goal of the JOIDES Ocean Paleoenvironment Panel to deepen Hole 462A in an attempt to penetrate the sill and flow complex and recover Jurassic rocks. This deepening became an objective of Leg 89. Further, the age, petrologic character, and thickness of the sill-flow complex led to the realization that the volcanic history of the western Pacific was more complex than simple hot-spot models had indicated. It was believed that by completely penetrating and sampling this complex we could arrive at more definite conclusions regarding its age, petrology, magnetic character, and genesis.

Leg 61 Background and Objectives

Introduction

The goal of the Leg 61 scientific party at Site 462 was to study the paleontologic, sedimentary, petrologic, tectonic, and magnetic histories of that area from Recent

[1] Moberly, R., Schlanger, S. O., et al., *Init. Repts. DSDP*, 89: Washington (U.S. Govt. Printing Office).

[2] Ralph Moberly (Co-Chief Scientist), Hawaii Institute of Geophysics, University of Hawaii, Honolulu, HI; Seymour O. Schlanger (Co-Chief Scientist), Department of Geological Sciences, Northwestern University, Evanston, IL; Miriam Baltuck, Deep Sea Drilling Project, Scripps Institution of Oceanography, La Jolla, CA (present address: Geology Department, Tulane University, New Orleans, LA); James A. Bergen, Department of Geology, Florida State University, Tallahassee, FL (present address: UNOCAL, P.O. Box 76, Brea, CA 92631); Walter Dean, U.S. Geological Survey, Denver Federal Center, Denver, CO; Peter A. Floyd, Department of Geology, University of Keele, Keele, Staffordshire, United Kingdom; Naoyuki Fujii, Department of Earth Sciences, Kobe University, Kobe, Japan; Janet A. Haggerty, Department of Geosciences, University of Tulsa, Tulsa, OK; James G. Ogg, Department of Geology and Geophysics, University of Wyoming, Laramie, WY; Isabella Premoli Silva, Istituto di Paleontologia, Milan, Italy (present address: Dipartimento di Scienze della Terra, Universitá di Milano, Milan, Italy); André Schaaf, Institut de Geologie, Strasbourg, France (present address: Université de Bretagne Occidentale, GIS Océanologie et Géodynamique, 29287 Brest Cedex France); Rainer G. Schaefer, Institut für Erdöl und Organische Geochemie, KFA Jülich, Federal Republic of Germany; William V. Sliter, Branch of Paleontology and Stratigraphy, U.S. Geological Survey, Reston, VA (present address: U.S. Geological Survey, Menlo Park, CA); Jill M. Whitman, Geological Research Division, Scripps Institution of Oceanography, La Jolla, CA.

[3] Holes 462 and 462A were drilled on Leg 61, the latter to a sub-botom depth of 1068 m, and are described in Larson, Schlanger, et al. (1981).

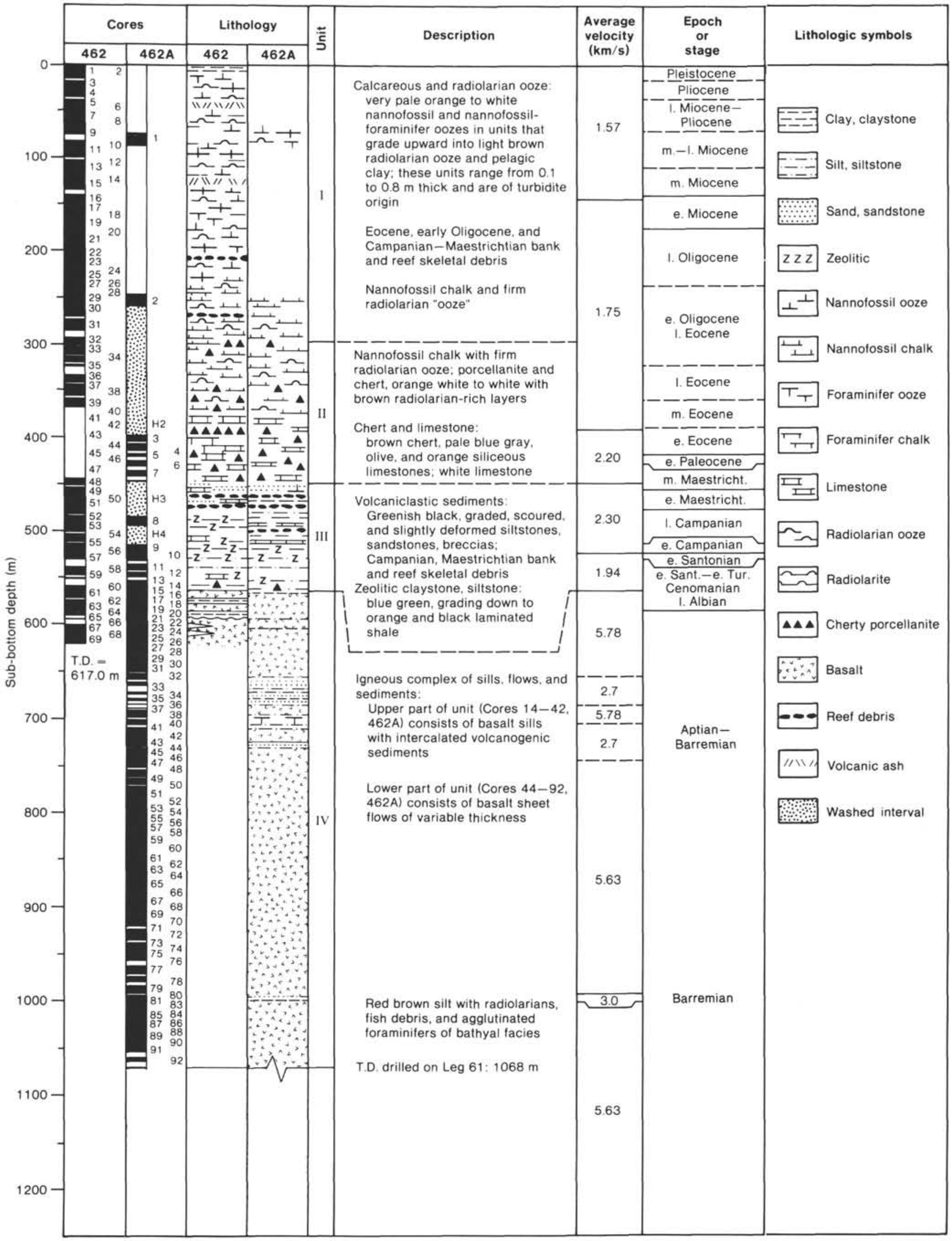

Figure 1. Columnar sections at Site 462, showing cored intervals, lithologic units, interval seismic velocities, and ages (from Larson, Schlanger, et al., 1981). (See Figure 22, Hole 462A for modifications derived from Leg 89 drilling.)

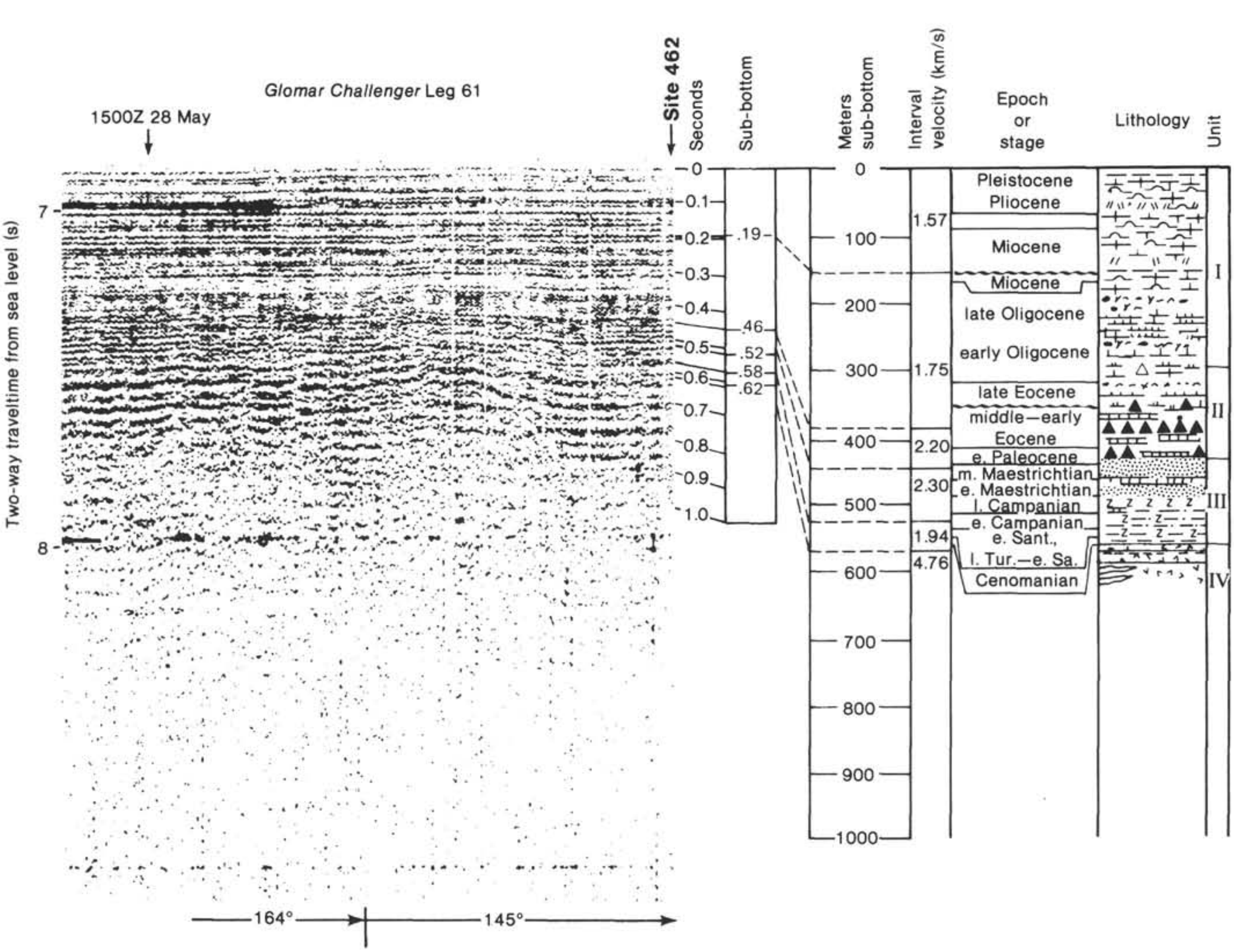

Figure 2. Correlation of drilling results and seismic data (from Larson, Schlanger, et al., 1981). See Figure 1 for an explanation of lithologic symbols.

to Late Jurassic by drilling a deep reentry site into the Nauru Basin west of the Ralik Chain of the Marshall Islands (Fig. 3). This area formed at a fast-spreading Pacific Plate boundary 145 to 155 Ma in the Late Jurassic (Figs. 4 and 5). It was thought that cores from this locale would better our understanding of biostratigraphic evolution and sedimentary processes in a Mesozoic open-ocean environment, the petrologic nature of fast-spreading oceanic crust, the tectonic history of the Late Jurassic Pacific Plate, and the nature of the Jurassic magnetic quiet zone.

Sedimentological and Paleoenvironmental Objectives

The basement, or plate, age at Site 462 in the Nauru Basin should be approximately 145 to 155 m.y., providing an opportunity to core sediments possibly as old as Oxfordian. The section there should thus encompass these stratigraphic intervals: late Barremian–Aptian–early Albian, and Cenomanian–Turonian, occupied by organic carbon-rich "black-shales" or sapropels, cored at many DSDP sites. These black shale sections are thought to be the result of the development of a widespread and thick oxygen minimum layer in the world ocean during relatively short and well defined times (Schlanger and Jenkyns, 1976).

Sedimentological, geochemical, and paleontological studies of strata deposited during the Nauru Basin stages (mentioned earlier) would make it possible to compare the effects of an oxygen minimum buildup in a relatively closed basin such as the Atlantic Ocean and Tethys Sea, where terrestrial carbonaceous input was high, with effects in a relatively open basin such as Pacific, where terrestrial carbonaceous input presumably was low. The Nauru Basin sediments should contain a clear record of a deep water oxygen minimum event—one without the complicating factor of a heavy terrestrial organic carbon overprint.

Geochemical and isotopic studies of Site 462 material should resolve some of the questions posed concerning the correlation of oxygen minimum expansions and global climatic changes. Further, because the development of oxygen minima may be linked to variations in upper water layer fertility, the fossil record at the site, which should contain information on the range and extension of new groups, would help in establishing such a linkage. Recovery of a complete fossiliferous section down

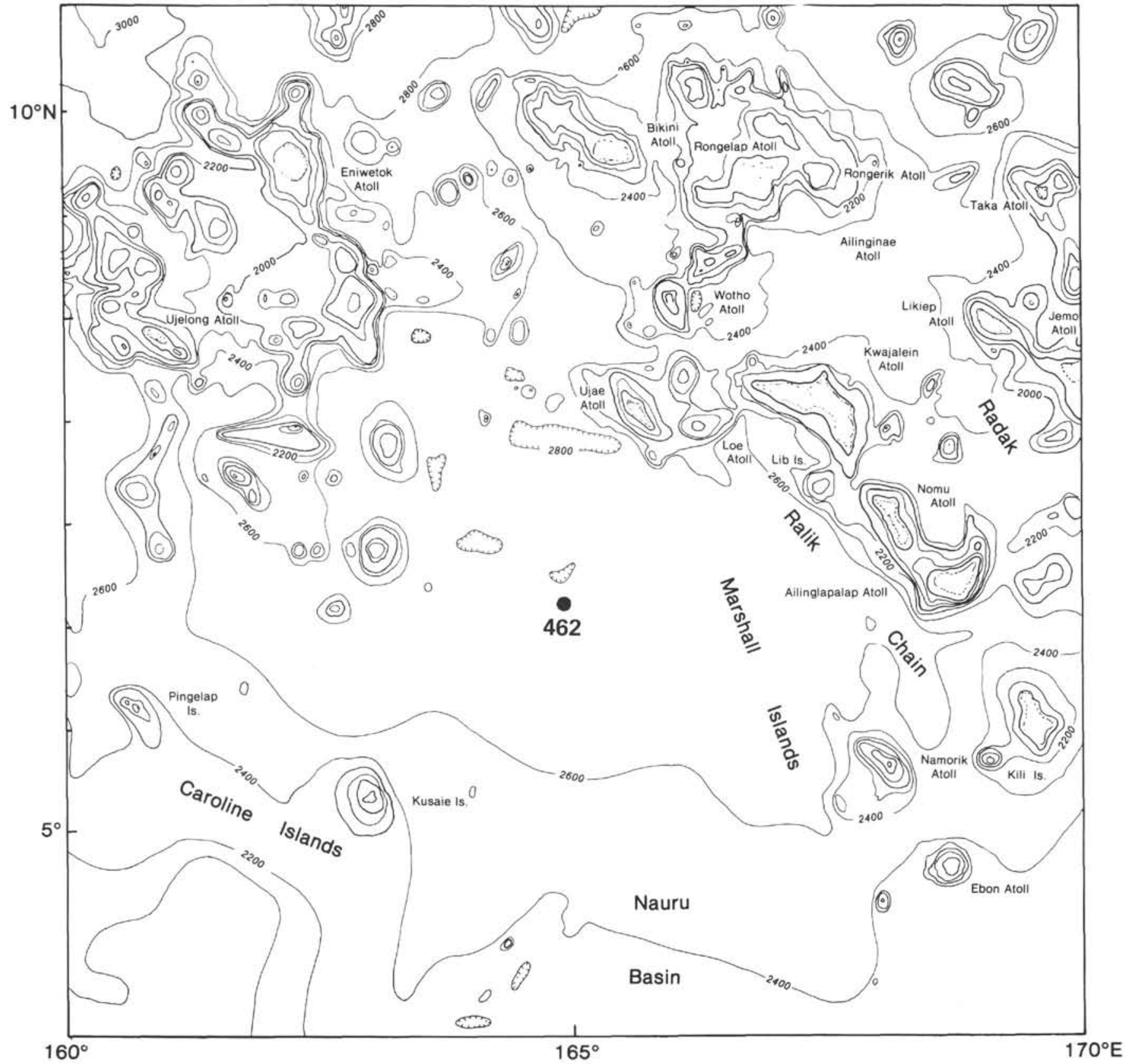

Figure 3. Regional bathymetric setting of Site 462 in the Nauru Basin, fringed to the north, east, and west by seamounts, guyots, and the Marshall and eastern Caroline islands (from Larson, Schlanger, et al., 1981).

to the Oxfordian would in itself be valuable in refining zonations and deciphering paleoenvironmental events.

The Cenozoic section at this site may, according to the site surveys, consist of interbedded pelagic sediments and turbidites. It is in a deep basin surrounded by atolls of the Marshall Islands and the volcanic islands of the Caroline Chain (Fig. 3). Further, *Kana Keoki* seismic records (Fig. 6) and a detailed bathymetric chart (Fig. 7) show levees and channels indicative of probable distal turbidite regimes. Therefore, we should be able to identify events such as the onset and cessation of volcanism that built the edifices in the Marshalls and eastern Carolines. Turbidite debris analysis should also give us information on reef buildup and, probably, island emergence in the area, as was done for the Leg 33 Line Islands area (Schlanger, Jackson, et al., 1976).

Petrologic Objectives

It has been a top priority to obtain relatively deep sections from oceanic crust formed at both slow- and fast-spreading ridges. Three DSDP legs (51, 52, 53) involved drilling such sites on 110-m.y.- old, slow-spreading crust in the western Atlantic Ocean. The Nauru Basin site was meant to sample fast-spreading , Mesozoic crust. The Nauru Basin formed at 4.7 cm/year, half-rate, and is an area of smooth oceanic crust, characterized by a well-defined magnetic lineation pattern.

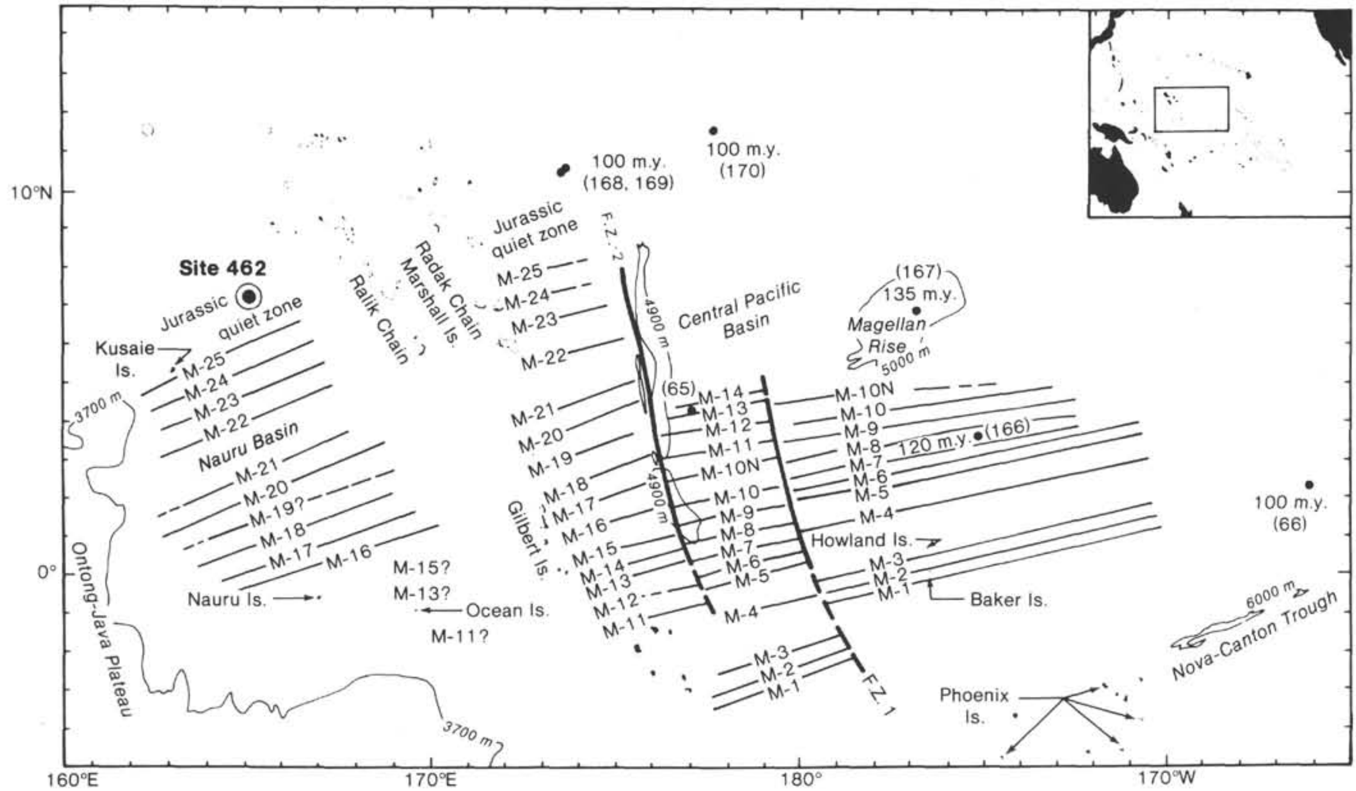

Figure 4. Mesozoic magnetic lineation patterns of the Nauru and Central Pacific basins, showing the location of Site 462 in the Jurassic quiet zone (from Larson, 1976).

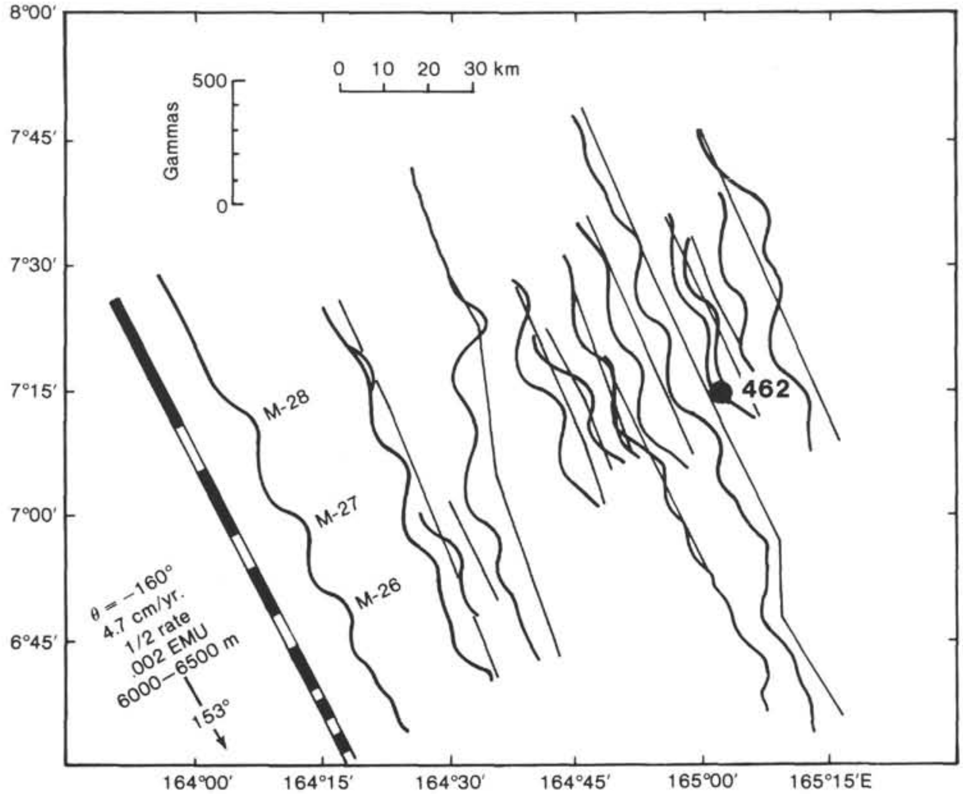

Figure 5. Cross-strike magnetic anomaly profiles across Anomalies M-26, M-27, and M-28 in the Jurassic quiet zone of the northern Nauru Basin. Data are from the *Kana Keoki* survey and a model profile based on the revised Late Jurassic magnetic time scale of Cande et al. (1978).

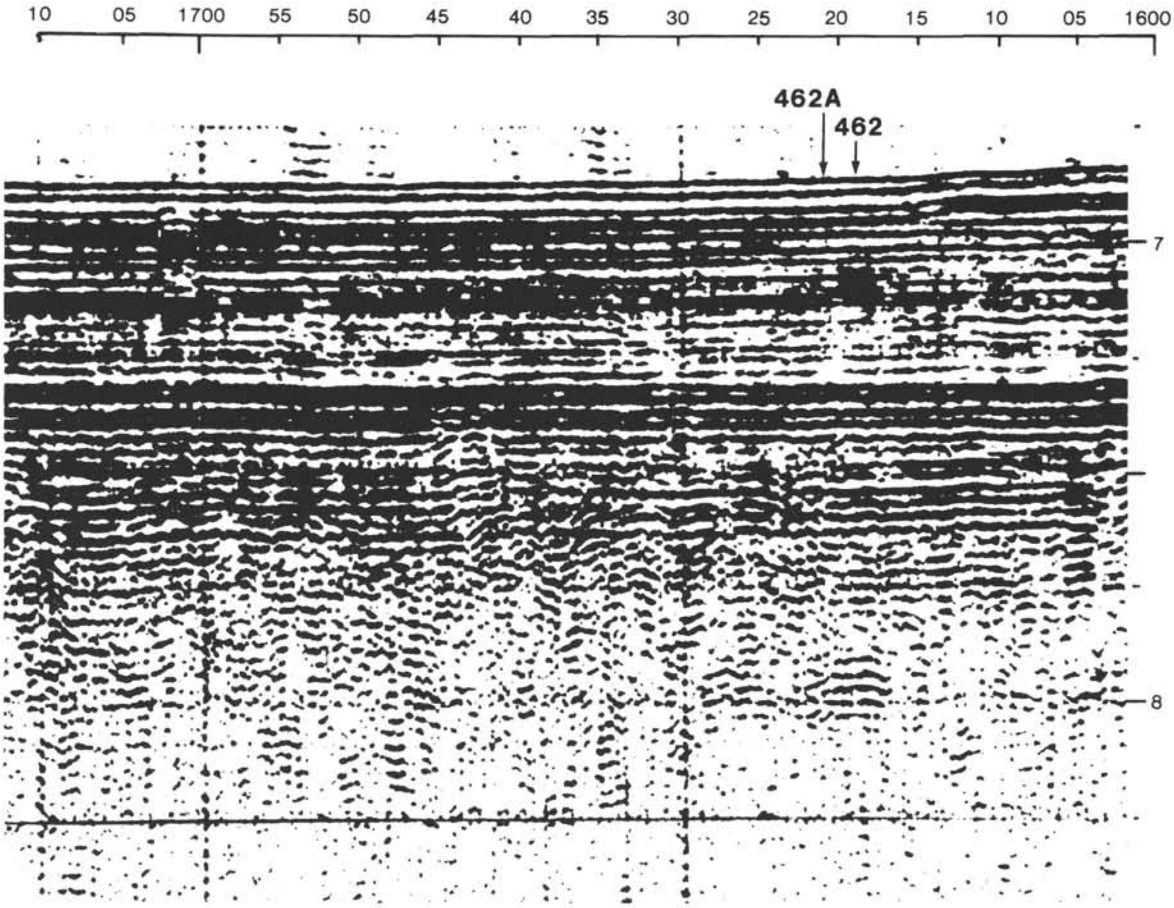

Figure 6. Seismic reflection profile made by *Kana Keoki* on 11 April 1977 during a site survey of the area (from Larson, Schlanger, et al., 1981). East is to the left, west to the right. Holes 462 and 462A are slightly south of this profile; arrows merely show their longitudinal positions.

The results from Atlantic Ocean drilling indicate that upper Layer 2 is constructed largely of extrusives, with many pillow-lava sequences separated by abundant glass-lined fragments. Is this also true for fast-spreading crust? This is an especially interesting question in the Nauru Basin, because the seismic-profile records show many smooth layers that may be indicative of significant intrusive activity.

Almost all of the Atlantic Ocean samples show alteration of basalts by cold water, and abundant production of smectite. Very few high-temperature metamorphosed samples have been recovered. Much relatively fresh glass was recovered from one of the deep sites on the 110-m.y.-old Atlantic crust. Is this also typical of fast-spreading crust, indicating a similar distribution of ridge crest isotherms and hydrothermal circulation history? Magnetic anomaly patterns, although subdued in amplitude, are remarkably well defined in the Nauru Basin, indicating that alteration has had little effect on the magnetic anomaly source layer.

Tectonic Objectives

The history of horizontal motion of the Pacific Plate back through the Early Cretaceous is relatively well known from studies of magnetic lineation patterns, magnetic studies of seamounts, and facies studies of sediments. The preceding Jurassic history is relatively unknown, because no Jurassic seamounts have been reported, magnetic lineation information is very limited, and no sediments of unequivocal Jurassic age have been recovered from the Pacific. Tentative studies of Jurassic magnetic lineation patterns suggest a more equatorial paleolatitude for the Late Jurassic Nauru Basin than the Early Cretaceous Central Pacific Basin just to the east (Fig. 4). This raises the possibility that in the Late Jurassic, the Pacific Plate was initially moving south or at least had a dominant counterclockwise rotational component. Sometime in the Late Jurassic or Early Cretaceous, this retrograde motion reversed, perhaps by rebounding off eastern Gondwanaland, and the Pacific Plate began the steady northward motion that persists today.

Studies of Mesozoic sedimentary facies coupled with paleomagnetic studies of the sedimentary and volcanic rocks of the Nauru Basin should confirm or deny this hypothesis. An equatorial sedimentary sequence at the base of the Nauru Basin section, overlain by higher latitude sediments, in turn overlain by a second equatorial sequence, would support the retrograde-motion hypothesis. Paleomagnetic inclination information should reveal the corresponding history of latitudinal motion, although nothing can be inferred concerning rotation of the Mesozoic Pacific Plate from the relative paleomagnetic declinations.

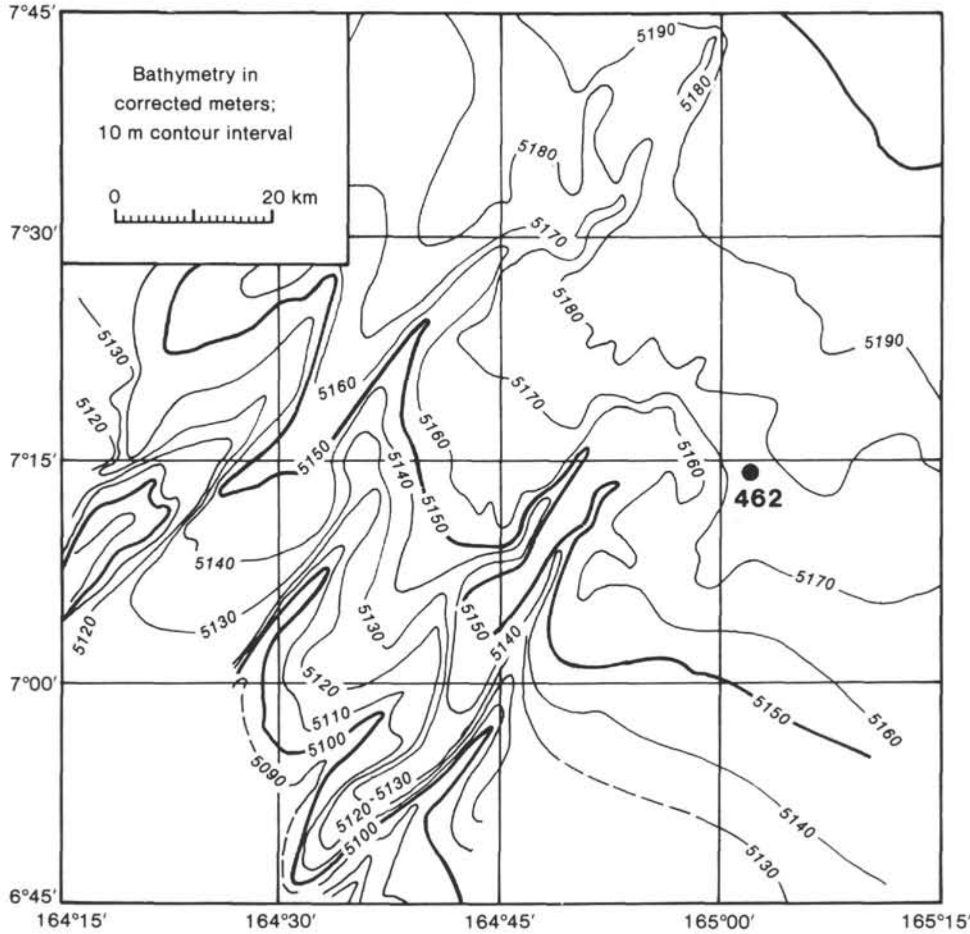

Figure 7. Detailed bathymetric chart of the Site 462 area, based on a *Kana Keoki* survey that outlines the channel-and-levee system that channels sediment to this area from the Ontong-Java Plateau (from Larson, Schlanger, et al., 1981).

Magnetic Objectives

Studies of the remanent paleomagnetic inclination information should contribute to our understanding of the Mesozoic tectonic evolution of the Pacific Plate. In addition, paleomagnetic and rock magnetic studies of Jurassic sedimentary and volcanic rocks should be of great interest in understanding the history of the Earth's magnetic field at that time.

The M-sequence of magnetic anomalies is always bounded on its old (Jurassic) end by an "envelope" of anomaly amplitudes that taper down from "normal" values at about 145 Ma to very small anomalies by 155 Ma. This latter portion of the record, nominally from 153 to 160 Ma, is called the Jurassic magnetic quiet zone (Figs. 4 and 5) and was the target of our drilling program in the northern Nauru Basin. In this area, very small but coherent magnetic anomalies (M-26, M-27, M-28) imply remanent magnetizations nearly an order of magnitude lower than Lower Cretaceous magnetic anomalies. Obtaining a significant Jurassic volcanic section should test the various hypotheses for the origin of these low-amplitude anomalies: fluctuations of the Jurassic dipole field intensity, field reversals during a time of generally low magnetic intensity, local variations in petrology, or a large increase in reversal frequency.

OPERATIONS

After leaving the East Mariana Basin and Site 585 on 2 November 1982 at 1709Z (Greenwich mean time), *Glomar Challenger* proceeded south across Ita Maitai Guyot and then southeastward through the western Marshall Islands and their associated seamounts toward Site 462. We passed between Enewetak and Ujelang atolls and over the lower flank of Heezen Guyot as we entered the Nauru Basin.

Our underway geophysical gear was the same as is described for the operations en route to Site 585. About 30 nautical miles from old Site 462, however, the air guns and magnetometer were retrieved and seismic sub-bottom and magnetic profiling ceased, in order to save ship positioning time when we neared the already well-surveyed site. Our final approach was nearly over the Leg 61 approach, and was controlled well by satellite navigation fixes. At 1832 hr. (0732Z) on 5 November we crossed the dead-reckoning location of Hole 462A, at 7°14.495′N, 165°01.898′E, and dropped an acoustic beacon. Our arrival on site was nearly 4 hr. earlier than we had estimated, as a result of favorable currents and exceptionally calm weather.

The piccolo was rigged while we were maneuvering back over the beacon that was descending to the seafloor, and while awaiting new satellite crossings. A series of fixes showed that the beacon was about 1035 m northwest of the recorded position of Hole 462A. We maneuvered closer and dropped a second beacon. Water depth, corrected to sea level, was 5177 m, during the Leg 61 drilling.

The bottom-hole components assembled by the drilling crew were shorter than normal and fitted with a bit having a large orifice useful for logging purposes or to clean cavings and bridges out of a hole. The BHA (bottom hole assembly) and drill pipe were lowered nearly to the seafloor; the reentry tool was lowered for 4 hr. through the drill string on the logging cable. The cone was detected about 7 m deeper than expected, but about 5 hr. was needed to accomplish the reentry operation. The exceptionally calm seas prevented rolling of the ship and, according to the ship's officers, that kept the string of pipe from swinging like a pendulum. The lightweight BHA may have exacerbated the problem. Normally a series of passes under the swath of a swinging drill string will soon give an opportunity to stab.

At 2016 hr. on 6 November we did drop the end of the drill string into the cone, reentering Hole 462A after a period slightly longer than 4 yr. and 3 mo. Our initial operation was to lower a temperature logging tool as deeply into the old hole as possible. It met with very slight obstructions at 470 and 515 m depth, and was blocked at 521 m. The tool was retrieved, and the drill string used to clean out the hole down into the basalt sills below 560 m. No difficulty was encountered. Presumably, within the igneous section there would be no danger of side tracking from the hole if substantial bridge or blockage by slumped rock was encountered with a regular drilling bit, and so the drill string was tripped from the hole. A regular BHA with a type F94CK bit was run down on the drill string, and the reentry sonar tool was lowered.

After about 2.5 hr. of scanning, we stabbed into the reentry cone at 0818 hr. on 8 November. Pipe was then run to the bottom of the hole, flushing out carefully en route. At 1630 hr. the bit reached bottom. The total depth at the end of Leg 61 was 1068.5 m; the drillers now reported a depth of 1071.7 m. The 3.2-m discrepancy may have resulted from a mismeasurement of pipe during either Leg 61 or this leg or both. Later we realized that some or all of the discrepancy may have been from a temporary change of sea level related to the 1982 El Niño event. So as not to have to change all the records of Leg 61 cores, yet to be able to use the length of the present drill string from drill floor to bit, we decided to cut the first core less than the usual 9 m and put any discrepancy within the amount of recovered versus not-recovered rock. We commenced cutting core.

Core 93, the first from Hole 462A during this leg (Table 1), was on deck at 0034 hr, on 9 November. Eight cores were cut with the bit. They were almost entirely of basalt sheet flows. Some softer volcanogenic zeolitic mudstone was recovered in a few of the cores. Veins of zeolite, pyrite, and smectite are common, especially in the lower cores. The upper several meters of Core 99 drilled quickly and gave poor recovery; the missing soft material probably was not basalt.

Table 1. Coring summary, Site 462, Hole 462A (Leg 89).

Core no.	Date (Nov., 1982)	Time	Depth from drill floor (m) top–bottom	Depth below seafloor (m) top–bottom	Length cored (m)	Length recovered (m)	Percent recovered
93	9	0034	6257.7–6262.6	1071.7–1076.6	4.9	1.78	36.3
94	9	0820	6262.6–6271.7	1076.6–1085.7	9.1	8.27	90.0
95	9	1536	6271.7–6280.9	1085.7–1094.9	9.2	8.81	95.8
96	9	2207	6280.9–6290.0	1094.9–1104.0	9.1	6.39	70.2
97	10	0307	6290.0–6299.2	1104.0–1113.2	9.2	6.67	72.5
98	10	1105	6299.2–6308.3	1113.2–1122.3	9.1	8.04	88.4
99	10	1445	6308.3–6317.5	1122.3–1131.5	9.2	1.32	14.3
100	11	0309	6317.5–6320.5	1131.5–1134.5	3.0	3.30	110.0
101	12	0953	6320.5–6328.9	1134.5–1142.9	8.4	5.88	70.0
102	12	1730	6328.9–6338.0	1142.9–1152.0	9.1	5.90	65.0
103	13	0219	6338.0–6347.2	1152.0–1161.2	9.2	1.57	17.1
104	13	1038	6347.2–6356.3	1161.2–1170.3	9.1	2.17	23.8
105	14	1954	6356.3–6360.3	1170.3–1174.3	4.0	3.73	93.3
106	15	0313	6360.3–6366.4	1174.3–1180.4	6.1	3.43	56.2
107	15	1238	6366.4–6375.5	1180.4–1189.5	9.1	0.06	1.0
108	15	2030	6375.5–6384.7	1189.5–1198.7	9.2	4.16	45.2
109	16	1154	6384.7–6395.0	1198.7–1209.0	10.3	2.95	28.6
					137.3	74.43	54.2

During the cutting of the lower part of Core 99 and short Core 100, behavior of the drill string indicated bit damage. The string was pulled with the core barrel for Core 100 within the BHA. The bit was on board at 0334 hr. on 11 November. Two of its four cones were very loose from failed bearings and one other was sufficiently wobbly to indicate that the bit had been pulled just before complete failure. It had lasted 31 hr., 40 min. A new type F94CK bit, standard BHA, and drill string were run from the ship.

Although there was a modest delay from breakdown of pipe handling equipment, our third reentry was a fast 1.6 hr., and pipe was run quickly to a few meters off bottom. The last 12 m had to be reamed larger, as the diameter of the first bit had been worn significantly. Coring then continued on 12 and 13 November in hard sheet flow basalts and probably some pillowed basalts. After retrieving the third core of the new bit (number 103), the drillers noted an abnormally high pump pressure, indicating an obstruction at the bit. A heavy chisel-ended rod was pumped down the drill stem ahead of a core barrel, and apparently cleared the obstruction. Cores 103 and 104 cut slowly and their recovery was poor, indicating probable bit damage. The bit was brought up on the drill string, arriving at the drill floor at 2115 hr., 13 November. It had been used for 25.6 hr. and had penetrated only 35.8 m. Bearing wear was nearly as bad as for the first bit, and tooth breakage was somewhat worse.

For a few hours on 13 November before the drill string was pulled from the hole, a second train of swells, coupled with wind gusts to 28 knots, caused the ship to roll to a maximum of 5°. The weight indicator for the drill string reached the new operating limits imposed for Leg 89 on two or three occasions. With that exception, roll was mainly less than 3° in what can best be described as an excellent environment that lasted through our several day occupation of Site 462, namely winds from 0 to 18 knots, seas rippled to 2 ft., and 3 to 5 ft. swells.

A new bit of the same type was added to the BHA and the round trip completed relatively quickly. The reentry maneuver was exceptionally fast, only 7 min. elapsing between scanning the cone at 15 m and stabbing into it. The final five cores were cut slowly but with good recovery, with two exceptions. After some problems in the seating of the core barrel, Core 107 was cut but only one piece of basalt a few centimeters in length was recovered. Core 109, the last core of the bit and of Leg 89's occupation of the site, drilled very slowly for the first 2 m and faster thereafter, and with more torque. Only basalt was recovered, and it is not known what it was that was not recovered—perhaps pillow edges or some other kind of basalt. The drilling rate was not fast enough to suggest that it may have been a mudstone or limestone. Figure 8 shows drilling rates.

At 1209 m total depth the hole was abandoned, clean of junk (it awaits further reentry after a change in engineering capabilities, such as 1200 m of aluminum drill pipe to substitute in the lower part of the drill string). The string was pulled from the hole, and the piccolo removed. The third bit had been used nearly 24 hr., and it had penetrated 38.7 m. Although its bearings were in fair condition, it had lost as many teeth as the first two bits. The "drive rows" of teeth, next to the outside, were nearly stripped clean on three of the four cones.

All in all we cored 137.3 m and recovered 74.43 m (54% average), mainly of sheet flow basalt with minor sedimentary rock and pillows. At 1654 hr. on 16 November, *Glomar Challenger* got under way on a southwest course toward our last site of the leg, SW-9, which is at DSDP 289 on the northeastern edge of the Ontong-Java Plateau.

LITHOLOGIC SUMMARY

Continuation of coring at Hole 462A recovered basalt and dolerite almost exclusively. Only in Sections 1 and 2 of Core 462A-99 (1122.3–1131.5 m sub-bottom depth) was sediment recovered that was demonstrably not contamination from uphole.

On the basis of textural and compositional similarity both of these occurrences resemble sediments cored within the igneous layers during the Leg 61 occupation of the site. These are olive gray (5Y 4/1) to dark greenish gray (5GY 6/1) and grayish blue green (5BG 6/2) that in smear slide and hand specimen appear to be claystone to clayey sandstone with traces of radiolarians and fish debris. The clay is probably volcanogenic and contains about 1 or 2% each of zeolite and altered volcanic glass. Wispy laminae in the lower sediment (Section 462A-99-2) contain up to 30% silt-sized altered volcanic glass.

The more significant of the two sediment occurrences is that in Sample 462A-99-1, 110–124 cm (Piece 11a and 11b, Fig. 9). This contains a sediment/basalt contact in a large piece indisputably proving that the sediment is in place between igneous Units 46 and 47. The contact be-

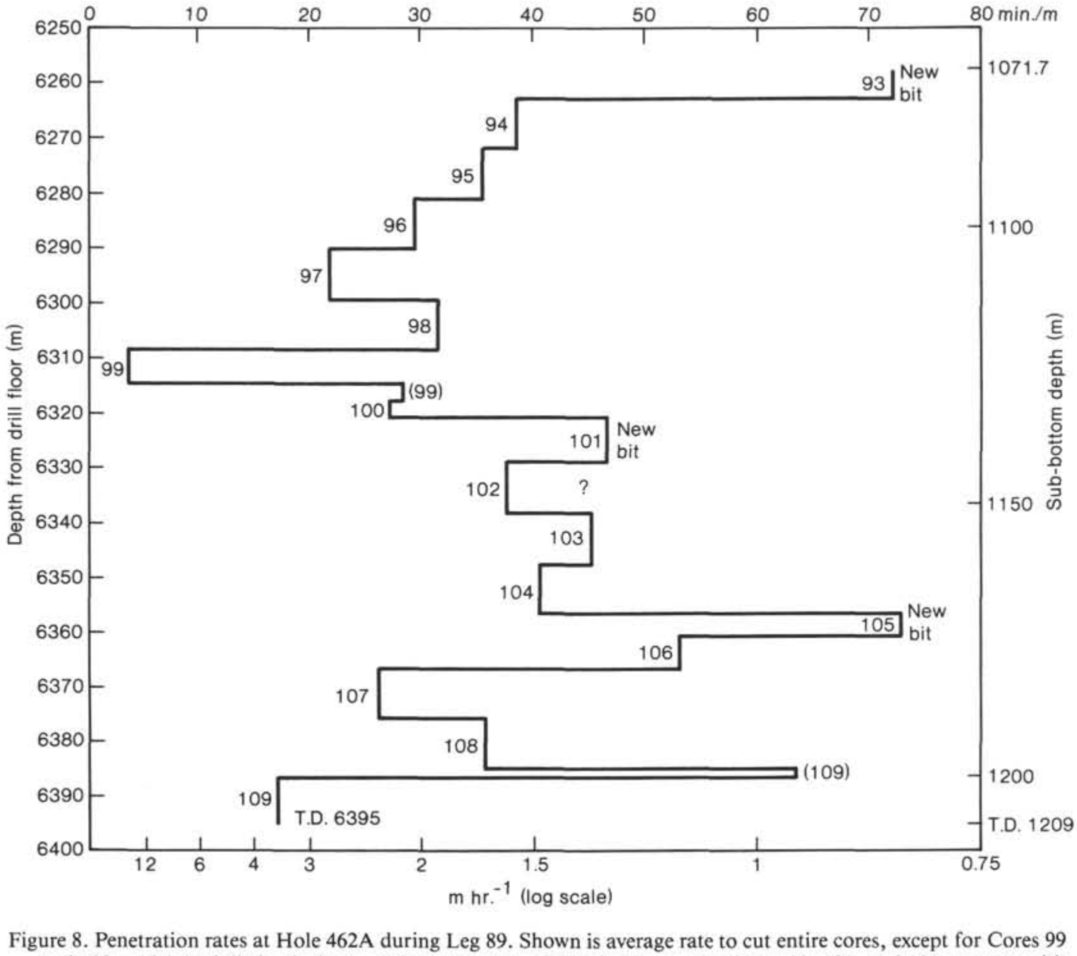

Figure 8. Penetration rates at Hole 462A during Leg 89. Shown is average rate to cut entire cores, except for Cores 99 and 109, which had distinctly faster and slower parts within the same core. Cores 93, 101, and 105 were cut with new bits (drillers normally cut such new cores slowly to break in new bits).

Figure 9. Hyaloclastite sediment on chilled basalt margin in Sample 462A-99-1, 110–124 cm (Pieces 11a and b).

tween sediment and underlying basalt is inclined at about 45° along a green (5G 2/1) margin of chilled, formerly glassy olivine-clinopyroxene basalt (see The Igneous Petrology section that follows). No upper contact of the sediment was recovered. The sediment consists of about 8 cm of dark greenish gray material with olive gray rounded clasts of sediment about 1 to 8 mm in diameter at the base of the sequence. It shows a very weak reaction to HCl. Smear slide analyses did not discern a significant percentage of silt or sand, but in thin section the texture is sandy. The rock is a poorly sorted, altered volcaniclastic, silty sandstone. The sediment is dominantly of hyaloclastic origin (thin section, Sample 462A-99-1, 115 cm); vitric and lithic basalt grains in a clay matrix have been altered to clay and zeolite.

Texture

Grain size ranges from 0.2 mm to a few micrometers in diameter, with a median of about 0.08 to 0.06 mm (coarse silt to very fine sand). Most grains are angular to subangular, blocky to prismatic polygonal, and equant to elongate in shape. A few vesicular grains, formerly glass but now replaced by zeolite with spherulitic clay as amygdules, have vesicles that are 0.04 to 0.09 mm in diameter. No shardlike grains were observed, and most former volcanic grains have the typical shape and sorting of hyaloclastite grains.

Composition

The angular sand and silt grains that made up most of the sediment have been altered to yellowish brown to greenish gray masses of zeolite and clay. These grains, particularly the numerous angular, translucent, pale grayish yellow grains of zeolite-replaced glass, show ghosts of igneous textures and microlites. Other evidence of former volcanic glass are grains of pale brown to golden brown to red brown palagonite in sand and silt sizes. Crystals of plagioclase, corroded plagioclase(?), zeolite-replaced plagioclase(?), and pyroxene and are within the size range of the other grains. A few rounded, sand-sized grains of red brown to gray green mudstone are present. Rare, silicified, hematite-coated radiolarians and more common hematite-coated siliceous masses of unidentified origin also are present. A few elongate fish bone fragments were seen.

Authigenesis and Origin

It is not known whether this sediment had a matrix of glass dust or other silt finer than the grains that can be distinguished now. The rock is cemented by yellow smectite of about 0.005 to 0.002 mm grain size, which we consider to be authigenic because of the fringing scaly texture that rims the framework grains. Centers of the larger cement patches have a microcrystalline mosaic texture. There are a few patches and veinlets of zeolite.

The composition and texture of the sediment was dominantly hyaloclastic in origin. The hyaloclastite material is admixed with small amounts of reworked mudstone, radiolarians, and other grains that have been transported only a short distance. Most of the glassy, labile sediment has altered to clay and zeolite and has been cemented by clay.

A radiolarian age determined from this sedimentary interval dates the sediment and the adjacent basalt as within the range of Late Jurassic to earliest Aptian (see the Biostratigraphy section that follows).

A second piece of sediment—462A-99-2, 36–37 cm (Piece 5)—is an isolated fragment of wavy laminated claystone and silty claystone about 1.5 cm in diameter. The laminae are wispy, possibly burrowed, silty claystone with traces of zeolite, fish debris, and silicified radiolarians, and silt-sized altered volcanic glass. A smear slide of material from one laminae shows it to be about 30%

silt and 70% clay, the silt fraction being celadonite- and smectite-alteration of volcanic glass. Interlaminae material is more than 90% clay.

BIOSTRATIGRAPHY

No foraminifers or nannofossils were recovered. Radiolarians only are reported on here.

In Hole 462A, three samples were examined: the sedimentary bed in Core 462A-99 (Sample 462A-99-1, 113–114 cm), small chips occurring in Core 462A-108, and chips and clay in the core catcher of Core 462A-109. In these three samples, radiolarians are very rare and poorly preserved. In Core 108 they are replaced by zeolites. Only *Holocryptocapsa hindei* was positively identified in 462A-99-1, 113–114 cm. This species has a range from the uppermost Jurassic to the lowermost Aptian.

Biostratigraphic Revision of 462A-80-1, 16–17 cm (Leg 61)

Seven determinations were provided by P. de Wever on Leg 61: *Crucella* sp., *Sethocapsa* sp., *Dictyomitra lacrimula, Eucyrtis micropora*(?), *Thanarla elegantissima, Thanarla* sp. aff. *T. conica*, and *Mirifusus mediodilatatus*. The two first determinations, identified only to genus, can be used. Two other species must be rejected: *Eucyrtis micropora*(?), a species difficult to determine (Foreman, 1975) and not biostratigraphically useful (Baumgartner et al., 1980); and *Thanarla* sp. aff. *T. conica*, a species poorly described by Aliev (1965), regarded as senior synonym of *Dictyomitra lacrimula* by Pessagno (1977), and with a range confined to the Valanginian. For these reasons, only three species are useful for biostratigraphic revision: *Archaedictyomitra lacrimula, Thanarla elegantissima*, and *Mirifusus mediodilatatus*.

Figure 10, which shows the known stratigraphic range for each species, shows that *Mirifusus mediodilatatus* and *Archaeodictyomitra lacrimula* are never overlapping. This implies reworking.

In the right of Figure 10 we have recorded three index species for the middle part of the Lower Cretaceous. *Pantanellium lanceola* is a ubiquitous species that is very common in all Mesozoic oceans; *Pseudodictyomitra leptoconica* and *Eucyrtis columbaria* are very common in Barremian from the western Pacific. The absence of these three species suggests the youngest age of this sample is late early Aptian. Thus 462A-80-1, 16–17 cm seems to be an upper lower Aptian fauna with a Lower Cretaceous (below lower Hauterivian) reworked fauna. (This material must be reexamined before a final conclusion is reached.)

Biostratigraphic Revision of 462A-46-1, 1–3 cm (Leg 61)

The same reasoning can be applied to 462A-46-1, 1–3 cm, in which the presence of *Emiluvia pessagnoi, Emiluvia chica*, and *Staurosphaera sedecimporata* seems to indicate an older age (Berriasian) for the reworked fauna. Thus it is possible that during the Aptian an inverse differential erosion provided the reworked material.

SEDIMENT ACCUMULATION RATES

There is no report on sediment accumulation rates for this hole.

ORGANIC GEOCHEMISTRY

The only sediment interval recovered in substantial quantities from this hole (462A-99-1, 110–124 cm) was analyzed for both its organic carbon content as well as for its hydrocarbon potential, using the CHN analyzer and the Rock-Eval instrument, respectively (see Site 585 Organic Geochemistry section for analytical details). The organic carbon contents were measured four times, and an average value of 0.065% was obtained. The calcium carbonate content was less than 1%. The Rock-Eval pyrolysis gave the following results:

S_1 = 0.021 mg hydrocarbons/g
S_2 = 0.052 mg hydrocarbons/g
S_3 = 2.84 mg CO_2/g
T_{max} = 349°C
I_H (hydrocarbon index) = 80 mg hydrocarbons/g C_{org}
I_p (production index or transformation ratio) = 0.29

The value for the oxygen index exceeds 4000 mg CO_2/g C_{org} and is therefore absolutely irrelevant.

On the basis of these data, the type of the organic matter represents a hydrogen-lean Type III kerogen. The elevated production index of nearly 0.3 indicates either the impregnation by migrated hydrocarbons or an advanced maturity stage. The latter possibility might be explained by thermal stress, which the organic matter underwent between the basalt flows. The low T_{max} value of 349°C, however, is not in accordance with the anticipated advanced maturity. A value of about 440°C would be expected for a mature kerogen. The high I_p value is thus best explained by the assumption of a slight hydrocarbon impregnation.

INORGANIC GEOCHEMISTRY

There is no geochemistry report for this hole.

IGNEOUS PETROLOGY

The basaltic sills and flows encountered in Hole 462A during Leg 61 (Larson, Schlanger, et al., 1981) were interpreted as a product of Early to mid-Cretaceous midocean volcanism erupted onto Jurassic oceanic basement. One of the objectives of deepening Hole 462A during Leg 89 was to drill through the "sill-flow" complex into Lower Cretaceous and Jurassic sediments, and eventually to penetrate true oceanic crust. This was not achieved, and the Leg 89 deepened hole only encountered, during about 130 m of drilling, further flows. Cores with good recovery were also entirely basalt with minimal sediment being recovered between flow units. Fast drilling sequences and poor recovery cores were also suspected of being predominantly volcanic and composed of thin glassy or fractured flow units.

This report describes the basalts encountered from about 1072 m sub-bottom, below the oldest flow unit (type B basalts, Unit 44) found during Leg 61 (Larson,

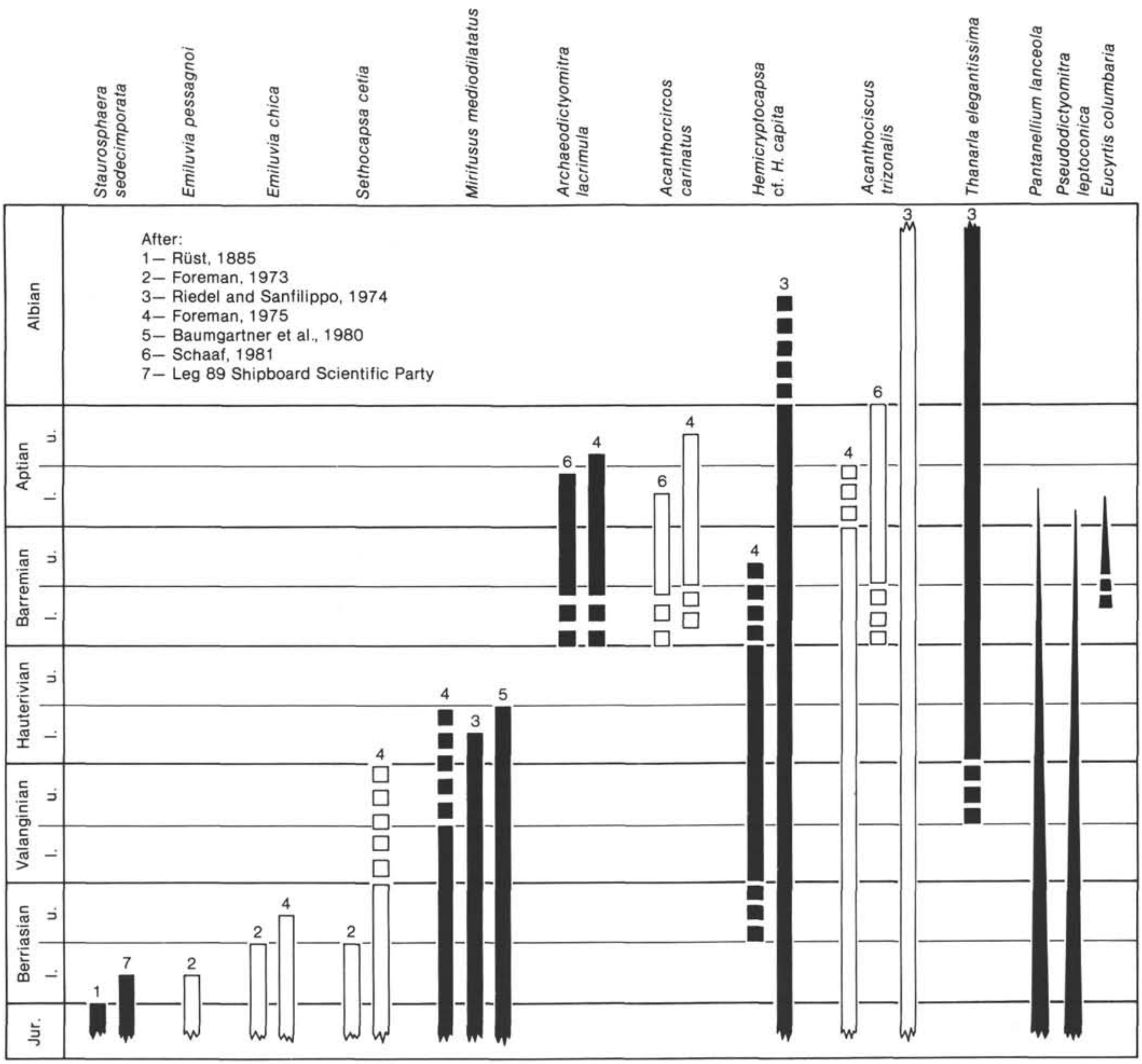

Figure 10. Biostratigraphic ranges of some Lower Cretaceous radiolarians. (Unfilled intervals indicate uncertain identifications by P. de Wever, Leg 61.) At the right are ranges of three common mid-Early Cretaceous index species not found in the samples (see text).

Schlanger, et al., 1981). Subsequent units below Unit 44 have been numbered sequentially.

Nature of the Volcanic Units and Their Boundaries

The basalts have been divided into 12 volcanic units (Fig. 11) on the basis of: (1) sedimentary and hyaloclastite interlayers, (2) the development of marginal quench textures, (3) the presence of chilled, but not necessarily quenched, margins, (4) marked megascopic grain-size reduction, and (5) mineralogical variation, especially in phenocryst content and proportions.

Consideration of the characteristic features of pillow lavas, lava flows, and sills (Fig. 12) suggests that the volcanic units represent individual submarine flows or groups of closely related flows. Thick units, such as Units 46 (31.3 m) and 52 (21.3 m) are predominantly holocrystalline or contain minor interstitial glass and do not develop any ophitic textured facies, pegmatitic zones, or granophyric patches, as often found in sills of similar thickness. Furthermore, small glassy subunits with skeletal crystals or slight changes in grain size and mineralogy may be observed within some thicker units—features that suggest a pile of rapidly extruded related flows.

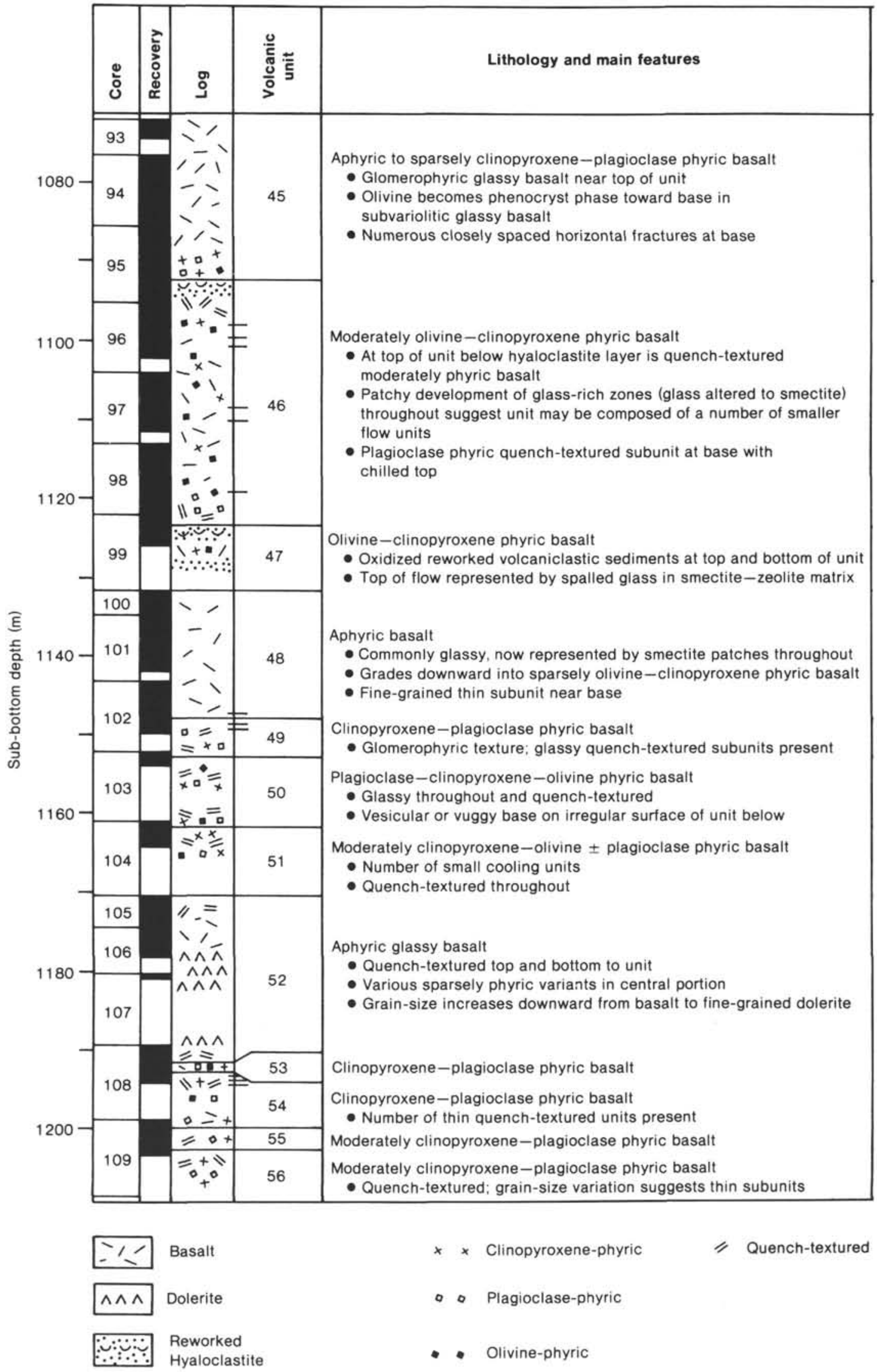

Figure 11. Graphic log and main lithologic features of volcanic units 45 to 56, Hole 462A.

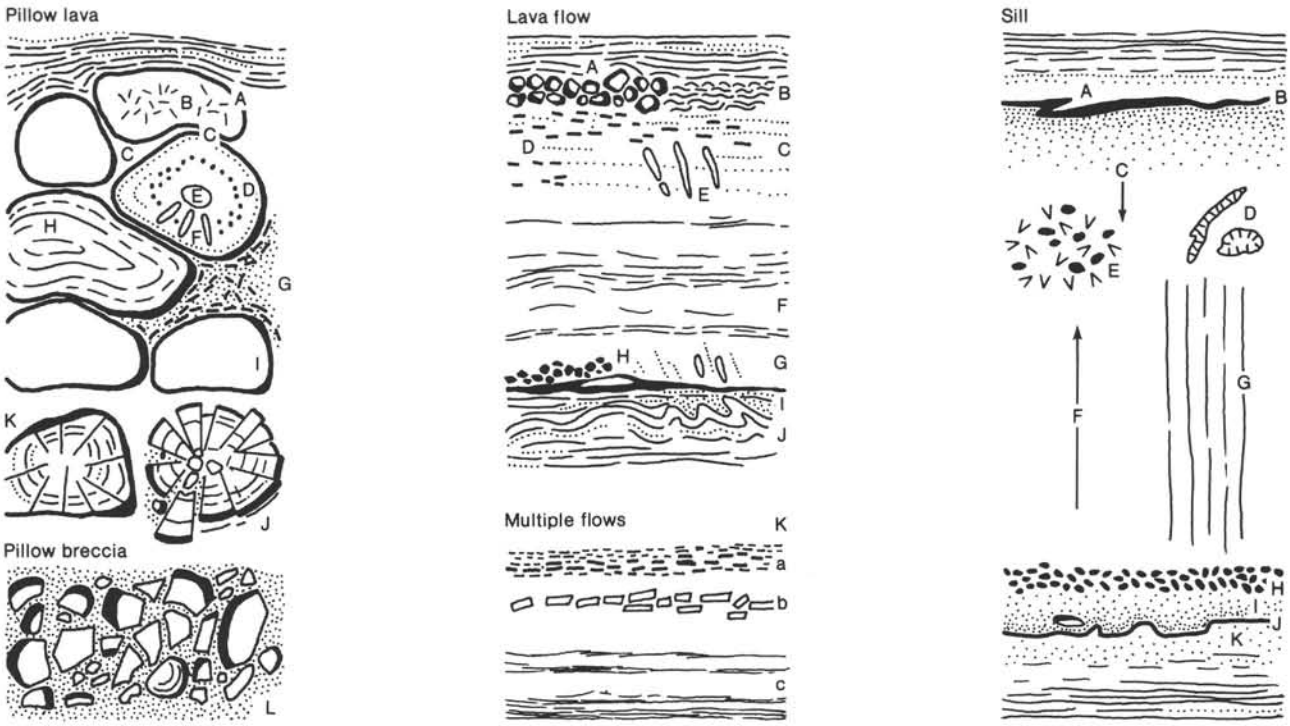

Elongate tubelike glassy cooling units, bun-shaped or ovoid in cross section; quench textures throughout, although hypocrystalline in centers of large-diameter tubes

Characteristic features:

Dark glassy rims (A)
Pale colored, partly crystalline interiors (B)
Moulding of individuals or interpillow space (C)
Small vesicles (rim zone) increasing in size inward, commonly has several concentric zones (D)
Central vacuole common (E)
May have radial pipe vesicles (F)
Interpillow spaces (G) filled with spalled glassy rims (= hyaloclastite), often altered to palagonite and smectite ± carbonate
If altered, concentric zonation accentuated (H)
Vertical and curved glassy margins (I)
Autobrecciation (J) along radial and concentric cooling fractures (K)

Pillow breccias (L) composed of crystalline pillow basalt fragments set in spalled glassy rims, commonly altered (= flow front or top)
Features — monolithologic, fragments angular, poorly sorted, matrix supported

Sheetlike variable thickness glassy cooling units with quench textures; fine-grained holocrystalline interiors common in thick or rapidly extruded multiple flows

Characteristic features:

Unaltered sediments contour flow top (A)
Blocky or corrugated glassy flow top (B)
Below flow top, typically laminated (C), zones of elongate vesicles (D), some near-vertical pipe vesicles (E)
Interior may be glassy or crystalline, typically flow laminated (F)
Some have a few orientated vesicles near base (G)
Flow base may be blocky and include xenoliths (H)
Basal sediments baked (I) or if wet may show wet-sediment deformation (J)

Multiple flows (K) may produce a sequence of glassy and crystalline sheets with "internal" junctions: high density vesicle layers (a), rapid change in grain size or phenocryst-rich layers (b), chilled glassy zones in holocrystalline matrix (c)

Massive holocrystalline sheetlike cooling unit that can be very thick; may exhibit internal magmatic differentiation

Characteristic features:

Baked contact sediments (A) are hard, lighter in color, and reduced; sometimes adinolized
Chilled margin (B) of fine-grained basalt and/or thin glassy zone
General increase in grain size downwards (C)
Granophyric patches and veins toward top (D)
Pegmatitic (or gabbroic) zone (E) about 2/3 up from base
Most of body is dolerite (F) that may grade from melanocratic (near base) to more leucocratic upward; ophitic texture
Columnar jointing typical (G)
Possible olivine ± pyroxene cumulate layer (H) close to base
Basal chilled margin of fine-grained basalt (I)
Irregular lower margin, sometimes with country rock xenoliths (J)
Baked contact sediments (K) are hard, lighter in color and reduced; sometimes adinolized

Figure 12. Composite, characteristic features of pillow lavas, sheet lava flows, and sills that were used to determine the nature of the basaltic rocks in Hole 462A.

There is little evidence for the "intrusion" of a flow into a cooling submarine lava pool under an already chilled flow top. In such a case, the "intruding" lava might form a more holocrystalline basalt with chilled margins at top and bottom, rather than quenched zones. Chilled margins between Units 50/51 and 54/55, however, exhibit quench textures at the junctions and are not holocrystalline.

Only in one questionable case (Unit 51) was a sequence of pillow lavas suspected with observable concentric quenched margins. Only two or so intact cooling units were so identified together with isolated basalt pieces exhibiting a rapid alteration in grain size from fine to coarse. They did not show some of the typical features illustrated in Figure 12, such as interpillow debris, although this may be a consequence of poor recovery during drilling.

The evidence for the top and bottom of the volcanic units is presented in Table 2, together with an indication of the reliability of the defined junction, for example, actually observed or inferred.

Lithological Variation of Volcanic Units

The dominant lithology of each unit is illustrated in Figure 11 and shows a crude alternation of relatively fresh aphyric and moderately phyric (2–10% phenocrysts) basalts. The proportion of phenocrysts can vary within a unit, however, such that predominantly aphyric units may contain a few phenocrysts concentrated into layers to produce sparsely phyric basalts. Most of the thicker units are essentially holocrystalline (Unit 45) or contain variable amounts of residual interstitial glass (Unit 48). On the other hand, the thin units are quench textured throughout (Units 49 and 50), although the proportion of residual melt (now quenched to glass) is variable. Apart from rare occurrences (for example, Unit 50), all the basalts are nonvesicular and indicate extrusion in a deep-water environment.

Compared with the type B flows sampled during Leg 61, aphyric basalts are again volumetrically important. Below 1072 m a greater preponderance of clinopyroxene and a lower proportion of olivine amongst the phenocryst assemblages is apparent.

Petrology of Main Basalt Types

The volcanic units are composed of a number of different basaltic types that can be classified according to the proportions and assemblages of phenocrysts present (Table 3). Many of the basalts contain residual interstitial glass (referred to as glassy basalts), and few are completely holocrystalline. Quench-textured basalts show phenocryst assemblages similar to those of the more crystalline types.

Textural variations relate to the cooling history of the unit—quenched at the margins or more crystalline in the slower cooling interiors of flows. Glassy basalt margins and some complete flow units are hyalopilitic, with large plumose clinopyroxenes and skeletal microlites of plagioclase. Remains of original glass (now altered) may be seen between the quenched crystallites. Farther away from the glassy margins, basalts are typically variolitic with intergrowths of skeletal and serrated "bow-tie" plagioclase and clinopyroxene. Isolated radiate groups of two or three plagioclase microlites (subvariolitic) are also common throughout many glassy basalts and are set in a granular clinopyroxene-plagioclase matrix. Textures in the coarser-grained interiors of aphyric flows are granular or intersertal, but never ophitic. Intersertal textured

Table 2. Thickness, location, and nature of the boundaries between volcanic units, Hole 462A.

Unit	Thickness (m)	Sub-bottom depth (m)	Boundary sample (core-section, cm level)	Nature of boundary[a] A	B	C	Boundary characteristics[b] (Nature of contact between each unit)
45	>20.4						t = glassy basalt (Unit 44, Leg 61), medium-grained dolerite b = quench texture, phenocryst density decrease
		1092.3	95-5, 65	X			
46	31.1						t = hyaloclastite, quench texture in basalt below b = quench texture
		1123.4	99-1, 112		X		(Reworked volcaniclastic sediment)
47	8.1						t = spalled glassy flow top to basalt
		1131.5	99-2/100-1			X	(Reworked volcaniclastic sediment)
48	16.5						b = quench texture, cpx-ol phyric basalt
		1148.0	102-4, 64		X		
49	4.6						t = quench texture, cpx-plag phyric basalt b = fine-grained ol-cpx phyric basalt
		1152.6	103-1, 55		X		
50	9.0						t = quench texture, three-phase phyric basalt b = vesicular base
		1161.6	104-1, 42	X			(Curved irregular contact)
51	8.8						t = chilled margin, quench texture b = phyric basalt, quench texture
		1170.4	105-1, 7		X		
52	21.3						t = aphyric basalt, quench texture b = quench texture
		1191.7	108-2, 71		X		
53	0.6						t = glass-coated quenched basalt pebble (breccia?) b = phyric glassy basalt
		1192.6	108-3, 12		X		
54	7.1						t = quench texture; grain-size decreases downwards b = chilled margin
		1199.7	109-1, 104	X			(Inclined contact)
55	2.0						t = quench texture
		1201.7	109-3			X	
56	>0.3						t = rapid grain-size variation, finer than Unit 55

[a] A = boundary visible within a single portion of core, B = adjacent, but individual pieces within same section, and C = inferred (poor recovery between sections or cores).
[b] t = top, b = bottom, also, cpx = clinopyroxene, ol = olivine, plag = plagioclase.

Table 3. Distribution of main basaltic types (X) and other variants (+) within volcanic Units 45 to 56, Hole 462A.

Basaltic type (includes both glassy and holocrystalline basalts)	Volcanic unit											
	45	46	47	48	49	50	51	52	53	54	55	56
Aphyric basalts												
1. Aphyric medium to coarse-grained basalt, some is glassy	X			X				X				
2. Fine-grained dolerite								+				
Sparsely and moderately phyric (1-10% phenocrysts) basalts												
3. Clinopyroxene-phyric basalt		+						+	+			
4. Olivine-clinopyroxene-phyric basalt		X		+			X	+				
5. Clinopyroxene-plagioclase-phyric basalt	+				X		+	+	X	X	X	X
6. Olivine-clinopyroxene-plagioclase-phyric basalt	+	+					+					
Phyric (>10% phenocrysts) basalts												
7. Olivine-phyric basalt		+										
8. Olivine-clinopyroxene phyric basalt		+	X									
9. Plagioclase-clinopyroxene-olivine basalt						X						

basalts commonly contain interstitial residues of glass that may be crowded with skeletal or granular magnetite.

The most commonly occurring phenocryst assemblages: (1) clinopyroxene-plagioclase, (2) olivine-clinopyroxene, and (3) olivine-clinopyroxene-plagioclase (Table 3) are typical of holocrystalline, glassy basalts and quench-textured basalts alike. As seen in Figure 13, the proportion of the matrix phases—clinopyroxene, plagioclase, and Fe ore (olivine is rarely observed in the matrix)—varies between the three main phenocryst assemblages just listed. Only the quench-textured basalts are characterized by a higher proportion of clinopyroxene and reflect the more primitive mafic-rich composition of the initial melt relative to the plagioclase-rich flow interiors. Other local modal variations also relate to the cooling history of specific units. For example, the concentration of olivine microphenocrysts at the base of Unit 45 probably represents the accumulation of early fractionated olivine within this slowly cooled, thick aphyric unit.

The modal quench compositions for different basaltic units plotted in Figure 14 show some variation and two possible differentiation trends toward plagioclase-rich compositions (Unit 51) and magnetite-rich compositions (Unit 50). In the absence of data on fresh glass, this suggests that there may be some variation in the initial melt compositions between volcanic units.

Petrographic data based on the examination of 48 thin sections are given in Table 4. The visual estimates are only approximate and the proportion of clay is probably too high in view of the low H_2O^+ content of most basalts determined. Petrographic details of two basaltic types are given later to illustrate some of the textural and mineralogical variations encountered. Photomicrographs of selected basalts are shown in Figures 15 to 17.

In summary, the modal and textural variations are largely the result of the cooling history of individual units, together with some differences in initial melt composition between units. Variation in phenocryst assemblages also suggests different magma compositions resulting from pre-eruptive fractionation processes within one or more magma chambers.

Detailed Petrography of Two Basaltic Types

Plagioclase-Clinopyroxene-Olivine Phyric Glassy Basalt

This basalt is typical of Units 50 and 51, although the proportions of phenocryst phases vary and olivine may not always be present. These basalts are characterized by the presence of the three main phenocryst phases, remnant glass, and a quenched hyalopilitic texture.

Subhedral olivine phenocrysts vary in size from 0.1 to 0.3 mm and are always replaced by yellowish brown smectite and a fine-grained iddingsitic opaque material. Carlsbad- and polysynthetic-twinned plagioclase phenocryst are lath-shaped and vary in composition from about An_{70} to An_{80}. Very fine zoning (type not defined) is only occasionally observed. Anhedral and subhedral clinopyroxene (varying from 0.1 to 0.2 mm, sometimes 0.6 mm in size) tends to form glomerocrysts, although in some places they may only be associated with plagioclase phenocrysts that are enclosed subophitically. Glomerophyric clinopyroxene is a characteristic feature of the majority of the basalts and is typically augite.

The matrix displays a hyalopilitic texture of large quenched clinopyroxene plumes and sheaves, small granules of magnetite and skeletal plagioclase microlites, together with some glass (now smectite) between the clinopyroxene crystallites. Clinopyroxene is intergrown with "bow-tie" serrated plagioclase microlites (variolitic texture) only where the plumose clinopyroxenes are larger and better crystallized away from the margin. Anhedral clinopyroxene prisms may also be found in these areas and may constitute about 20% of the total clinopyroxene content. Complete clinopyroxene sheaves are internally peppered and externally rimmed by small magnetite granules (about 0.006 mm), although less rapid quenching allows the magnetite to grow larger and become concentrated in the intersheaf glassy areas. Plagioclase microlites (An_{54-60}) may occur as subvariolitic groups of

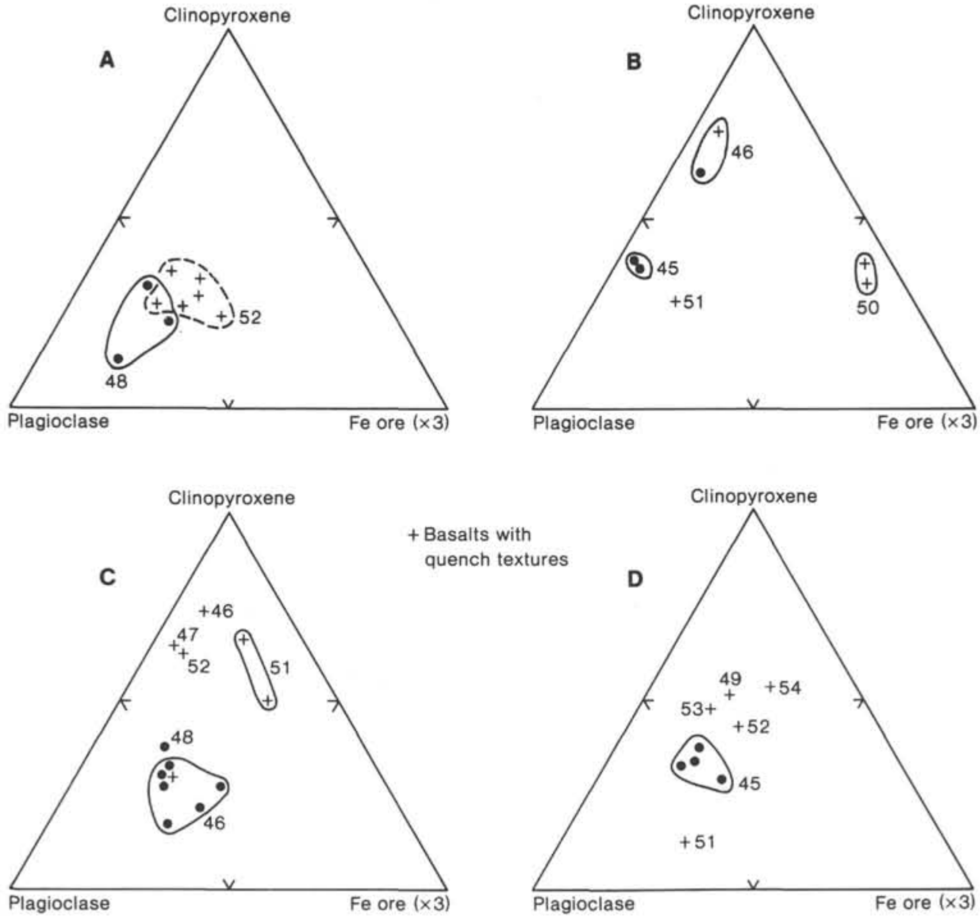

Figure 13. Relative modal proportions (visual estimates only) of (A) matrix clinopyroxene, plagioclase, and Fe ore in aphyric basalts, (B) olivine-clinopyroxene-plagioclase variably phyric basalts, (C) olivine-clinopyroxene variably phyric basalts, and (D) clinopyroxene-plagioclase variably phyric basalts. Samples are numbered according to their volcanic unit (45 to 54).

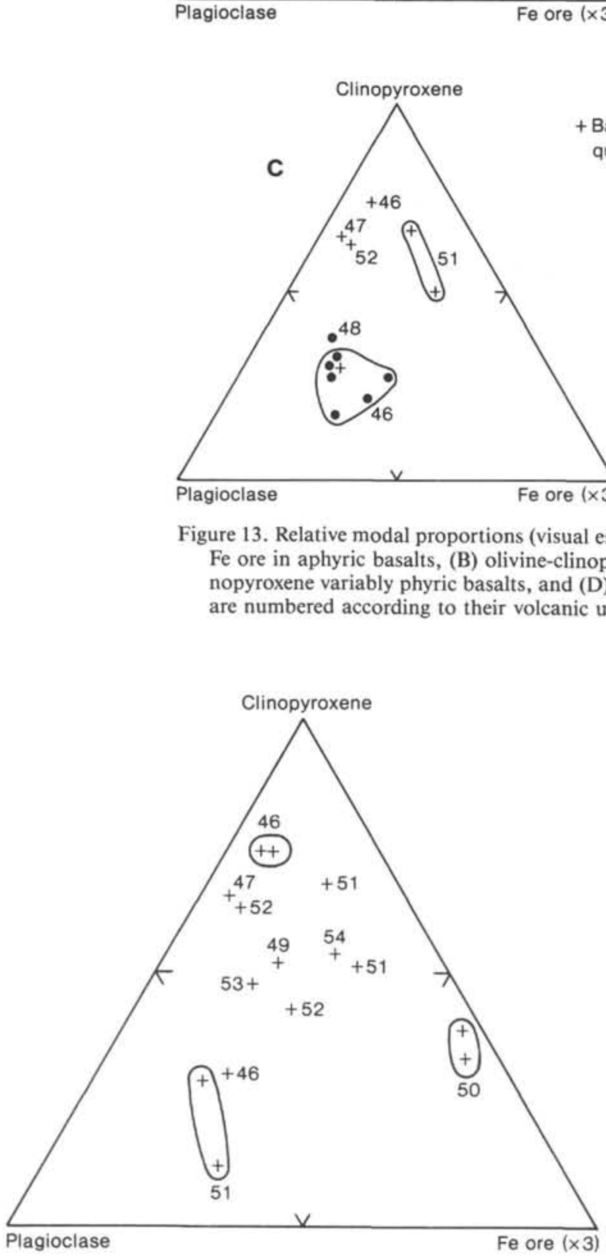

Figure 14. Relative modal proportions (visual estimates only) of matrix clinopyroxene, plagioclase, and Fe ore in quench-textured basalts from various volcanic units (numbered).

two or three skeletal "bow-tie" crystals or may form long, curving, serrated individuals, or small-cored narrow prisms with forked ("swallow-tailed") terminations. Skeletal magnetite is often enclosed (and replaced?) by a dark opaque clay material that obscures its outline and under plane polarized light gives the impression of more Fe ore than is readily apparent under vertical reflected light.

Aphyric or Sparsely Clinopyroxene-Plagioclase Phyric Basalt

This basalt is typical of Unit 45 and has a granular texture of anhedral to subhedral clinopyroxene prisms and plagioclase laths. Slightly porphyritic clinopyroxene (augite) may occur as glomerocrysts that are isolated from any plagioclase phenocrysts (An_{70-72}). Matrix augite forms small anhedral grains (0.05–0.2 mm) that may occasionally be twinned. Plagioclase is labradorite (commonly An_{50-55}; some basalts have An_{60-65} in groundmass plagioclases) and exhibits both carlsbad and polysynthetic twinning in the same crystal. Magnetite makes up a good proportion of the matrix (average 10%), forming anhedral grains (0.1–0.3 mm) commonly obscured by dark brownish smectite. Glassy equivalents of these basalts tend to have intersertal textures with interstitial

Table 4. Summary of petrographic data from thin section examination of basalts, Hole 462A.

Core-section, cm interval (volcanic unit)	Rock type	Texture	Phenocrysts (%)				Matrix (%)				Fe	Alteration (%)		
			ol	cpx	plag	(An%)	ol	cpx	plag	(An%)	ore	carb	clay	zeol
93-1, 85-86 (45)	Sparsely plag-cpx glomerophyric B	Intersertal	—	1	1		—	27	40	(55-60)	5	1	25	—
94-1, 122-123 (45)	Sparsely plag phyric B	Granular	—	—	1		— (+1% amphibole)	38	35	(54)	15	—	10	1
94-4, 19-20 (45)	Sparsely plag-cpx phyric B	Granular	—	0.5	0.5		— (+1% pyrite)	30	33	(60-65)	5	—	30	—
94-6, 133 (45)	Sparsely plag-cpx glomerophyric B	Granular	—	0.5	0.5	(70-72)	—	30	44	(50-55)	10	—	15	—
95-2, 61-62 (45)	Sparsely cpx glomerophyric B	Granular	—	1	—		—	25	44	(55)	10	—	20	—
95-5, 40-41 (45)	Sparsely cpx-plag phyric ol B	Granular	—	0.5	0.5		tr	25	34		5	—	35	—
95-5, 59-60 (45)	Altered ol-cpx-plag phyric ol B	Subvariolitic and granular	4	4	1	(72)	tr	20	30	(55)	1	—	40	—
95-5, 63-64 (45)	Altered ol-cpx-plag phyric glassy B	Subvariolitic	2	2	1		— (+ tr glass)	20	24		2	1	48	—
95-5, 89-90 (46)	Altered ol-cpx phyric glassy B	Subvariolitic	3	2	tr		tr	10	30		5		50	
95-5, 127-128 (46)	Altered cpx glomerophyric B	Granular	6	3	—		—	17	40	(60)	5	—	35	—
95-6, 101-102 (46)	Altered ol-cpx phyric B	Granular and intersertal	3	2	—		—	25	35		5	—	30	—
96-3, 32-33 (46)	Ol-cpx phyric B	Granular and intersertal	10	1	—		—	20	36	(62-65)	5	—	28	—
96-3, 140-143 (46)	Sparsely ol-cpx phyric B	Granular	1	1	—		—	25	40	(60)	5	—	28	—
96-5, 130-131 (46)	Altered ol-cpx phyric B	Granular and intersertal	5	2	—		—	20	43	(55-60)	10	—	20	—
97-5, 110-111 (46)	Ol phyric B	Granular	7	tr	tr		—	18	40		15	—	20	—
98-6, 25-26 (46)	Ol-cpx phyric B	Granular and intersertal	10	2	—		—	25	33		10	—	20	—
98-6, 47-48 (46)	Altered ol-cpx phyric glassy B	Hyalopilitic	8	5	tr		—	20	32		5	—	30	—
98-6, 99-100 (46)	Altered ol-cpx phyric B	Hyalopilitic	3	5	—		—	69	15		2	—	15	—
98-7, 47-48 (46)	Cpx-ol-plag phyric B	Hyalopilitic	1	5	2		—	60	15		2	—	15	—
99-1, 100 (46)	Altered ol phyric and cpx-plag glomerophyric B	Granular and subvariolitic	6	2	1		—	44	20		2	—	25	—
99-1, 115	Vitric tuff (= reworked hyaloclastite)	Altered glass shards in pale yellow smectite matrix												
99-1, 129 (47)	Ol-cpx phyric glassy B	Hyalopilitic	2	15	—		—	42	20		1	—	20	—
100-2, 28-29 (48)	Aphyric B	Subvariolitic and intersertal	tr	—	—		—	10	52	(65-68)	5	1	30	2
101-1, 68-69 (48)	Aphyric glassy B	Subvariolitic and intersertal	—	—	—		—	30	50		5	—	15	—
101-4, 57-58 (48)	Aphyric glassy B	Subvariolitic and intersertal	—	—	—		—	22	50		8	—	20	—
102-4, 7-8 (48)	Sparsely cpx-ol phyric glassy B	Intersertal and granular	1	1	—		— (+5% palagonite)	35	43	(55-60)	5	—	10	—
102-4, 132-133 (49)	Altered cpx-plag phyric glassy B	Hyalopilitic	—	4	1	(55-60)	—	44	25	(50-55)	5	—	21	—
103-1, 60-61 (50)	Plag-cpx-ol phyric glassy B	Hyalopilitic	2	4	10	(70-80)	—	52	5		25	—	2	—
103-1, 74-75 (50)	Plag-cpx-ol phyric glassy B	Hyalopilitic	1	4	10		—	42	10		25	—	2	—
104-1, 40-44 (51)	Altered cpx-plag-ol phyric B	Granular	2	4	2		— (+ tr amphibole and pyrite)	22	40		5	—	25	—
104-1, 80-84	Altered cpx-ol phyric glassy B	Hyalopilitic	1	3	—		—	51	10		5	—	30	—
104-1, 126-127 (51)	Altered cpx-ol phyric glassy B	Hyalopilitic	1	3	—		—	46	15		10	—	25	—
105-1, 3-4 (51)	Altered cpx-plag glomerophyric glassy B	Intersertal	—	4	1	(65)	—	10	48	(54)	8	—	30	1
105-1, 11-12 (52)	Sparsely cpx phyric glassy B	Hyalopilitic and variolitic	—	1	—		tr (+5% palagonite)	25	34	(50-54)	10	—	25	—
105-1, 80-81 (52)	Altered, cpx-ol phyric glassy B	Hyalopilitic	1	1	—		—	59	10	(52-55)	8	tr	20	—
105-2, 4-5 (52)	Aphyric glassy B	Intersertal and variolitic	—	—	—		tr	30	45		10	—	15	—
106-1, 21-22 (52)	Aphyric glassy B	Intersertal and variolitic	—	—	—		—	30	50	(52-55)	10	—	10	—
106-2, 3-4 (52)	Aphyric glassy B	Intersertal and variolitic	—	—	—		—	30	50	(50-55)	15	—	5	—
106-2, 147-148 (52)	Aphyric glassy B	Intersertal and variolitic	—	—	—		—	40	45	(55-60)	10	—	5	—
106-3, 3-4 (52)	Aphyric fine-grained dolerite	Poorly variolitic	—	—	—		—	40	50	(50)	7	—	3	—
108-1, 10-11 (52)	Aphyric fine-grained dolerite	Granular	—	—	—		—	20	40	(47-54)	5	—	35	—
108-2, 55-56 (52)	Sparsely cpx-plag phyric glassy B	Granular	—	1	1		—	40	30	(60-63)	8	—	20	—
108-2, 66-67 (52)	Sparsely cpx phyric glassy B	Hyalopilitic	tr	2	—		—	40	20		8	tr	30	—
108-2, 74-75 (53)	Altered cpx phyric glassy B	Hyalopilitic	—	3	—		—	45	15	(56)	2	—	35	—
108-2, 108-109 (53)	Altered cpx-plag phyric glassy B	Variolitic	tr	3	1		—	41	30		5	—	20	—
108-3, 26-27 (54)	Altered cpx-plag glomerophyric glassy B	Hyalopilitic	—	5	1	(64)	—	46	15	(50-52)	8	—	25	—
109-1, 100-103 (55)	Altered cpx-plag phyric glassy B	Variolitic	—	5	1		—	40	30	(55)	10	—	14	—
109-2, 145-148 (55)	Altered cpx-plag phyric glassy B	Subvariolitic and granular	—	8	2		—	20	30		8	—	32	—

Note: B = basalt, ol = olivine, cpx = clinopyroxene, plag = plagioclase. Proportions of phenocrysts, primary phases, and alteration products represent visual estimates only; tr = trace; carb = carbonate; zeol = zeolite; — = not observed.

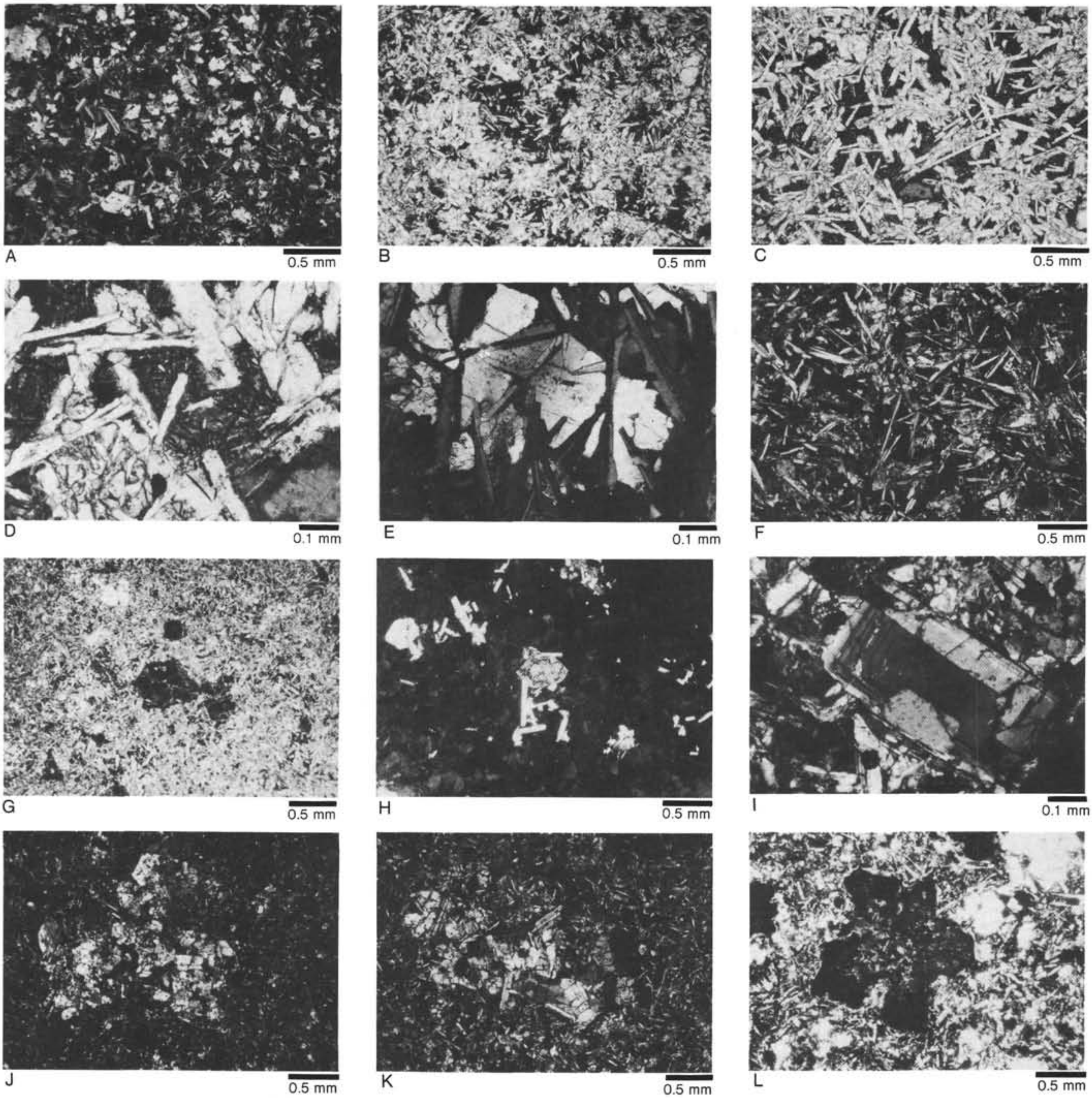

Figure 15. Textures of holo- and hypocrystalline basalts from Hole 462A (xp = cross polarized light, ppl = plane polarized light). (A) Granular-textured aphyric basalt, largely composed of anhedral clinopyroxene and stumpy plagioclase laths (xp); Sample 462A-94-4, 19–20 cm. (B) Patchy development of interstitial glass, now altered to smectite (dark areas), with granular clinopyroxene and small plagioclase laths (xp); Sample 462A-95-6, 102–103 cm. (C) Poorly developed intersertal texture with Fe ore-rich interstitial glass (dark areas) (ppl); Sample 462-105-2, 4–5 cm. (D) Interstitial glass crowded with dark acicular magnetite needles (enlargement of center of 15C). Palagonitized glass area in right-hand bottom corner has a fringe of fibrous smectite (ppl); Sample 462A-105-2, 4–5 cm. (E) Clusters of serrated "bowtie" plagioclase microlites subophitically enclosed within a clinopyroxene prism (xp); Sample 462A-106-1, 21–22 cm. (F) Subvariolitic texture of poorly developed radiate groups of single or double elongate skeletal plagioclase microlites with anhedral clinopyroxene granules (xp); Sample 462A-100-2, 28–29 cm. (G) Smectite (dark) pseudomorphing poorly defined olivine phenocrysts in center of field (ppl); Sample 462A-95-5, 59–60 cm. (H) Clumps of plagioclase microphenocrysts and a single smectite-replaced olivine phenocryst in a matrix (dark) of clinopyroxene spherulites (ppl); Sample 462A-103-1, 60–61 cm. (I) Plagioclase phenocryst showing an internal, albite-twinned core surrounded by two zoned growth areas and a clear unzoned rim (xp); Sample 462A-94-6, 133 cm. (J) Glomerocrystic aggregate of anhedral-subhedral clinopyroxene prisms (xp); Samples 462A-95-5, 59–60 cm. (K) Glomerocrystic aggregate of subhedral clinopyroxene prisms and minor plagioclase laths (xp); Sample 462A-108-2, 108–109 cm. (L) Irregular vug (or coalesced vesicles) infilled with variably crystalline smectite (dark) that becomes coarser-grained toward the center (ppl); Sample 462A-109-2, 145–148 cm.

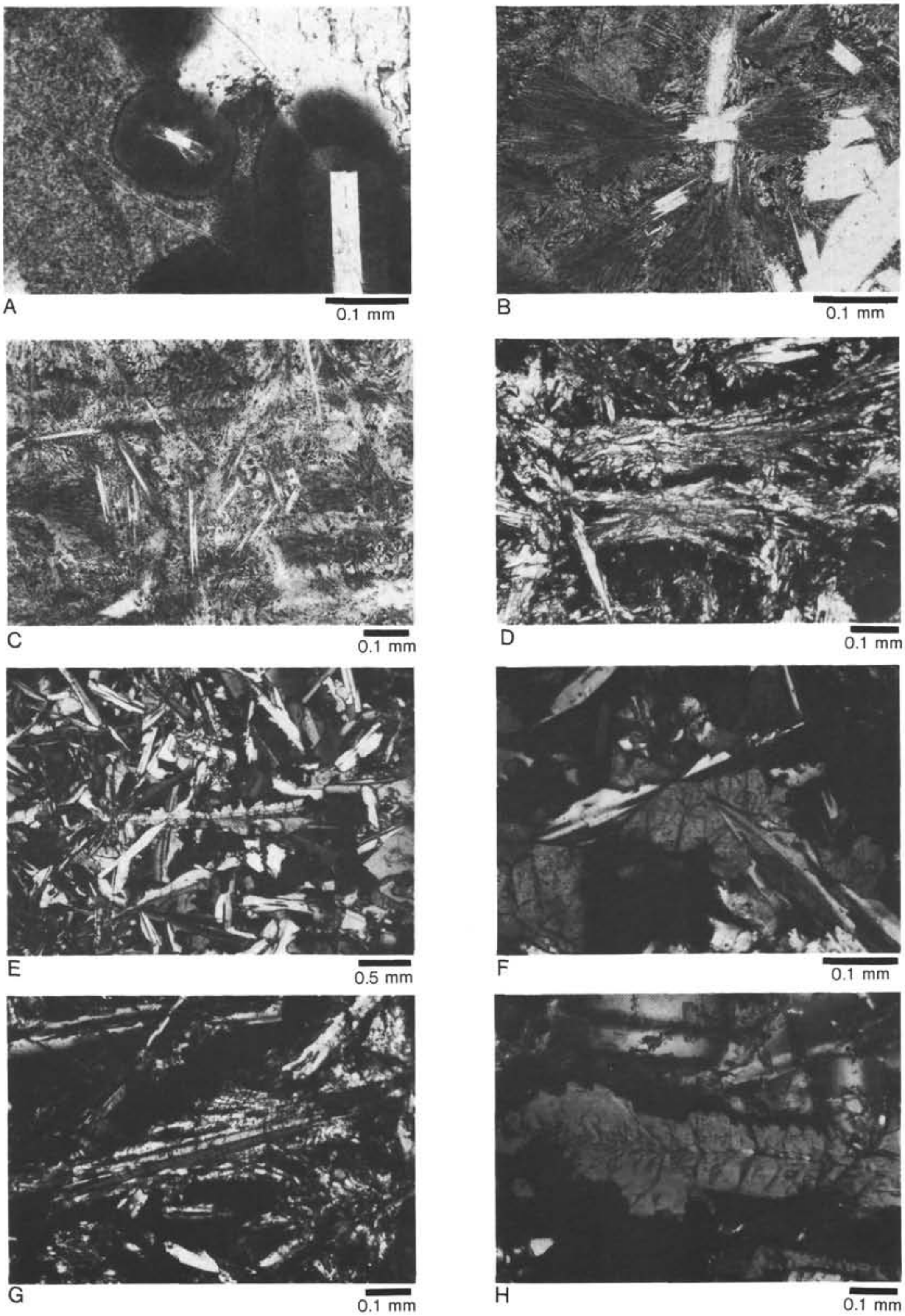

Figure 16. Textures of quenched basalts from Hole 462A, (ppl = plane polarized light, xp = cross polarized light) (A) Dark Fe ore-rimmed spherulites of fibrous pyroxene crystallites nucleated on plagioclase microphenocrysts. The originally vitreous matrix is now composed of clear palagonite (right-hand side, top corner) and granular smectite (left-hand side) (ppl); Sample 462A-103-1, 60–61 cm. (B) Variolite of plumose clinopyroxene nucleated on terminations of plagioclase microlites (ppl); Sample 462A-103-1, 60–61 cm. (C) Skeletal and "swallow-tailed" plagioclase microlites scattered throughout a matrix of plumose clinopyroxene variolites (ppl); Sample 462A-102-4. 100–101 cm. (D) Two well-developed variolites of clinopyroxene sheaves (ppl); Sample 462-102-4, 132–133 cm. (E) Open-structured spherulite of radiate skeletal "bowtie" plagioclase microlites (xp); Sample 462A-106-2, 3–4 cm. (F) Detail of spherulite composed of a few skeletal plagioclase microlites subophitically enclosed by anhedral clinopyroxene (xp); Sample 462A-105-1, 11–12 cm. (G) Detail of a variolite showing a coaxial microlite intergrowth of twinned plagioclase (center) and acicular clinopyroxene (xp); Sample 462A-100-2, 28–29 cm. (H) Elongate, skeletal, dendritic clinopyroxene crystal (xp); Sample 462A-108-1, 10–11 cm.

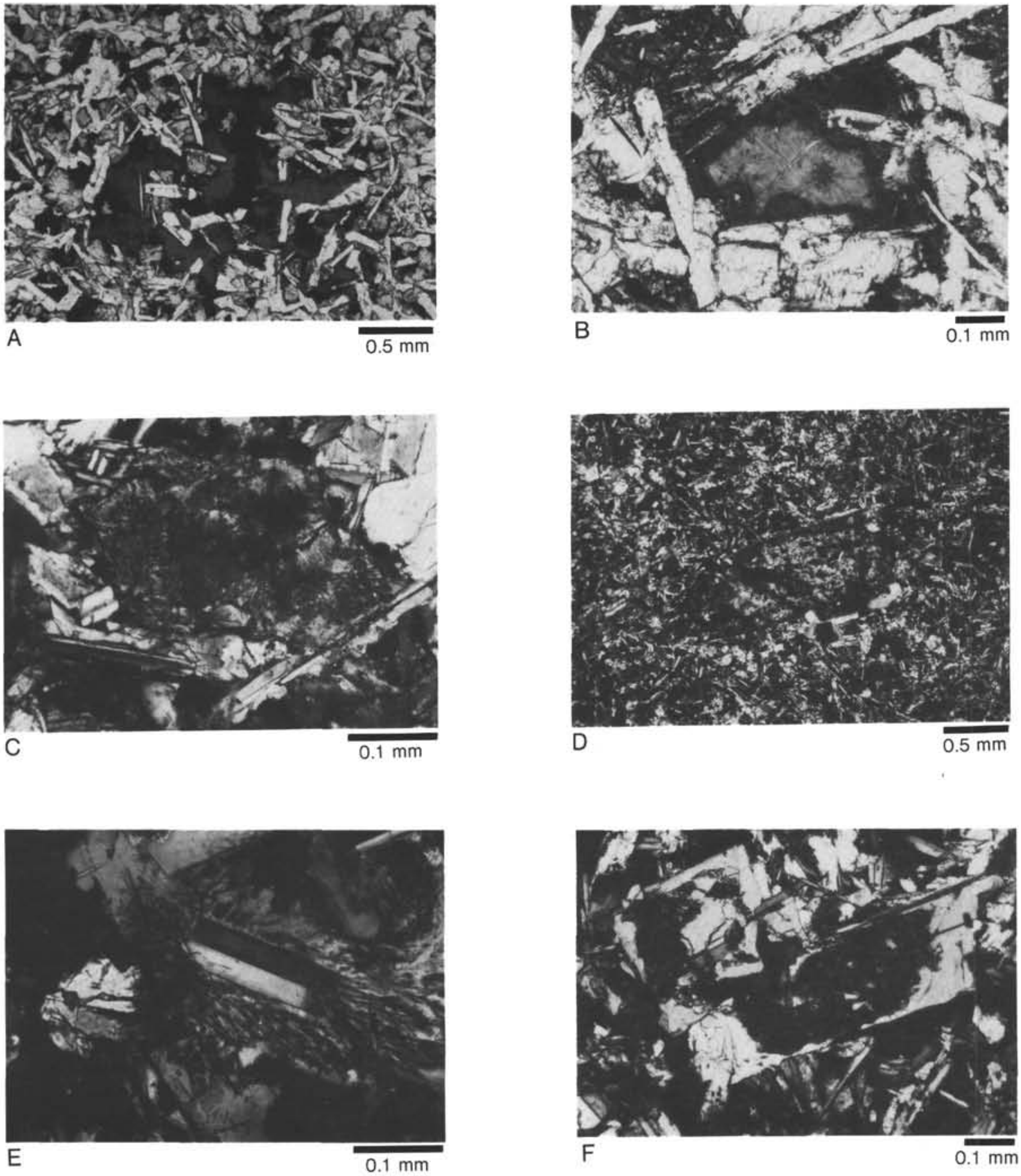

Figure 17. Alteration features in basalts from Hole 462A (xp = cross polarized light, ppl = plane polarized light). (A) Fibrous smectite (dark) replacing interstitial palagonitized glass (gray) (ppl); Sample 462A-102-4, 7–8 cm. (B) Interstitial palagonite (gray) replaced by a thin marginal zone and inward growth hemispheres of fibrous smectite (dark) (ppl); Sample 462A-105-2, 4–5 cm. (C) Dark mass of fibrous and platy smectite alteration products replacing olivine microphenocryst (outlined) (xp); Sample 462A-97-5, 110–111 cm. (D) Originally zoned plagioclase phenocryst patchily replaced in the core and completely in the rim zone by smectite (xp); Sample 462A-108-2, 108–109 cm. (E) Feathery zeolite nucleated on a largely unaltered twinned plagioclase lath (xp); Sample 462A-105-1, 3–4 cm. (F) Group of plagioclase microphenocrysts with the central portion of one largely replaced by dark platy smectite (xp); Sample 462A-108-2, 108–109 cm.

residual glass altered to brown smectite. Magnetite grains are commonly associated with the glassy areas.

Secondary Alteration and Fracturing

Bulk Rock Alteration

Although smectite clays are found throughout the basalt flows and within fractures, the degree of alteration is generally low, with an alteration code (see Site 585 report) of B to C. They are relatively fresh compared with many submarine midoceanic ridge flows, having high, typically basaltic, specific gravity (average 2.94) and low H_2O^+ contents (average 0.86 wt.%). In general terms, brownish smectites (dark green in hand specimen) replace glass and olivine throughout the basalts, whereas zeolites, calcite, and K-feldspar are relatively rare and Fe oxides not observed (except in reworked hyaloclastite fragments).

In detail, thin section examination shows that yellow brown to dark brown smectites (together with an unidentified opaque clay) typically replace interstitial glass in aphyric and glassy quenched basalts. Only rarely are golden yellow palagonite remnants seen surrounded by yellow to brown zones of smectite. Palagonitized vitrophyric glass may also exhibit thin smectite alteration zones around the enclosed phenocrysts (for example, the top of Unit 52). Alteration zoning of glass generally indicates a diffusion-controlled process as well as the migration of fluids via grain-glass boundaries.

Olivine is always replaced by dark brown smectites and an opaque iddingsitic material; only rarely has calcite been observed in association with smectite replacing olivine phenocrysts (Unit 52; Core 105-1).

Toward the base of Hole 462A (Unit 52 downward) cloudy brownish smectites commonly replace the cores of (zoned?) plagioclase laths. Larger areas of coaxial brown and green smectite fibers may replace both plagioclase and clinopyroxene to some degree. Also in these areas are small, individual, acicular colorless to pale green prisms. They are probably a zeolite (rather than amphibole), as many apparently have straight extinction and low birefringence.

Rare vesicles and vugs are smectite-lined and toward the top of Unit 49 (Core 102-4, 132-133 cm) are zoned from a rim of golden yellow brown smectite to a thin dark brown opaque zone and a core of well-crystallized, radiate pleochroic yellow green and green celadonite(?).

Fractures and Veins

Fractures are ubiquitous in Hole 462A basalts and are represented by two major sets: (1) a conjugate pair of steeply dipping (60–70°) fractures, and (2) subhorizontal, often closely spaced, fractures. A few near-vertical crosscutting fractures may also be observed. The rarity of slickensides on fracture infillings suggests little movement has taken place between adjacent blocks.

The distribution of fractures in Unit 45 (Fig. 18) shows a top zone of steep fractures (92–100% of total fractures), a large middle zone where both sets occur in roughly similar proportions, and a basal zone dominated by subhorizontal fractures that increase in frequency downward. About 20 cm from the base of the unit no fractures are observed. It is suggested that the subhorizontal set represents fracturing along or parallel to some initial flow lamination or platy cooling zones within the unit. Their paucity at the top of the unit may be the result of slower cooling under a thickening blanket of subsequently extruded flows and a superimposed vertical stress system.

In the vast majority of cases, fractures contain infillings of various combinations of low-temperature minerals: (1) dark green clay–pyrite is the commonest association and is found throughout the basalt pile, (2) green clay–zeolites with or without minor calcite, (3) zeolites, and (4) calcite–quartz. The green clay was found to be (Fe-rich?) saponite; zeolites are heulandite, minor phillipsite, and stilbite—with the last by far the most abundant (all XRD confirmed). In 462A-99-1 (Piece 1) were some well-crystallized stilbite plates containing small inclusions of two other minerals; one formed acicular, quartz-coated(?) fibers (probably another zeolite) and the other, small dark green spheres of radiating prisms (epidote or pumpellyite?).

In summary, low-temperature alteration in the lower zeolite facies is indicated by the presence of Fe-saponite, celadonite, stilbite, heulandite, and phillipsite, and by the lack of chlorite, higher-grade zeolites, prehnite, and actinolite, all of which typify higher metamorphic grades. The ubiquitous presence of pyrite in veins and basalt matrix, together with the lack of oxidation throughout, suggests alteration took place in a reducing, slightly acid to neutral, environment and was not caused by the downward percolation of oxygenated seawater. Zeolite-calcite veins of later origin indicate a change to slightly more alkaline conditions and higher CO_2 activities.

Summary

1. The volcanic sequence is composed of an alternating series of aphyric and moderately phyric flow basalts containing various proportions of clinopyroxene, plagioclase, and olivine as phenocryst phases. The basalt flows represent the continuation downward of the lower flow unit (type B basalts) found during Leg 61 and are divided into 12 volcanic units.

2. The thicker volcanic units are often aphyric holocrystalline or glassy basalts and in some cases represent a packet of rapidly extruded smaller cooling units. The thinner volcanic units are often quench-textured throughout and represent individual flows.

3. Although glass and olivine characteristically replaced by brownish smectites throughout the basaltic pile, the degree of alteration is generally low. No fresh glass remains, although palagonite is present in a few cases.

4. Alteration took place in the lower zeolite facies under slightly acid to mildly alkaline, low CO_2-activity, reducing conditions.

PALEOMAGNETICS

Routine paleomagnetic sampling and analysis were performed on the Aptian basalt flow complex drilled at Hole 462A (7°15′N; 165°01′E; 14.3° mean dipole inclination, 3° present field inclination), DSDP Leg 89 in order to determine magnetic polarity, magnetic inclinations of flow units, and mean paleolatitude. Steiner (1981) reported in detail on the paleomagnetism and magnetic properties of the overlying continuation of this basalt complex drilled on Leg 61, and therefore no further shore-based studies of magnetic properties were deemed necessary.

Within these 137 m of basalt, 35 minicores were collected with orientation relative to the axis of the drill string (deviation from vertical was 1° at Core 93 and less than 0.5° at Core 104). Several of these samples are from fine-grained phyric basalt near chill margins or flow boundaries, but the majority are of the typical phyric to aphyric granular basalts. The entire basalt complex drilled on Leg 89 is interpreted as a sequence of massive sheet flows with only a few pillow basalt flows.

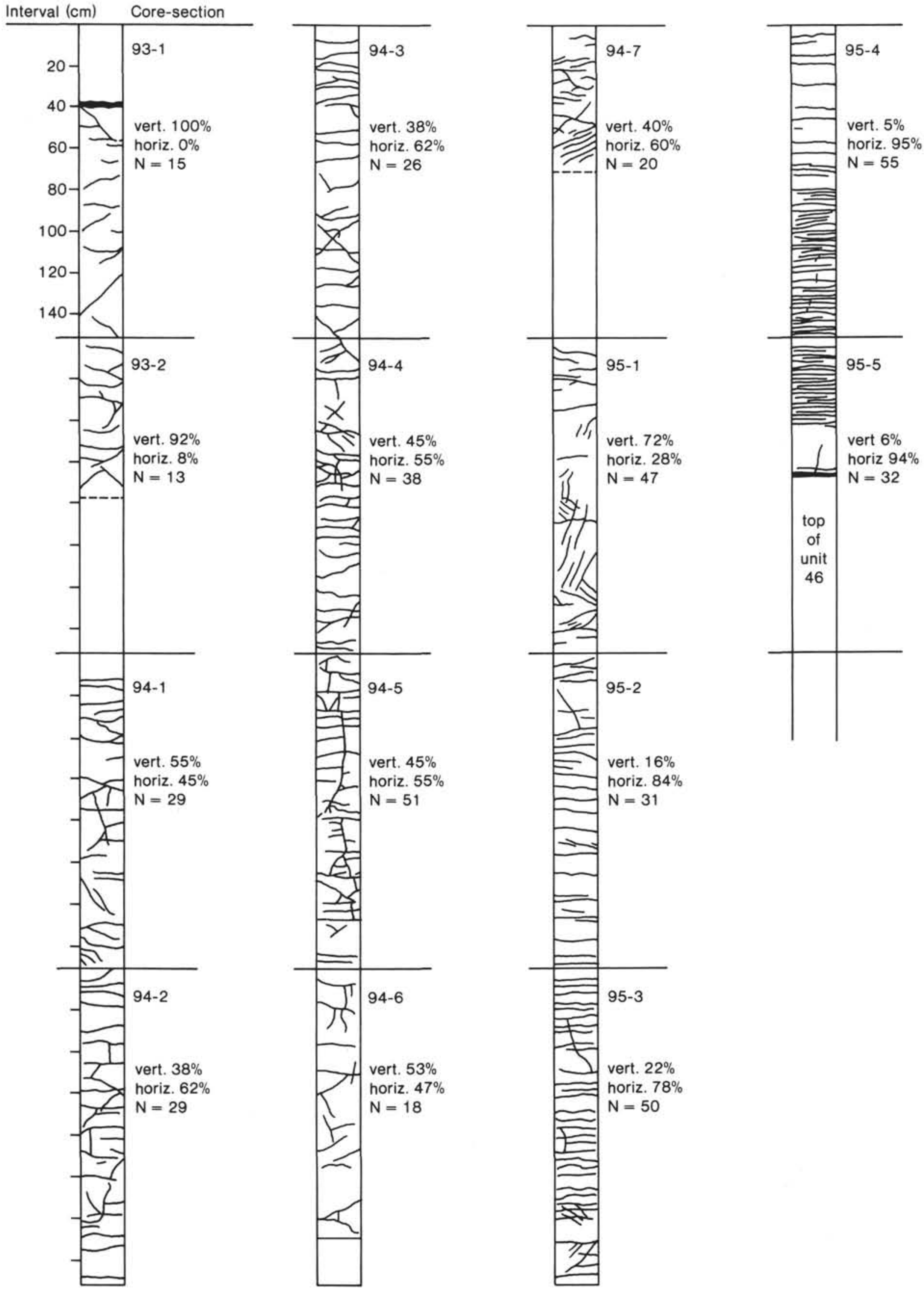

Figure 18. Graphic fracture log of volcanic Unit 45, showing number (N) and percentage of approximately vertical (vert.) and horizontal (horiz.) fractures within different sections.

METHOD

All measurements were preformed on a Digico fluxgate magnetometer on board the *Glomar Challenger*. This instrument is partially shielded and has a 1.5 to 2.0 Gauss magnetic field near the sample insertion opening (lab field = 0.7 Gauss). Therefore extraneous induced magnetic components were a problem at higher demagnetization steps. The internal field changed with each roll and course change of the ship, therefore the background field was not always cancelled by the inverted set of measurements (personal communication, K. Krumsiek, 1981, DSDP Leg 81 Site 552 shipboard report). The Digico also lacked a reliable calibration, and a measurement performed on the 1× range had almost twice the apparent intensity of the same sample if measured using the 10× range. Calibration samples of pink limestone brought from the University of Wyoming proved to be too weak to give a reliable signal/noise intensity value on the Digico. Therefore, the intensity values recorded may be systematically magnified or reduced by some unknown factor (but probably are within 50 to 200% of the actual value). For consistency, all measurements were performed at 1× range, 64 spins, and 4 positions with corrections for sample volume. The directions of magnetization are probably accurate to ±3° (the measured drift of the calibration sample during a measurement), though a systematic bias of up to 5° in declination (but not inclination) is suspected, based on additional measurements made on a cryogenic magnetometer at the University of Wyoming.

Magnetic susceptibility of each minicore cylinder axis was measured on a Bison Model 3101 susceptibility bridge using a correction factor of 4.9/height of sample (determined by Shaul Levi on Leg 70, personal communication, 1979). Susceptibility was measured both before and after the progressive demagnetization of each sample. Anisotropy of susceptibility was analyzed separately by N. Fujii as a special study (this volume).

Progressive alternating fields (AF) demagnetization was performed using a Schoenstedt GSD-1 single-axis demagnetizer. Generally, five to eight steps from 30 to 300 Oe were used on each sample, with the increment spacing dependent on the behavior of the sample.

Magnetic Properties

The intensity and direction magnetization at each demagnetization step, initial and final susceptibilities, and median destructive field of both the total intensity and the intensity of the horizontal component (MDF and MDF_{xy}) for each sample is tabulated in Table 5. The median destructive field of the horizontal component is calculated because of a strong "soft" VRM produced along the Z-axis (downward), as discussed later.

NRM and Drilling-Induced Remanence

The NRM intensities range from 1 to 17 × 10^{-3}emu/cm^3. This range is similar to the NRM intensities of the flow units in the overlying basalt complex, but is less than half of the typical intensities of the sill units in that complex (Steiner, 1981). The NRM inclinations range from 83.5° to −51.6. A steep downward component was removed by AF demagnetization and is interpreted as an artifact of the drilling process. Therefore, the NRM measured in the lab is not the *in situ* NRM of the basalts.

Drilling-produced overprint is frequently observed during coring of basaltic rocks (rarely of sediments), but the process of acquisition has never been adequately explained. Petersen (1979) measured a 5 Gauss field near the drill bit and suggested that the pressure of the drill produced a piezomagnetic effect in the cored material. On Leg 89 there was a field greater than 10 Gauss associated with the drill pipe (the probe meter went off scale), but only a 2 Gauss field in the drill bit assembly and core barrel. Dave van Alstine (personal communication, 1980) observed that drilling-induced magnetic remanence increased with depth and was reduced when using a nonmagnetic core barrel. Steiner (1981) observed a steep upward drilling-induced component of the NRMs of the Site 462 basalts, which is opposite to the downward component observed during the Leg 89 continuation of drilling at the site. In general, fine-grained basalts are less susceptible to acquiring drilling remanence than coarse-grained basalts. These observations suggest that the actual coring process is only partially responsible for producing the overprint, and that the ambient field within the drill string may play an important role. Probably during the previous drilling at Site 462, the drill string had a magnetic field opposite to the direction during this leg.

Susceptibility

The initial magnetic susceptibilities are tightly grouped in a 1.8 to 3.7 × 10^{-3}emu (G/Oe) range. This is more than twice the typical susceptibilities recorded by Steiner (1981) for the overlying basalt complex, but perhaps this only reflects the use of the correction factor (2.3 for a 2.1-cm-high minicore) determined by later shipboard investigators for this particular instrument. In general, fine-grained basalts have less susceptibility and show less overprinting by drilling-induced remanence than coarse-grained basalts (e.g., Ade-Hall and Johnson, 1976; Bleil and Smith, 1980), therefore these provide the more reliable directions of original magnetic remanence. Susceptibility increased by about 10% after AF demagnetization.

Demagnetization Behavior

The bulk of the drilling-induced remanence and present-day overprint was removed by AF demagnetization above 100 OE. Most of the samples displayed negative inclinations after the 150-Oe step. The few exceptions were some coarser-grained samples that developed severe viscosity and therefore did not yield stable measurements, and one sample (462A-100-3, 49 cm), which behaved in a manner opposite that of the other samples and is probably from a block accidentally inverted during removal from the core catcher.

Polarity

The polarity of all samples was normal.

Magnetic Units

The stable inclinations of magnetization are tabulated in Table 6. To qualify as "stable inclination," the mean inclination had to remain constant (±2°) for two or more consecutive measurements at progressively higher AF demagnetization steps above 100 Oe; the stable inclination is the average of this set. Slightly over 60% of the samples satisfied this criterion. Three samples had stable inclination prior to an onset of viscous instability, which was judged to be representative of the "stable inclination," even though the higher demagnetization steps were not acceptable.

Clusters of similar stable inclinations were inferred to represent basalt units, which were erupted over a short interval of time, and hence recorded only a brief span of secular variation. Eight such magnetic units were identi-

Table 5. Paleomagnetic analysis of basalts of Hole 462A.

Sample (core-section, cm level) (description)	AF demag. step (Oe)	Intensity (10^{-6} emu/cm^3)	Declination (°)	Inclination (°)	Comments	Susceptibility and mean destructive field (MDF)
93-1, 64	0 (NRM)	2060	324	−2.8		Init. susc. = 3090×10^{-6}
	20	1960	333	−17.4		Final susc. = 3330×10^{-6}
	40	1810	332	−39.7		MDF = 150 Oe
	60	1600	326	−47.3		MDF_{xy} = 60 Oe
	85	1370	333	−50.1		
	120	1100	330	−51.5		
	160	1020	330	−48.3		
	210	600	336	−44.1		
	280	360	324	−31.5	Viscous	
	360	250	327	−20.9		
93-2, 76	0 (NRM)	3020	291	69.7		Init. susc. = 3130×10^{-6}
	15	2690	301	69.0		Final susc. = 3270×10^{-6}
	30	2180	298	55.2		MDF = 45 Oe
	50	1370	309	40.6		MDF_{xy} = 100 Oe
	75	990	309	18.0		
	100	780	300	2.4		
	130	170	312	−4.3		
	160	146	313	−6.2	Slightly viscous	
	200	120	319	−4.6		
94-3, 39	0 (NRM)	5810	140	60.6		Init. susc. = 3340×10^{-6}
	40	2400	110	48.1		Final susc. = 3440×10^{-6}
	70	870	97	24.6		MDF = 30 Oe
	100	330	83	0.3		MDF_{xy} = 30 Oe
	140	170	42	−16.6	Viscous	
	170	140	10	−22.3		
94-6, 140	0 (NRM)	5250	108	80.4		Init. Susc. = 2935×10^{-6}
	40	2670	95	76.4		Final susc. = 3070×10^{-6}
	100	520	50	70.3		MDF/MDF_{xy} = 40 Oe
	150	240	334	56.0	Viscous	
	220	190	335	21.9		
95-1, 84	0 (NRM)	4320	259	59.1		Init. susc. = 3220×10^{-6}
	30	2830	266	41.9		Final susc. = 3250×10^{-6}
	80	1530	282	−5.8		MDF = 50 Oe
	110	1660	282	−45.8		MDF_{xy} = 110 Oe
	140	1310	290	−51.2		
	170	1000	287	−50.8		
	210	650	292	−49.2		
	250	390	297	−48.1		
	300	280	303	−40.5	Slightly viscous	
95-5, 56	0 (NRM)	4100	51	18.2		Init. susc. = 2096×10^{-6}
(20 cm above chill	20	3190	54	9.3		Final susc. = 2310×10^{-6}
margin)	40	2260	55	−19.3		MDF = 120 Oe
	60	3050	56	−37.0		MDF_{xy} = 55 Oe
	80	3490	53	−43.9		
	110	2870	52	−51.9		
	160	770	44	−53.6		
	200	500	42	−55.8		
	250	290	41	−52.2		
	300	160	25	−56.1		
	360	110	24	−49.8		
	2 days later	95	1	−37.8		
95-1, 86	0 (NRM)	10850	238	−51.6		Init. susc. = 2220×10^{-6}
(just below chill	10	10860	237	−50.0		Final susc. = 2790×10^{-6}
margin)	25	10800	240	−51.7		MDF = 80 Oe
	50	10090	240	−52.4		MDF_{xy} = 100 Oe
	75	8160	240	−53.6		
	100	3100	241	−49.9		
	150	2390	240	−49.8		
	200	1700	243	−50.2		
	250	1060	249	−47.9		
	300	400	243	−50.9		
	350	370	253	−57.6		
	2 days later	160	250	−56.6		
95-7, 28	0 (NRM)	3730	248	69.2		Init. susc. = 2646×10^{-6}
	40	1920	286	55.1		Final susc. = 2800×10^{-6}
	80	1180	311	12.2		MDF = 40 Oe
	130	940	312	−15.8		MDF_{xy} = 100 Oe
	160	600	311	−20.4		
	200	260	328	−23.2	Slightly viscous	
	250	140	332	−18.2		
96-1, 57	0 (NRM)	5500	309	58.1		Init. susc. = 2770×10^{-6}
	50	3720	325	-33.1		Final susc. = 2854×10^{-6}
	80	3455	325	−47.0		MDF = 130 Oe
	110	3200	332	−50.8		MDF_{xy} = 120 Oe
	150	2060	340	−49.5		
	200	1370	338	−50.3		
	250	990	342	−45.2	Slightly viscous	
	300	670	342	−40.0		
96-4, 14	0 (NRM)	5530	255	79.3		Init. susc. = 3095×10^{-6}
	50	2160	241	69.5		Final susc. = 3141×10^{-6}
	100	675	273	58.9		MDF = 40 Oe
	150	285	301	31.7		MDF_{xy} = 80 Oe
	200	205	319	5.2	Viscous	
97-1, 101	0 (NRM)	1040	232	51.0		Init. susc. = 1865×10^{-6}
	20	910	236	48.9		Final susc. = 2075×10^{-6}

Table 5 (continued).

Sample (core-section, cm level) (description)	AF demag. step (Oe)	Intensity (10^{-6} emu/cm^3)	Declination (°)	Inclination (°)	Comments	Susceptibility and mean destructive field (MDF)
97-1, 101	50	430	248	31.2		MDF = 45 Oe
	100	220	262	2.5		MDF_{xy} = 55 Oe
	150	130	281	−4.0		
	200	90	293	−12.2		
	250	84	305	−11.6	Viscous	
	300	59	308	−4.6		
97-3, 99	0 (NRM)	4230	155	45.4		Init. susc. = 3000 × 10^{-6}
	30	3050	155	26.2		Final susc. = 3280 × 10^{-6}
	70	1520	159	−18.0		MDF = 50 Oe
	100	1060	160	−31.3		MDF_{xy} = 65 Oe
	140	590	159	−41.4		
	180	350	158	−43.5		
	230	150	152	−57.9		
	280	70	145	−74.4	Viscous	
98-1, 79	0 (NRM)	6490	124	72.4		Init. susc. = 2675 × 10^{-6}
	50	2480	120	56.0		Final susc. = 2710 × 10^{-6}
	100	490	92	25.9		MDF = 40 Oe
	130	215	61	−1.6	Viscous	MDF_{xy} = 50 Oe
	160	170	21	−24.0		
98-5, 74	0 (NRM)	6500	201	65.3		Init. susc. = 2740 × 10^{-6}
	30	3660	207	54.1		Final susc. = 2800 × 10^{-6}
	70	1110	219	13.9		MDF = 35 Oe
	100	640	228	−12.4		MDF_{xy} = 60 Oe
	140	365	250	−25.3		
	180	270	265	−27.0	Slightly viscous	
	220	300	270	−27.8	Viscous	
99-1, 51	0 (NRM)	4460	73	79.2		Init. susc. = 3105 × 10^{-6}
	40	1910	64	57.2		Final susc. = 3465 × 10^{-6}
	80	770	57	18.8		MDF = 35 Oe
	120	330	44	−15.2		MDF_{xy} = 100 Oe
	150	260	39	−22.6		
	180	170	28	−30.2	Slightly viscous	
	220	135	15	−23.7	Viscous	
	260	115	350	−18.0		
99-2, 2	0 (NRM)	13200	204	−51.7		Init. susc. = 2100 × 10^{-6}
(near chill margin?)	520	60	235	−49.5		Final susc. = 2530 × 10^{-6}
(fine-grained)	2 days later	30	264	−48.5		
100-1, 136	0 (NRM)	3580	198	23.4		Init. susc. = 2780 × 10^{-6}
	20	3240	199	9.7		Final susc. = 3170 × 10^{-6}
	40	2600	202	−6.0		MDF = 90 Oe
	70	2020	204	−18.8		MDF_{xy} = 100 Oe
	100	1650	203	−20.3		
	140	1270	205	−23.0		
	180	990	205	−23.0		
	220	690	204	−23.7		
	270	415	212	−25.3		
	330	260	215	−23.8		
100-3, 49	0 (NRM)	1540	236	−54.8	This block from	Init. susc. = 3060 × 10^{-6}
	20	1200	250	−45.5	core-catcher	Final susc. = 3400 × 10^{-6}
	50	500	268	−9.2	seems to be	MDF = 40 Oe
	100	360	274	16.7	inverted	MDF_{xy} = 50 Oe
	150	290	278	21.8		
	200	200	286	23.9		
	270	135	288	21.6		
	350	90	302	13.6		
101-1, 91	0 (NRM)	6746	245	82.1		Init. susc. = 2593 × 10^{-6}
(coarse-grained)	40	3140	285	79.9		Final susc. = 2859 × 10^{-6}
	100	450	315	44.7		MDF = 40 Oe
	150	228	320	5.5		MDF_{xy} = 50 Oe
	200	154	328	−7.5		
	250	107	323	−13.6	Viscous	
	300	97	328	−8.8		
101-4, 69	0 (NRM)	7400	160	83.5		Init. susc. = 3443 × 10^{-6}
(coarse-grained)	60	1650	352	81.9		Final susc. = 3580 × 10^{-6}
	120	423	347	40.6		MDF = 30 Oe
	180	241	335	6.1		MDF_{xy} = 40 Oe
	240	241	341	7.9	Viscous	
	300	210	337	7.9		
102-2, 73	0 (NRM)	5700	213	69.2		Init. susc. = 3280 × 10^{-6}
	70	1260	221	72.0		Final susc. = 3300 × 10^{-6}
	130	276	297	60.7		MDF = 30 Oe
	200	221	333	20.1	Viscous	MDF_{xy} = 30 Oe
102-4, 89	0 (NRM)	6510	47	−4.7		Init. susc. = 2486 × 10^{-6}
(fine-grained top of flow unit)	20	6450	47	−3.6		Final susc. = 2659 × 10^{-6}
	50	6460	51	−4.1		MDF = 190 Oe
	80	6178	52	−6.8		MDF_{xy} = 170 Oe
	120	5280	47	−13.1		
	170	3710	47	−17.5		
	220	2558	49	−19.2		
	280	1650	45	−20.8		
	350	965	45	−19.7		
	400	620	45	−23.0		
102-4, 124	0 (NRM)	5965	346	−5.1		Init. susc. = 2673 × 10^{-6}
(fine-grained)	50	5570	340	−10.8		Final susc. = 2964 × 10^{-6}

Table 5 (continued).

Sample (core-section, cm level) (description)	AF demag. step (Oe)	Intensity (10^{-6} emu/cm^3)	Declination (°)	Inclination (°)	Comments	Susceptibility and mean destructive field (MDF)
102-4, 124	150	2637	345	−18.4		MDF = 140 Oe
(fine-grained)	220	1282	350	−17.7		MDF_{xy} = 130 Oe
	280	585	347	−19.7		
	360	242	364	−18.2		
102-5, 16	0 (NRM)	4250	73	17.9		Init. sucs. = 3085 × 10^{-6}
(fine-grained)	100	2280	67	−14.5		Final susc. = 3393 × 10^{-6}
	180	950	67	−21.4		MDF = 110 Oe
	200	745	68	−22.0		MDF_{xy} = 110 Oe
	250	385	63	−25.2		
	300	225	63	−25.5		
	350	139	54	−22.4		
103-1, 107	0 (NRM)	5350	134	29.0		Init. susc. = 2595 × 10^{-6}
(fine-grained with	60	3250	121	5.7		Final susc. = 3004 × 10^{-6}
augite clusters)	120	1617	114	−16.1		MDF = 80 Oe
	170	860	108	−24.4		MDF_{xy} = 85 Oe
	220	428	111	−28.3		
	270	237	110	−28.3		
	320	126	100	−32.6	Slightly viscous	
104-1, 106	0 (NRM)	3335	53	−11.9		Init. susc. = 2399 × 10^{-6}
	30	3409	46	−13.6		Final susc. = 2770 × 10^{-6}
	80	3150	47	−20.7		MDF = 160 Oe
	130	2082	48	−24.1		MDF_{xy} = 140 Oe
	180	1285	50	−26.0		
	230	720	47	−27.6		
	280	419	47	−25.7		
	330	244	47	−25.0		
105-1, 15	0 (NRM)	6917	53	2.4		Init. susc. = 2764 × 10^{-6}
	40	6730	51	−10.5		Final susc. = 3304 × 10^{-6}
	80	5124	47	−19.9		MDF = 120 Oe
	130	2982	47	−24.9		MDF_{xy} = 110 Oe
	190	1500	43	−33.0		
	250	684	45	−28.0		
	330	299	46	−26.5		
105-3, 47	0 (NRM)	17000	174	70.6		Init. susc. = 3664 × 10^{-6}
(coarse-grained)	40	6610	160	68.1		Final susc. = 3774 × 10^{-6}
	80	2113	168	67.4		MDF = 30 Oe
	140	405	130	74.8	Viscous	MDF_{xy} = 30 Oe
	200	128	8	54.4		
106-1,55	0 (NRM)	8900	169	62.7		Init. susc. = 3753 × 10^{-6}
(coarse-grained)	60	2500	173	50.8		Final susc. = 3888 × 10^{-6}
	120	499	180	46.0		MDF/MDF_{xy} = 40 Oe
	200	78	230	69.5	Viscous	
106-2, 123	0 (NRM)	7810	200	78.0		Init. susc. = 3031 × 10^{-6}
(coarse-grained)	100	430	311	60.0		Final susc. = 3179 × 10^{-6}
	130	185	316	47.5		MDF = 40 Oe(?)
	150	133	324	31.4		MDF_{xy} = 45 Oe(?)
	180	99	322	12.2		
	210	80	325	3.2	Viscous	
108-1, 77	0 (NRM)	7760	125	83.0		Init. susc. = 3484 × 10^{-6}
(granular)	40	3165	161	81.0		Final susc. = 3611 × 10^{-6}
	90	720	38	83.6		MDF = 40 Oe
	140	297	343	52.2	Viscous	
108-2, 141	0 (NRM)	5030	289	63.6		Init. susc. = 3640 × 10^{-6}
(medium-grained)	50	2728	300	47.0		Final susc. = 3894 × 10^{-6}
	100	1126	310	13.1		MDF = 55 Oe
	150	525	320	−2.7		MDF_{xy} = 90 Oe
	200	301	318	−9.7		
	250	182	316	−9.4		
	300	150	320	−7.4	Slightly viscous	
108-3, 42	0 (NRM)	4560	168	24.2		Init. susc. = 2910 × 10^{-6}
	300	235	165	−12.6		Final susc. = 3358 × 10^{-6}
	350	130	168	−11.0		MDF — not determined
	400	72	164	−12.6	Slightly viscous	
109-1, 93	0 (NRM)	4380	351	59.7		Init. susc. = 2948 × 10^{-6}
(fine-grained)	40	2995	350	40.8		Final susc. = 3260 × 10^{-6}
	80	1970	349	10.4		MDF = 70 Oe
	120	1475	355	−0.9		MDF_{xy} = 90 Oe
	160	1060	346	−6.5		
	200	670	349	−8.8		
	250	410	347	−9.7		
	300	258	344	−9.6		
	350	154	340	−6.8	Slightly viscous	
109-2, 86	0 (NRM)	8945	121	74.0		Init. susc. = 3334 × 10^{-6}
(medium-grained)	50	3230	103	65.0		Final susc. = 3499 × 10^{-6}
	100	972	84	47.5		MDF = 40 Oe
	140	476	70	28.0		MDF_{xy} = 50 Oe
	180	284	57	18.0	Viscous	
	230	244	45	3.6		

Note: All intensities of samples in Cores 93 to 100 must be multiplied by 1.33 to be consistent with the calibration factor used in Cores 101 to 109. MDF_{xy} = mean destructive field for horizontal component of magnetization.

Table 6. Stable inclinations, Hole 462A, basalt flows.

Sample (core-section, cm level)	AF demag. steps (Oe)	Stable inclination	Magnetic Unit [mean inclination (± error)]	Corresponding igneous unit
93-1, 64	85, 120, 160	−50.0	1	
95-1, 84	140, 170, 210	−50.4	[−51.2 (±1.5)]	Unit 45 and uppermost
95-5, 56	110, 160, 200, 250	−53.4		46 (baked margin?)
95-5, 86	75, 100, 150, 200	−51.1		
95-7, 28	160, 200	−21.3	2—probably multiple units	Upper part of Unit 46
96-1, 57	110, 150, 200	−50.2	[−38 (±15)]	
97-3, 99	140, 180	−42.4		
98-1, 79	160	−24.0	3	
98-5, 74	140, 180, 200	−27.2	[−25.6 (±1.6)]	Lower part of Unit 46
99-1, 51	150, 180, 220	−25.5		
			4	
99-2, 2	NRM, 520	−50.7	[−50.7]	Unit 47
100-1, 136	140, 180, 220	−23.2	5	
100-3, 49	150, 200, 270	−22.4	[−22.8 (±0.4)]	Unit 48
102-4, 89	226, 280, 350	−19.9	6	
102-4,124	220, 280, 360	−18.5	[−20.8 (±2.5)]	Unit 49
102-5, 16	200, 250, 300	−23.8		
103-1, 107	220, 270	−28.3	7	
104-1, 106	180, 230, 280, 330	−26.1	[−27.9 (±1.5)]	Units 50 and 51 and top of 52
105-1, 15	190, 250, 350	−29.2		
108-2, 141	200	−9.7	8	
108-3, 42	300	−12.6	[−10.7 (±1.5);	Unit 54
109-1, 93	250, 300	−9.7	may still have overprinting]	

fied. These were found to correlate well within the igneous units identified by petrographic characteristics. The only exceptions are the three samples from the lowest part of Cores 95 to 97, which display no grouping, yet all fall within the upper half of igneous Unit 46. One explanation is that igneous Unit 46 consists of multiple eruptive and cooling events. Magnetic Units 5 and 6 have similar mean inclinations but show different behavior during demagnetization, and therefore were separated. In two cases, the magnetic unit extended into the uppermost centimeters of the underlying igneous flow unit, indicating a thermal resetting of the magnetism of this contact zone.

Paleolatitude

The magnetic units are too few in number to have sampled the secular variation adequately or to provide sufficient statistics for a precise determination of the mean paleolatitude. With this caution in mind, mean inclination statistics (Kono, 1980) were applied to the data. Each magnetic unit was considered to be a single value with the exception of magnetic Unit 2, for which each sample was taken separately, and of Unit 8, which was judged to have inadequate removal of overprinting and thus was omitted. The resulting mean inclination is −35.9° (N = 9, k = 18, 95% confidence circle [standard deviation] = 6.9°, 95% confidence circle [alpha-95] = 11.9°). The mean paleolatitude is 19.9°S (standard deviation = 4.7°, alpha-95 = 8°).

The mean paleolatitude of the overlying basalt flows (igneous Units 22, 23, 26, 29, and 34 of extrusive basalt of the thick basalt flow-sill complex) is 20.6°S (2.4° alpha-95). This paleolatitude was recomputed from Steiner (1981) using the statistical method of Kono (1980). Data from igneous Unit 30 were omitted, because this unit was interpreted as containing sills intruded into the flows; therefore it may have undergone multiple thermal remagnetization events and may represent a different time of magnetization than the other flows. The two nearly identical mean paleolatitudes imply that northward movement of the site was insignificant (within the error limits) during the emplacement of the basalt flows within the basalt flow-sill complex.

Summary

The basalt flow series drilled during the continuation of Site 462 has a minimum of eight magnetic units (episodes of flow emplacement). The polarity of these is normal and the mean paleolatitude is 19.9°S (alpha-95 = 8°), similar to the results obtained by Steiner (1981) from the overlying basalt complex.

PHYSICAL PROPERTIES

METHODS

Sliced chips from minicores were measured for wet bulk density, water content, and porosity by the gravimetric seawater displacement method. Compressional wave velocity and 2-min. GRAPE wet bulk density measurements were preformed for minicores, using methods described in Boyce (1976). The same minicores were also measured for magnetic susceptibility using Bison Model 3101 susceptibility bridge. For both sound velocity and magnetic susceptibility, the measurements in three mutually perpendicular directions, including one vertical (subscript V) and one along the minicore axis (subscript Hl), were performed. Anisotropy of compressional wave velocity A(V) is defined $A(V) = 3(V_{H1} + V_{H2} - 2V_V)/2(V_{H1} + V_{H2} + V_V)$. Apparent anisotropy of magnetic susceptibility (χ) is tentatively defined as $A(\chi) = 2(\chi_{H2} - \chi_V)/\chi_{H2} + \chi_V)$, for minimizing the effect of shape on susceptibility. Because of the scarcity of sediments recovered, no physical property measurement was made on sediments.

Results

All measured values of sound velocity, wet bulk density, water content, porosity, and magnetic susceptibility are listed in Table 7, and their variations with depth are shown in Figure 19. Values of compressional wave velocity in the vertical direction range from about 5.0 to 6.2 km/s, which are comparable to those of Layer 2, and the mean value is 5.87 km/s whereas the averaged value for three orientations is 5.86 km/s. No apparent change of physical properties is found throughout the layers of basaltic sills and flows beginning from the sub-bottom depth of 560 m drilled during Leg 61 (Larson, Schlanger, et al., 1981). No apparent correlation with petrologic units is observed, although the chilled margins were not sampled. Because the thicker sediment layers are at most several meters below 560 m sub-bottom depth, as revealed by the recovered cores in Legs 61 and 89, the layers of basaltic sills and flows could be recognized as part of Layer 2 from the seismic point of view.

Variations of magnetic susceptibility are within a factor of approximately two with a mean value of 3.13×10^{-3} (cm g s). The basaltic flows are magnetically homogeneous (i.e., magnetic mineral compositions are very uniform when compared with the results of Legs 51 to 53 in the Atlantic [Levi et al., 1980]).

Anisotropies of compressional wave velocity and magnetic susceptibility range from −4.3 to 5.5% (−0.2 in average) and from −16 to 10% (0.5% in average) from on board measurements, respectively, and are discussed in more detail by Fujii and Hamano (this volume).

LOGGING AND DOWNHOLE MEASUREMENTS

Introduction

The temperature structure at Hole 462A is of particular interest from three points of view: (1) The heat flow variation in the older part of the oceanic crust is still poorly understood. (2) Also, it is not known whether the heat flow values become constant with ages older than 80 Ma) or decrease as a "root-t" trend. Hole 462A had remained undisturbed for 4.25 yr. after the Leg 61 drilling, and presumably the hole was completely at thermal equilibrium. (3) Lastly, there was some uncertainty in the interpretation of logs obtained in 1978. During Leg 61, the Tokyo T-probe was used and two Gearhart-Owen temperature logs were obtained from Hole 462, which is about 460 m south-southwest from Hole 462A (Larson, Schlanger, et al., 1981). The equilibrium temperature distribution, extrapolated from the two Gearhart-Owen T-logs, showed some discrepancy with that obtained by the Tokyo T-probe, as seen in Figure 20 (Boyce, 1981).

Lowering a temperature logging sonde to obtain downhole temperature measurements was therefore the first operation we undertook after reentering Hole 462A. The Schlumberger High-Resolution Thermometer (HRT) was calibrated by a standard mercury thermometer at 0.8

Table 7. Physical properties of basalts, Hole 462A.

Sample (core-section, interval in cm)	Sub-bottom depth (m)	Compressional velocity[a] (km/s) V_V	V_{H1}	V_{H2}	A(V)[b] (%)	Wet bulk density (g/cm)³ GRAPE	Gravimetric	Wet water content (%)	Porosity (%)	Impedance[c] (10^5 g/cm²s)	Magnetic susceptibility[d] χ (10^{-3} cmgs)	$A(\chi)$ (%)	Remarks
93-1, 63–65	1071.7–1076.6	5.87	5.88	6.01	1.3	2.82	2.87	1.90	5.5	16.7	3.32	5.8	Unit 45
93-2, 75–77		6.16	6.10	5.99	−1.9	2.77	2.96	0.83	2.5	17.7	3.30	−0.1	Unit 45
94-3, 38–40	1076.6–1085.7	5.81	5.99	5.85	1.9	2.76	2.93	1.81	5.3	16.5	3.44	5.4	Unit 45
94-6, 139–141		6.08	6.21	6.07	1.0	2.88	2.95	1.19	3.5	17.7	3.01	2.3	Unit 45
95-1, 83–85	1085.7–1094.9	6.02	6.11	6.07	1.2	2.85	2.98	1.50	4.5	17.6	3.09	5.9	Unit 45
95-7, 27–29		5.96	6.03	5.95	0.5	2.75	3.01	2.59	7.8	17.2	2.68	1.1	Unit 46
96-1, 56–58	1094.9–1104.0	6.08	6.08	6.11	0.3	2.85	2.92	1.49	4.4	17.5	2.79	−14.5	Unit 46
96-4, 13–15		5.84	6.02	5.73	0.6	2.84	2.89	2.01	5.8	16.7	3.12	4.9	Unit 46
97-1, 100-102	1104.0–1113.2	4.95	5.41	5.05	5.5	2.70	2.82	3.72	10.5	13.7	1.98	2.6	Unit 46
97-3, 98–100		5.36	5.50	5.35	1.2	2.75	2.83	3.68	10.4	15.0	3.27	0.6	Unit 46
98-1, 78–80	1113.2–1122.3	6.11	6.12	6.27	1.4	2.84	2.92	1.04	3.0	17.6	2.67	−3.4	Unit 46
98-5, 73–75		6.09	6.25	6.10	1.4	2.80	2.98	1.47	4.4	17.6	2.78	2.6	Unit 46
99-1, 50–52	1122.3–1131.5	5.65	5.50	5.64	−1.4	2.81	2.91	1.96	5.7	16.2	3.29	2.2	Unit 46
100-1, 135–157	1131.5–1134.5	5.71	5.44	5.73	−2.2	2.76	2.90	2.90	8.4	16.2	3.18	2.3	Unit 48
100-3, 48–50		5.62	5.66	5.61	0.3	2.77	2.87	1.93	5.6	15.9	3.46	1.5	Unit 48
101-1, 90–92	1134.5–1142.9	5.56	5.63	5.57	0.7	2.79	2.89	2.50	7.2	15.8	2.66	1.1	Unit 48
101-4, 68–70		6.07	5.98	6.04	−1.0	2.82	2.79	2.40	6.7	17.0	3.57	−1.4	Unit 48
102-2, 72–74	1142.9–1152.0	6.10	5.88	6.04	−2.3	2.81	2.89	1.34	3.9	17.4	3.33	−16.2	Unit 48
103-1, 106–108	1152.0–1161.2	5.88	5.75	5.84	−1.5	2.77	2.83	2.61	7.4	16.5	2.67	5.5	Unit 50
104-1, 105–107	1161.2–1170.3	5.65	5.55	5.64	−1.0	2.76	2.81	1.91	5.4	15.7	2.51	5.9	Unit 51
105-1, 14–16	1170.3–1174.3	5.83	5.69	5.74	−2.0	2.74	2.86	2.13	6.1	16.3	2.91	9.7	Unit 52
105-3, 46–48		6.09	5.67	6.00	−4.3	2.96	2.86	0.93	2.7	17.7	4.09	−5.9	Unit 52
106-1, 54–56	1174.3–1180.4	6.02	5.82	5.99	−1.9	2.80	2.73	2.52	6.9	16.7	3.91	4.7	Unit 52
106-2, 122–124		6.06	5.91	6.00	−1.8	2.81	2.97	1.04	3.1	17.5	3.21	−0.9	Unit 52
108-1, 76–78	1189.5–1198.7	6.12	6.00	6.12	−1.0	2.78	2.90	1.06	3.1	17.4	3.72	−8.4	Unit 52
109-2, 85–87	1198.7–1209.0	5.99	5.93	5.98	−0.6	2.70	2.80	1.72	4.8	16.5	3.53	−0.4	Unit 55

[a] Orientations are V: vertical, H1: horizontal along minicore axis, and H2: horizontal.
[b] $A(V) = 3(V_{H1} + V_{H2} - 2V_V)/2(V_{H1} + V_{H2} + V_V)$.
[c] Impedance is calculated by $V_V \times$ (mean of wet bulk densities).
[d] χ = initial susceptibility averaged for magnetic field along minicore axis (H1). $A(\chi) = 2(\chi_{H2} - \chi_V)/(\chi_{H2} + \chi_V)$. For Cores 93 to 100, values are after AF demagnetization.

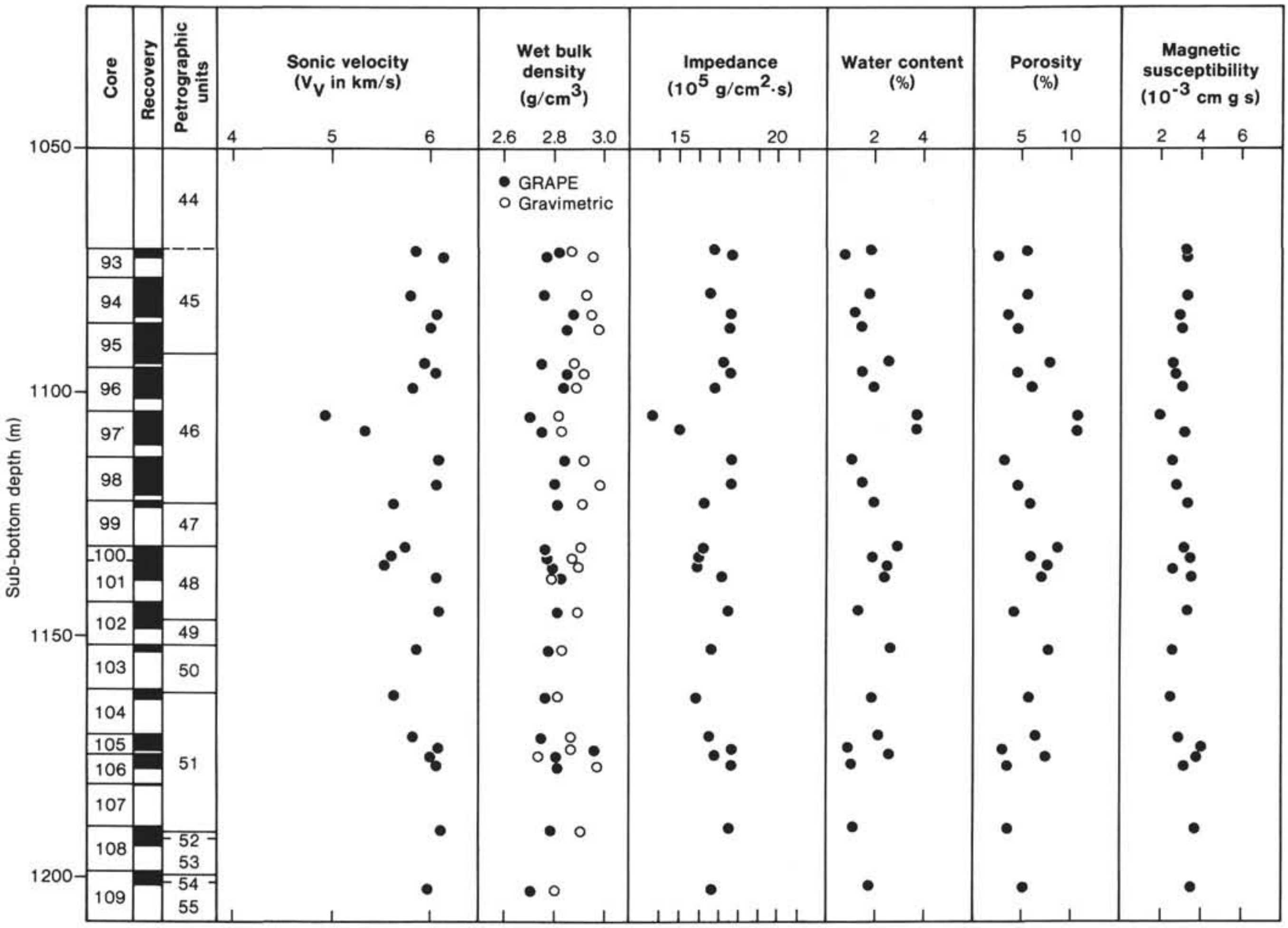

Figure 19. Physical properties of basalts, Hole 462A, Leg 89.

and 26.5°C before and after the logging run, which began at 0300 hr. and ended at 0700 hr., 7 November 1982.

Results

As shown in Figure 20, the temperature rises very slowly to the sub-bottom depth of 395 m but next it rises abruptly with a very steep gradient to the depth of 520 m where the tool was obstructed by sediments bridging across the hole. A maximum temperature of 24.6°C was obtained. A part of the actual record is shown in Figure 21. After the tool reached the bridge and was pulled up, the reality of the measured temperature distribution was confirmed by a similar record obtained during the retrieval of the tool (dashed curve in Fig. 20). The depths of steep temperature rise between 400 and 470 m coincide with the narrowing of the hole diameter, and the chert-rich limestone layer.

Estimation of Downhole Flow Rate

The model of downhole flow of bottom water through the hole is preferred in the Nauru Basin Hole 462A because (1) the bottom-hole temperatures measured by the Tokyo T-probe indicate a normal temperature gradient of 0.045°C/m in the upper 220 m, and (2) the second Gearhart-Owen temperature log showed a slight increase, which is probably due to the relatively less disturbed temperature distribution around the hole. By using a constant flow-rate model (Becker et al., 1983; Fujii, this volume), a volumetric downflow rate of approximately 1700 l/hr. can be calculated by the matching of the temperature distribution to the depth of 395 m. In this model, the (volumetric) flow rate through the hole and the temperature gradient of the undisturbed region are assumed constant. The former condition implies that the layer of the steep temperature rise (400–520 m depth) is permeable and dominated by lateral outward flow. Below this depth no effective downhole flow through the hole can be expected because slumped sediments had blocked the hole. Below that bridge, presumably the temperature had equilibrated with that of the undisturbed distribution; unfortunately, we could not measure that temperature distribution. To maintain the downflow for at least 4.25 yr., underpressure in the sediments is also required. Although the possibility of underpressure in basaltic basement near a ridge flank has been pointed out by Anderson and Zoback (1982), Site 462 is not near a ridge. The distance from Hole 462A to the nearest seamounts is about 200 km.

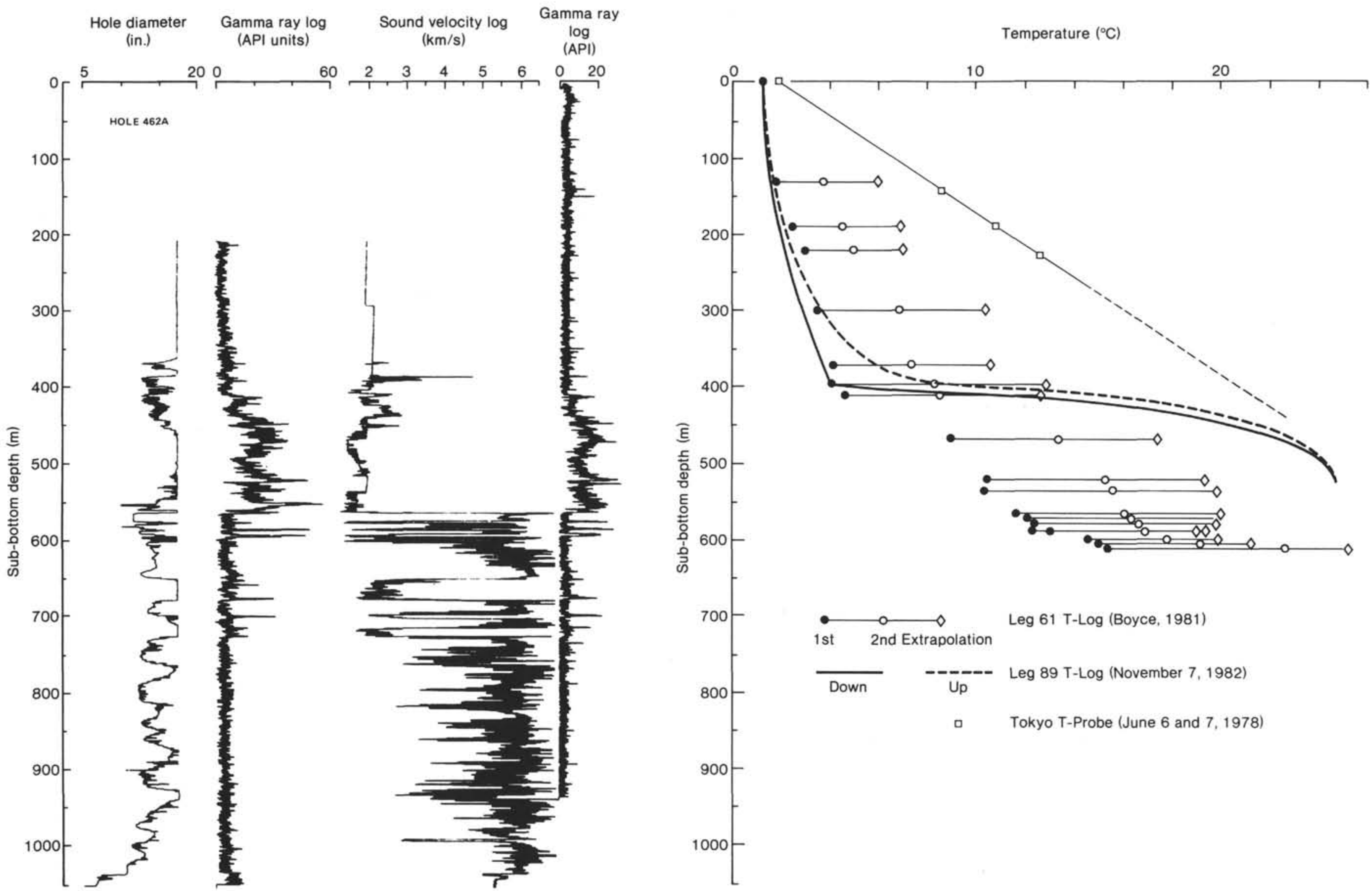

Figure 20. Results of the temperature logs (solid and dashed curves). Other symbols are from Leg 61 (Boyce, 1981). On the left-hand side, records of other logs are shown (from Larson, Schlanger, et al., 1981).

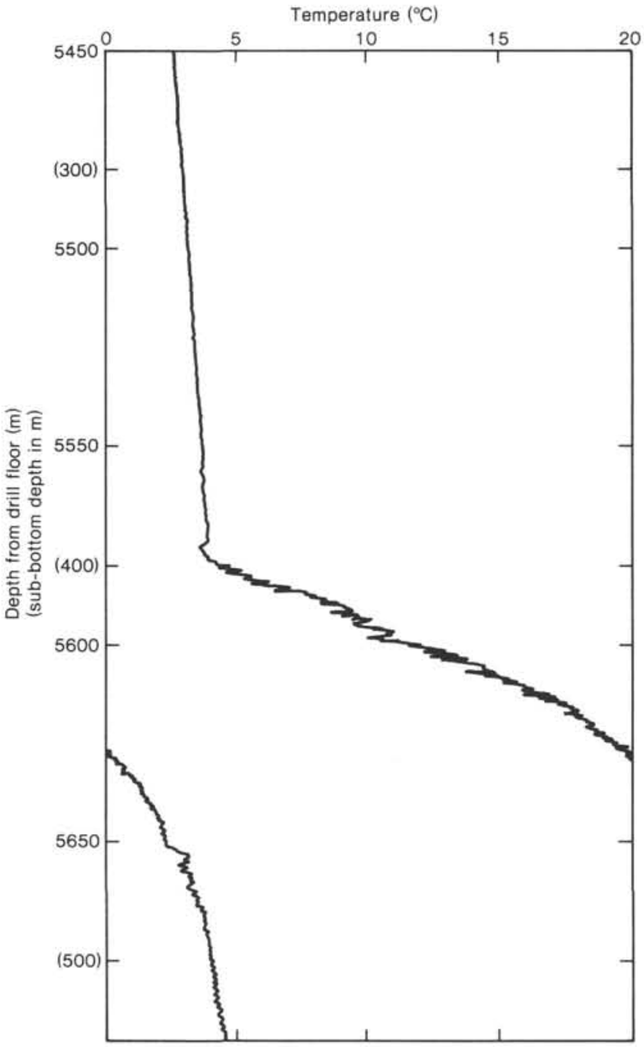

Figure 21. A part of the temperature logs at Site 462, Leg 89.

Implications

As noted by Becker et al. (1983), the downhole flow is not a direct consequence of hydrothermal, natural convection, but is a forced convection driven by the pore-fluid underpressure. The striking similarities of the magnitude of flow rate and required aquifer depth are obvious between Holes 395A and 462A. The plate tectonic situation, however, is considerably different. Among the previously suggested DSDP holes with downhole flow of bottom water (Holes 335, 395A, 396, 454A, 504B, and 462A), all, with the exception of 462A, are expected to have the presence of hydrothermal circulation within the basaltic basement. Instead, around Hole 462A in the Nauru Basin, no such hydrothermal circulation within the basement or in the sedimentary cover has been expected so far.

If such a downhole flow through the holes drilled were a common phenomenon in the oceanic sediments, the requirement of the presence of underpressure in the deep-sea sediments puts forth a fundamental problem in the development of the seafloor.

SEISMIC STRATIGRAPHY

There is no seismic stratigraphy report for this hole.

SUMMARY AND CONCLUSIONS

Drilling at Hole 462A, which was terminated on 27 July 1978 because of time limitations on Leg 61, had bottomed at a TD of 1068.5 m in basalt sheet flows. Within the sill and flow complex that occupied the interval between 563 and 1068.5 m, several intercalations of sediment had been cored. The age of the deepest of these sediment layers recovered in Core 462A-80 was interpreted, on the basis of the radiolarians, as being Barremian. The sediment is a red brown siltstone containing, besides radiolarians, fish debris and agglutinated benthic foraminifers representative of faunas from bathyal to abyssal depths. The Nauru Basin was then thought to have been perhaps 5 km deep during the Barremian. The presence of this Barremian sediment was taken as indicating that the sill-flow complex was not the basement, if we take basement to mean the lithospheric plate generated at a ridge crest approximately 150 Ma—the age predicted for the plate below the Nauru Basin, based on the position of Site 462 on the older boundary of Anomaly M-26.

Hole 462A was reoccupied on 5 November 1982. After 11 days at the site the hole had been deepened to 1209 m with 17 cores taken; the deepening amounted to 140.5 m (Fig. 22).

The volcanic sequence cored in this 140.5 m interval is composed of an alternating series of aphyric and moderately phyric flow basalts containing various proportions of clinopyroxene, plagioclase, and olivine as phenocryst phases. The basalt flows represent the continuation downward of the lower flows (type B basalts) found during Leg 61, the lowest of which was designated as Unit 44, and are divided into 12 volcanic units, 45 through 56. The thicker volcanic units commonly are aphyric holocrystalline or glassy basalts and in some cases represent a packet of rapidly extruded smaller cooling units. The thinner volcanic units are often quench-textured throughout and represent individual flows. Except for a questionable occurrence of pillow structures in Unit 51 (Core 462A-104), all of the units are apparently sheet flows.

Although glass and olivine are characteristically replaced by brownish smectites throughout the basaltic pile, the degree of alteration is generally low. No fresh glass remains, although palagonite is present in a few cases. Alteration took place in the lower zeolite facies under slightly acid to mildly alkaline, low CO_2-activity, reducing conditions.

In Section 462A-99-1, a few centimeters of zeolitic hyaloclastic sediment was recovered in contact with a chilled, glassy margin of a basalt flow. Radiolarians from this sediment include *Holocryptocapsa hindei*, which has a range from uppermost Jurassic to lowermost Aptian.

Shipboard revision of radiolarian-based age determinations of Cores 462A-46 and -80 is significant but needs further work. Core 462A-46 was thought to be Aptian-Barremian. It is now thought (see section on Biostratig-

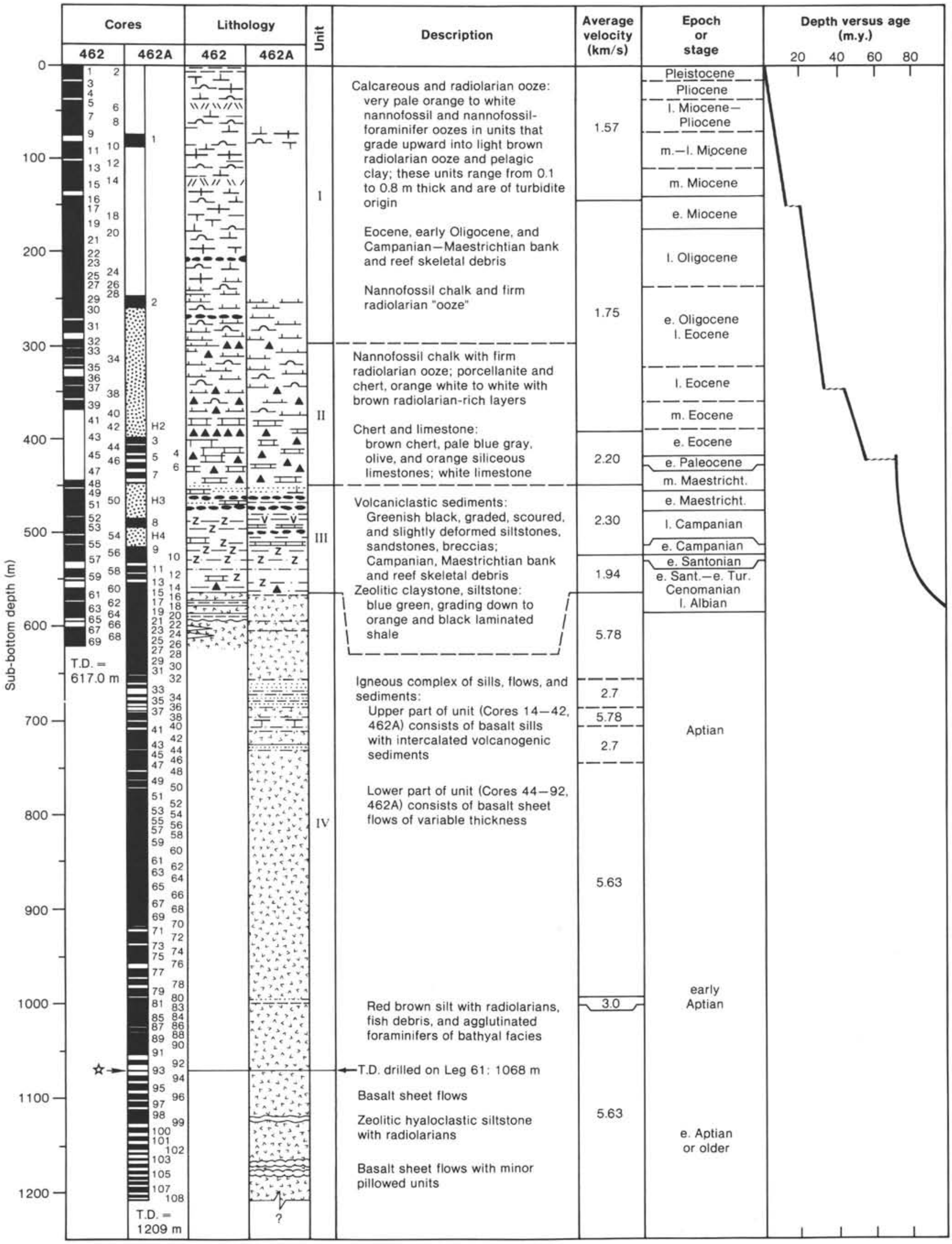

Figure 22. Columnar sections at Site 462, showing cored intervals, lithologic units, interval seismic velocities, and ages. Data from Leg 89 has been added to Leg 61 results. See Figure 1 for an explanation of lithologic symbols.

raphy) that the sediment is Aptian but contains a reworked Berriasian fauna. Core 462A-80 was thought to be Barremian but now is interpreted to be of upper lower Aptian; the sediment also contains a reworked lower Cretaceous (below lower Hauterivian) radiolarian fauna. These revisions are important because they show that older sediments are in the vicinity. The stratigraphic ages shown on Figure 22 are the Leg 89 revisions to the Leg 61 stratigraphic ages shown in Figure 1.

Paleomagnetic data were obtained from thirty-five minicores that were analyzed using progressive alternating field (AF) demagnetization. A steep positive inclination (probably an artifact of the drilling and exposure to the highly magnetic drill pipe) was overprinted on a primary negative inclination in every sample. As the site was south of the Equator during the Cretaceous, this implies that the entire basalt flow complex is of normal polarity. The inclinations are tightly grouped within individual flow units, and these cluster means range from $-51.2°$ ($\pm 1.5°$) to $-10.7°$ ($\pm 1.5°$).

The mean inclination of the magnetic units that could be distinctly identified is $-35.9°$ ($\pm 7°$), implying a paleolatitude of 19.9°S ($\pm 5°$). This is comparable to the paleolatitude of the overlying basaltic complex drilled on Leg 61 of 20.6°S ($\pm 2.4°$) (recalculated from Steiner, 1981, as explained in Ogg, this volume). The two nearly identical mean paleolatitudes imply that northward movement of the site was insignificant during the emplacement of the igneous complex. Resetting of the thermal remanent magnetism at the tops of some units to match that of the overlying unit is good evidence, along with the chilled margins, that these layers are flows, not sills.

A temperature log was run in Hole 462A for several reasons: (1) the hole had remained undisturbed for 4.25 yr. since Leg 61 and presumably was at thermal equilibrium; (2) there was some uncertainty about the interpretation of the logs run in 1978; and (3) the question remained whether heat flow values become constant with age or decrease as a "root-t" trend. The results of the temperature log run on Leg 89 showed that seawater is flowing down into the hole at a rate of about 1700 l/hr. This downhole flow condition is similar to that described by Anderson and Zoback (1982) and Becker et al., (1983). At Site 462 the downward flow is interpreted as a forced convection resulting from pore-fluid underpressure in the sediment column above the basalt sill-flow complex and not because of hydrothermally driven circulation (Fujii, this volume). This raises the interesting question as to the origin of underpressure in deep sea sediment sections.

Although Jurassic sediments were not reached at this site the hole remains clean, the reentry cone is easily seen on the reentry scanning tool, and the sediment layers in the sill-flow complex show that there are older sediments than Aptian in the Nauru Basin; conditions are propitious for a return to the site when a longer drill string can be deployed.

REFERENCES

Ade-Hall, J. M., and Johnson, H. P., 1976. Review of magnetic properties of basalts and sediments, Leg 34. *In* Yeats, R. S., Hart, S. R., et al., *Init. Repts. DSDP*, 34: Washington (U.S. Govt. Printing Office), 769–777.

Aliev, K. S., 1965. Radiolaryii nizhnemelovykh otlozhenii Severo-Vostochnogo Azerbaidzhana i ikh stratigraficheskoe znachenie. *Izvd. Akad. Nauk Azerbaidz.*, S. S. R., Baku, 3:1–124.

Anderson, R. N., and Zoback, M. D., 1982. Premeability, underpressures, and convection in the oceanic crust near the Costa Rica Rift, eastern equatorial Pacific. *J. Geophys. Res.*, 87:2860–2868.

Baumgartner, P. O., de Wever, P., and Kocher, R., 1980. Correlation of Tethyan Late Jurassic-Early Cretaceous radiolarian events. *Cah. Micropal.*, 2:23–85.

Becker, K. M., Langseth, M. G., and von Herzen, R., 1983. Deep crustal geothermal measurements, Hole 504B, DSDP Legs 69 and 70. *In* Cann, J. R., Langseth, M. G., Honnorez, J., von Herzen, R. P., White, S. M., et al., *Init. Repts. DSDP*, 69: Washington (U.S. Govt. Printing Office), 223–235.

Bleil, U., and Smith, B., 1980. Paleomagnetism of basalts, Leg 51. *In* Donnelly, T., Francheteau, J., Bryan, W., Robinson, P., Flower, M., Salisbury, M., et al., *Init. Repts. DSDP*, 51, 52, 53, Pt. 2: Washington (U.S. Govt. Printing Office), 1351–1362.

Boyce, R. E., 1976. I. Definitions and laboratory techniques of compressional sound velocity parameters and wet-water content, wet-bulk density, and porosity by gravimetric and gamma ray attenuation techniques. *In* Schlanger, S. O., Jackson, E. D., et al., *Init. Repts. DSDP*, 33: Washington (U.S. Govt. Printing Office), 931–958.

_______, 1981. Electrical resistivity, sound velocity, thermal conductivity, density-porosity, and temperature, obtained by laboratory techniques and well logs: Site 462 in the Nauru Basin of the Pacific Ocean. *In* Larson, R. L., Schlanger, S. O., et al., *Init. Repts. DSDP*, 61: Washington (U.S. Govt. Printing Office), 743–761.

Cande, S. C., Larson, R. L., and La Breque, J. L., 1978. Magnetic lineation in the Jurassic quiet zone. *Earth Planet Sci. Lett.*, 41: 434–440.

Foreman, H., 1973. Radiolaria of Leg 10 with systematics and ranges for the families Amphipyndacidae, Artostrobiidac, and Theoperidae. *In* Worzel, J. L., Bryant, W., et al., *Init. Repts. DSDP*, 10: Washington (U.S. Govt. Printing Office), 407–474.

_______, 1975. Radiolaria from the North Pacific, DSDP, Leg 32. *In* Larson, R. L., Moberly, R., et al., *Init. Repts. DSDP*, 32: Washington (U.S. Govt. Printing Office), 579–676.

Kono, M., 1980. Statistics of paleomagnetic inclination data. *J. Geophys. Res.*, 85:3878–3882.

Larson, R. L., 1976. Late Jurassic and Early Cretaceous evolution of the western central Pacific Ocean. *J. Geomagnet. Geoelec.*, 28:219–236.

Larson, R. L., Schlanger, S. O., et al., 1981. *Init. Repts. DSDP*, 61: Washington (U.S. Govt. Printing Office).

Levi, S., Bleil, U., Smith, B. M., and Rigotti, P. A., 1980. Comparison of paleomagnetic and rock magnetic of basalt samples from Deep Sea Drilling Project Legs 51, 52, and 53. *In* Donnelly, T., Francheteau, J., Bryan, W., Robinson, P., Flower, M., Salisbury, M., et al., *Init. Repts. DSDP*, 51, 52, 53 Pt. 2: Washington (U.S. Govt. Printing Office), 1337–1350.

Pessagno, E. A., 1977. Lower Cretaceous radiolarian biostratigraphy of the Great Valley Sequence and Franciscan Complex, California Coast Ranges. *Cushman Foundation Spec. Publ.*, 15:1–87.

Peterson, N., 1979. *Glomar Challenger* drillings: the magnetic field produced by the drill and drill string. *In* Dmitriev, L., Heirtzler, J., et al., *Init. Repts. DSDP*, 46: Washington (U.S. Govt. Printing Office), 377–378.

Riedel, W. R., and Sanfilippo, A., 1974. Radiolaria from the Southern Indian Ocean, Leg 26. *In* Davies, T. A., Luyendyk, B. P., et al., *Init. Repts. DSDP*, 26: Washington (U.S. Govt. Printing Office), 771–813.

Rüst, D., 1885. Beiträge zur Kenntniss der fossilen Radiolarien aus Gesteinen des Jura. *Palaeontographica*, 31, Ser. 3 (Vol. 7):273–321.

Schaff, A., 1981. Late Early Cretaceous Radiolaria from the Deep Sea Drilling Project, Leg 62. *In* Thiede, J., Vallier, T., et al., *Init. Repts. DSDP*, 62: Washington (U.S. Govt. Printing Office), 419–470.

Schlanger, S. O., Jackson, E. D., et al., 1976. *Init. Repts. DSDP*, 33: Washington (U.S. Govt. Printing Office).

Schlanger, S. O., and Jenkyns, H. C., 1976. Cretaceous oceanic anoxic events—causes and consequences. *Geologie en Mijnbouw*, 55: 179-184.

Steiner, M. B., 1981. Paleomagnetism of the igneous complex, Site 462. *In* Larson, R. L., Schlanger, S. O., et al., *Init. Repts. DSDP*, DSDP 61: Washington (U.S. Govt. Printing Office), 717-729.

Zoback, M. D., and Anderson, R. N., 1983. The implications of fracture and void distribution from borehole televiewer imagery for the seismic velocity of the upper oceanic crust at Deep Sea Drilling Project Holes 501 and 504B. *In* Cann, J. R., Langseth, M. G., Honnorez, J., Von Herzen, R. P., White, S. M., et al., *Init. Repts. DSDP*, 69: Washington (U.S. Govt. Printing Office), 255-270.

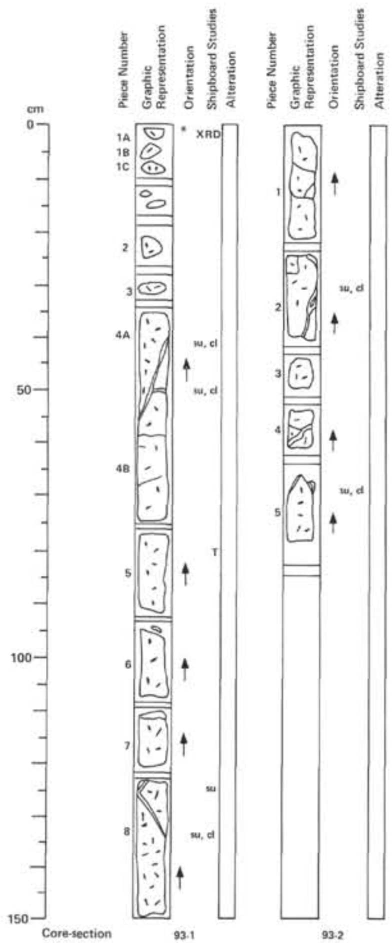

89-462A-93 Depth: 1071.7–1076.6 m

Section 1:

Macroscopic description:

1. Medium bluish gray (5B 5/1) homogeneous aphyric granular textured basalt (*relatively medium-grained throughout*, grains ~1 mm). Possible microglomerophyric olivine/pyroxene occur as dark spots (especially in Piece 2).
2. Poorly developed conjugate set of 2–4 mm wide pyrite ± dark clay veins in Pieces 4 and 8 (pyritized minor fractures). Veins dip at ~60° to horizontal.

Pieces 1A, B, and C sediment pieces are cavings, Pieces 2 and 3 possible cavings. 10–15 cm: two pieces of brown (5YR 4/4 and 10YR 3/2) zeolitic claystone.

* All pieces represent one cooling unit – Unit 45 (following Leg 61); possible lava flow?

XRD: Confirms that dark green clay-like vein infilling is saponite.

Section 2:

Macroscopic description:

1. Continuation of above, part of Unit 45; same cooling unit as no obvious internal junctions.
2. Medium bluish gray (5B 5/1) homogeneous sparsely to moderately pyroxene microphyric basalt.
3. Pyrite and clay veins in Pieces 2 and 5. Sporadic very thin pyrite veins only seen under binocular microscope in most pieces.

Possibility of exchange between Pieces 3 and 4.

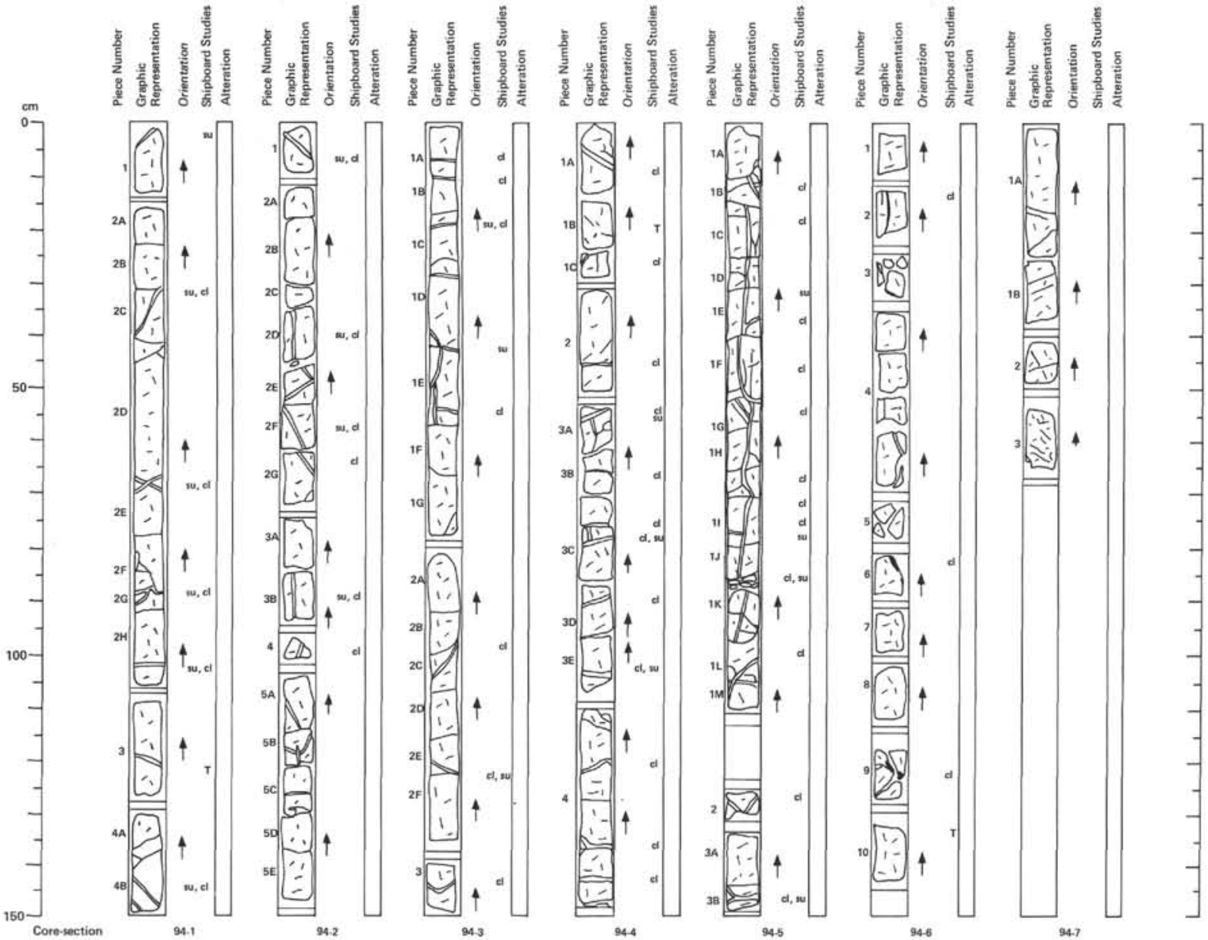

89-462A-94 Depth: 1076.6–1085.7

Section 1:

Macroscopic description:

1. Medium bluish gray (5B 5/1) homogeneous sparsely to moderately pyroxene microphyric basalt. Some slight variation in (a) density of phenocrysts and (b) ratio of felsics to mafics (Piece 3 is more felsic than others).
2. Pyrite and clay veins, some irregular fractures. Thin (1 mm) felspathic vein in Piece 3.

Same cooling unit as before (Unit 45).

Section 2:

Macroscopic description:

1. Medium bluish-gray (5B 5/1) homogeneous aphyric to sparsely pyroxene microphyric basalt (relatively coarse for a basalt).
2. Little variation, except relative proportion of mafics to feloics and then very minor, and similar to Section 1. Same cooling unit as before (Unit 45).
3. Numerous pyrite-bearing veins, generally steep, some subhorizontal.

Section 3:

Macroscopic description:

Medium bluish gray (5B 5/1) homogeneous sparsely pyroxene microphyric basalt – as before (still Unit 45). Very minor changes in grain size, presence or absence of phenocrysts and mafic/felsic ratio e.g. Piece 2F.

Dark green soft 'clay' of veins is smectite (XRD suggest saponite, see Core 93, Section 1).

Slickensides on clay in vein in Pieces 2C and slickensides in Piece 2E.

Section 4:

Macroscopic description:

1. Homogeneous medium bluish gray (5B 5/1) sparsely pyroxene microphyric basalt. Same as previous sections. Unit 45 continued; no internal junctions.
2. Pyrite-saponite veinlets – largely infilling fractures.

Section 5:

Macroscopic description:

1. Homogeneous bluish-gray (5B 5/1) sparsely phyric pyroxene microphyric basalt. Continuation of Unit 45.
2. Vertical saponite vein from 14–84 cm and continued 87–97 cm interval contains variable pyrite (2 mm thick in Piece 1D).

Section 6:

Macroscopic description:

1. Medium bluish gray (5B 5/1) homogeneous sparsely pyroxene microphyric basalt – as before, no internal junctions, part of Unit 45.
2. Minor 'clay' (saponite?) ± pyrite veining.

Section 7:

Macroscopic description:

1. Homogeneous medium bluish gray (5B 5/1) sparsely pyroxene microphyric basalt; phenocrysts randomly distributed (Unit 45).
2. Numerous veinlets and infilled fractures with dark saponite ± pyrite.

Whole core is microfractured and veined, increases downwards to a maximum in Section 5. Most are relatively steeply dipping (50° to vertical), cut by a later set of subhorizontal fractures (no pyrite).

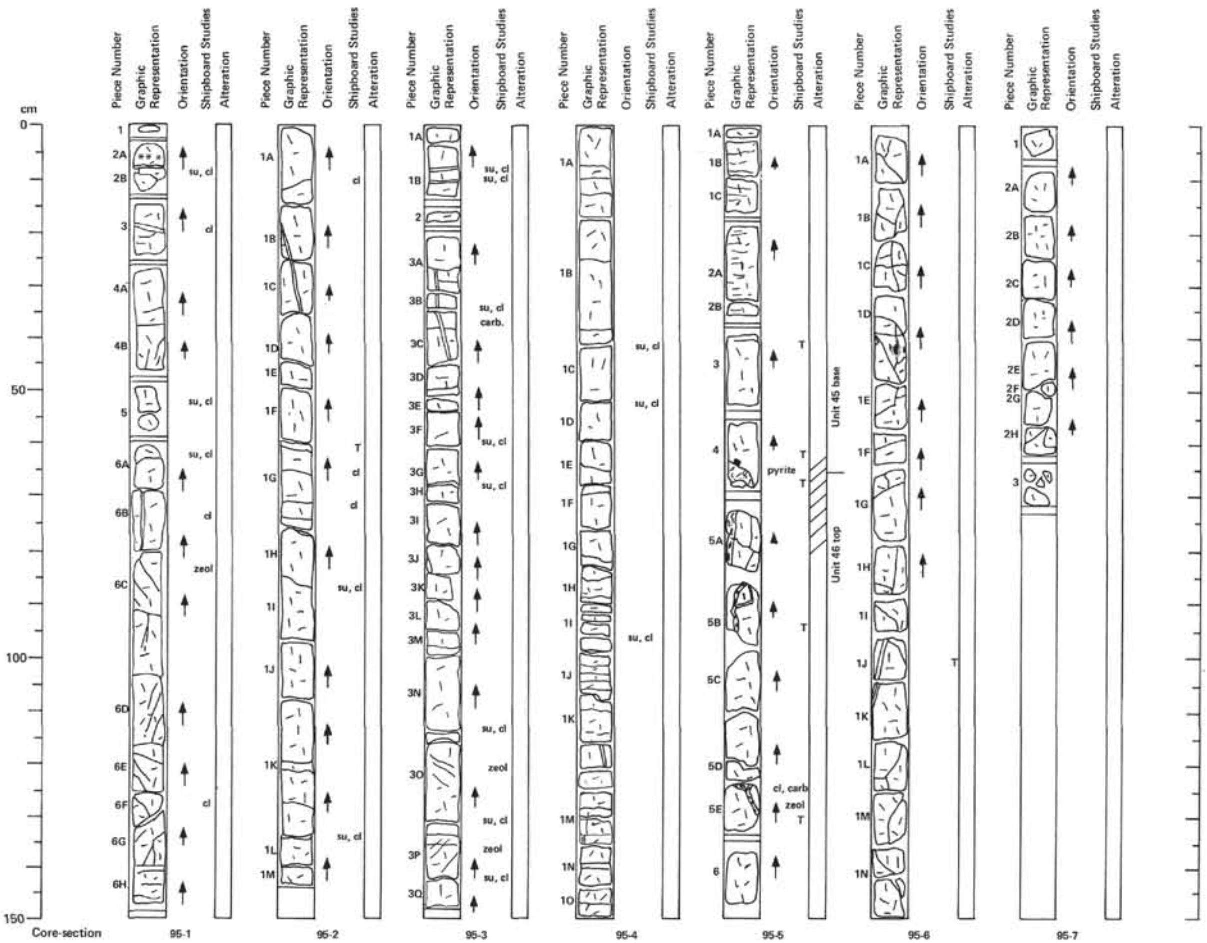

89-462A-95 Depth: 1085.7–1094.9 m

Section 1:

Macroscopic description:

1. Homogeneous medium bluish gray (5B 5/1) aphyric to sparsely pyroxene microphyric basalt. Similar to Core 94 – continuation of Unit 45.
2. Numerous very thin (<0.5 mm) saponite ± pyrite veinlets. Majority form a steep dipping conjugate set, together with a few subhorizontal veinlets. At 80–90 cm soft white zeolite(?) veinlets.
3. Piece 2A – 2 mm pyroxene-rich layer (subhorizontal).

Section 2:

Macroscopic description:

1. Homogeneous medium bluish gray (5B 5/1) aphyric to sparsely pyroxene microphyric basalt (Unit 45) (less phyric than Section 1).
2. Pyrite-saponite veinlets mainly subhorizontal and thinner in this core relative to Core 94.

Section 3:

Macroscopic description:

1. Homogeneous medium bluish gray (5B 5/1) aphyric to sparsely pyroxene microphyric basalt. Still Unit 45. Some variation in phenocryst density.
2. Most pyrite-saponite veinlets are subhorizontal. On broken surface pyrite cubes scattered in dark soft clay flakes. Conjugate zeolite(?) veinlets in Pieces 3O and 3P.

Section 4:

Macroscopic description:

1. Homogeneous medium bluish gray (5B 5/1) aphyric to sparsely pyroxene microphyric basalt (still Unit 45).
2. Most subhorizontal fractures are infilled with pyrite and saponite (not all marked graphically as veins). Increase in density of subhorizontal fractures down core and this section, e.g. top of section: 1 or 2 per 10 cm, at base of section: 5 per cm. Steep and vertical veinlets less in evidence.

Section 5:

Macroscopic description:

1. 0–64 cm homogeneous medium bluish gray (5B 5/1) aphyric to sparsely pyroxene microphyric basalt. Phenocryst density marked decreases in 55–64 cm interval and basalt marginally finer grained. Represents chilled base to Unit 45.
2. 64–110 cm chilled upper flow top to next unit (Unit 46) – fine-grained olivine-pyroxene glomerophyric basalt with vertical hyaloclastite zone (green smectite – replaced spalled shards in carbonate matrix). To base of section thin smectite, carbonate ± zeolite infilled fractures in homogeneous sparsely pyroxene microphyric basalt.

Piece 1C: numerous horizontal closely spaced fractures.

Section 6:

Macroscopic description:

1. Homogeneous medium bluish gray (5B 5/1) sparsely olivine pyroxene phyric and ahpyric basalt. Marginally finer grained than in Unit 45. Random and patchy distribution of phenocrysts.
2. Horizontal and steep infilled (pyrite and saponite) fractures throughout.
3. Near vertical brecciated zone between 97–109 cm.

Brecciated zone with dark margin and green smectite fragments, some carbonate (Piece 1J).

Section 7:

Macroscopic description:

1. As Section 6 above: Unit 46 basalt.

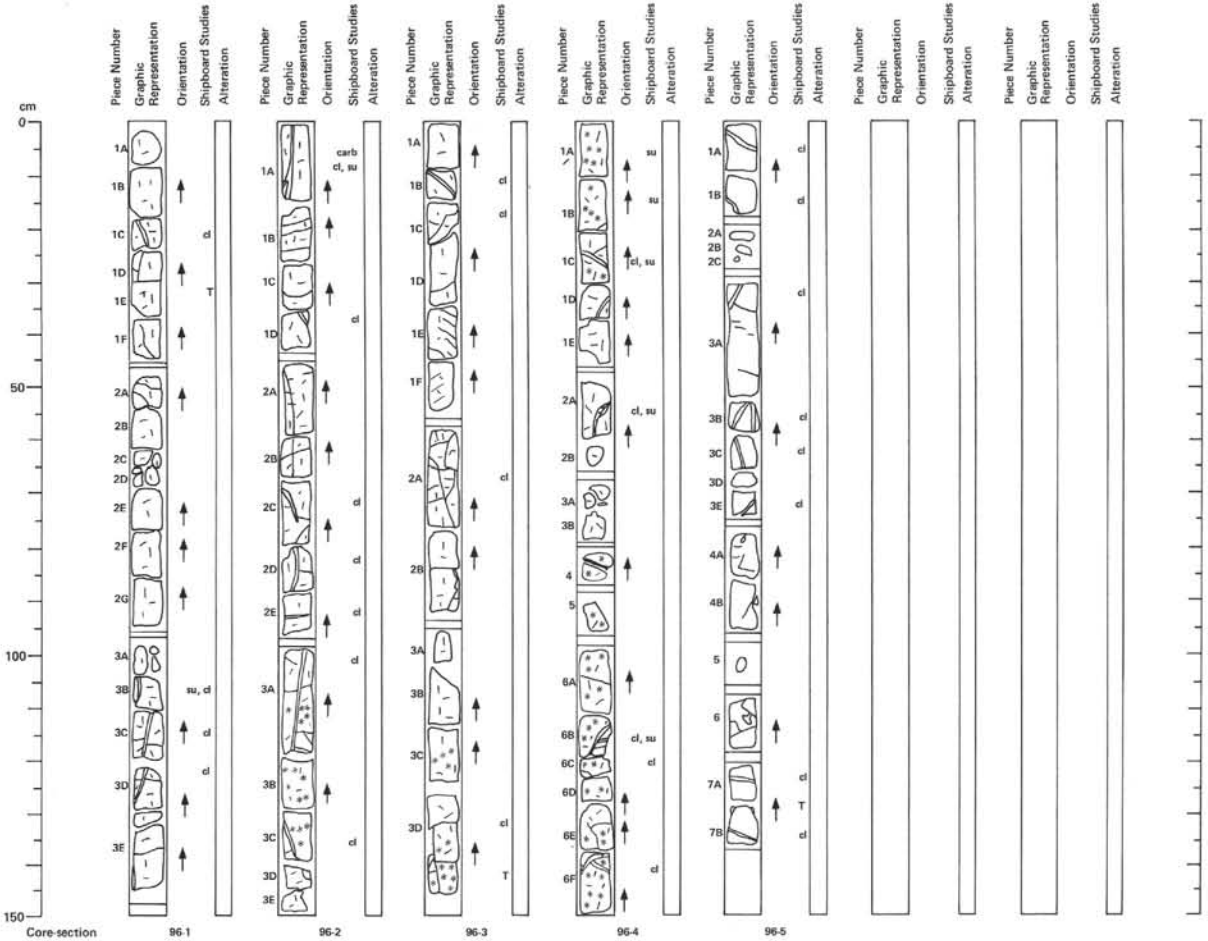

89-462A-96

Depth: 1094.9–1104.0 m

Section 1:

Macroscopic description:

1. Homogeneous bluish gray (5B 6/1) sparsely olivine-pyroxene microphyric basalt throughout.
2. Steep, curving (60–70° to the horizontal) saponite-pyrite ± carbonate-infilled fractures, generally ~1 mm wide.

Section 2:

Macroscopic description:

As Section 1 – Unit 46. Sparsely olivine-pyroxene microphyric basalt.

110–137 cm: Irregular layering and patchy concentration of pyroxene phenocrysts.

Section 3:

Macroscopic description:

As in Section 1, same unit – 46. Sparsely olivine-pyroxene microphyric basalt.
Poorly layered, patchy development of pyroxene phenocrysts (glomerophyric patches) at 120–146 cm.

Piece 2A: Very fractured.

Section 4:

Macroscopic description:

As in Section 1, still Unit 46. Homogeneous sparsely olivine-pyroxene microphyric basalt, except irregular layers and patches of pyroxene – glomerophyric throughout most of section. "Layers" from subhorizontal to 25° dip; sulphide (pyrite) may be associated (e.g. Pieces 1A and B) in matrix as well as in veinlets.

Section 5:

Macroscopic description:

As before, Section 1, still Unit 46. Sparsely olivine-pyroxene microphyric basalt.
Veinlets, many infilled with saponite, lack of pyrite.
En echelon set of microfractures in Piece 3A.

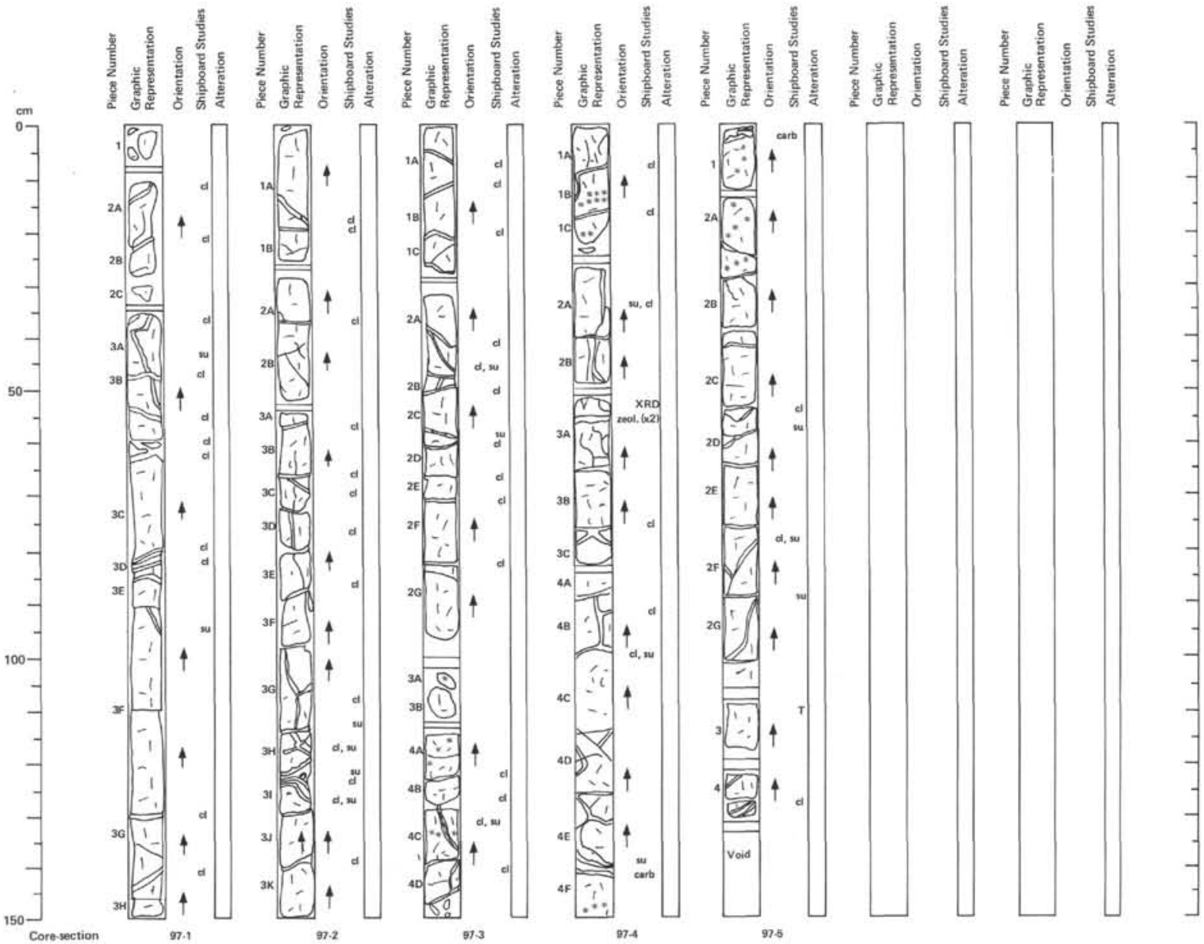

89-462A-97

Depth: 1104.0–1113.2 m

Section 1:

Macroscopic description:

Homogeneous bluish gray (5B 6/1) aphyric and sparsely-olivine pyroxene microphyric basalt (still Unit 46). Pyrite-saponite veins – pyrite forms radiate plumose crystals.

Section 2:

Macroscopic description:

As before, still Unit 46. Sparsely olivine-pyroxene microphyric basalt. Irregular masses of pyrite in matrix and associated with steep veins in Piece 3H.

Section 3:

Macroscopic description:

As before, Section 1, Unit 46. Sparsely olivine-pyroxene microphyric basalt. Pyroxene layers and patches in Piece 4 – not true igneous layering.

Section 4:

Macroscopic description:

As Section 1, Unit 46. Sparsely olivine-pyroxene microphyric basalt. Vein at 55 cm contains two zeolites (white and prismatic; grayish white radiate masses).

XRD: Heulandite, minor phillipsite and milky white quartz.

Section 5:

Macroscopic description:

As before, Section 1, Unit 46. Sparsely olivine-pyroxene microphyric basalt. Veinlets rich in pyrite in Pieces 2F and 2G.

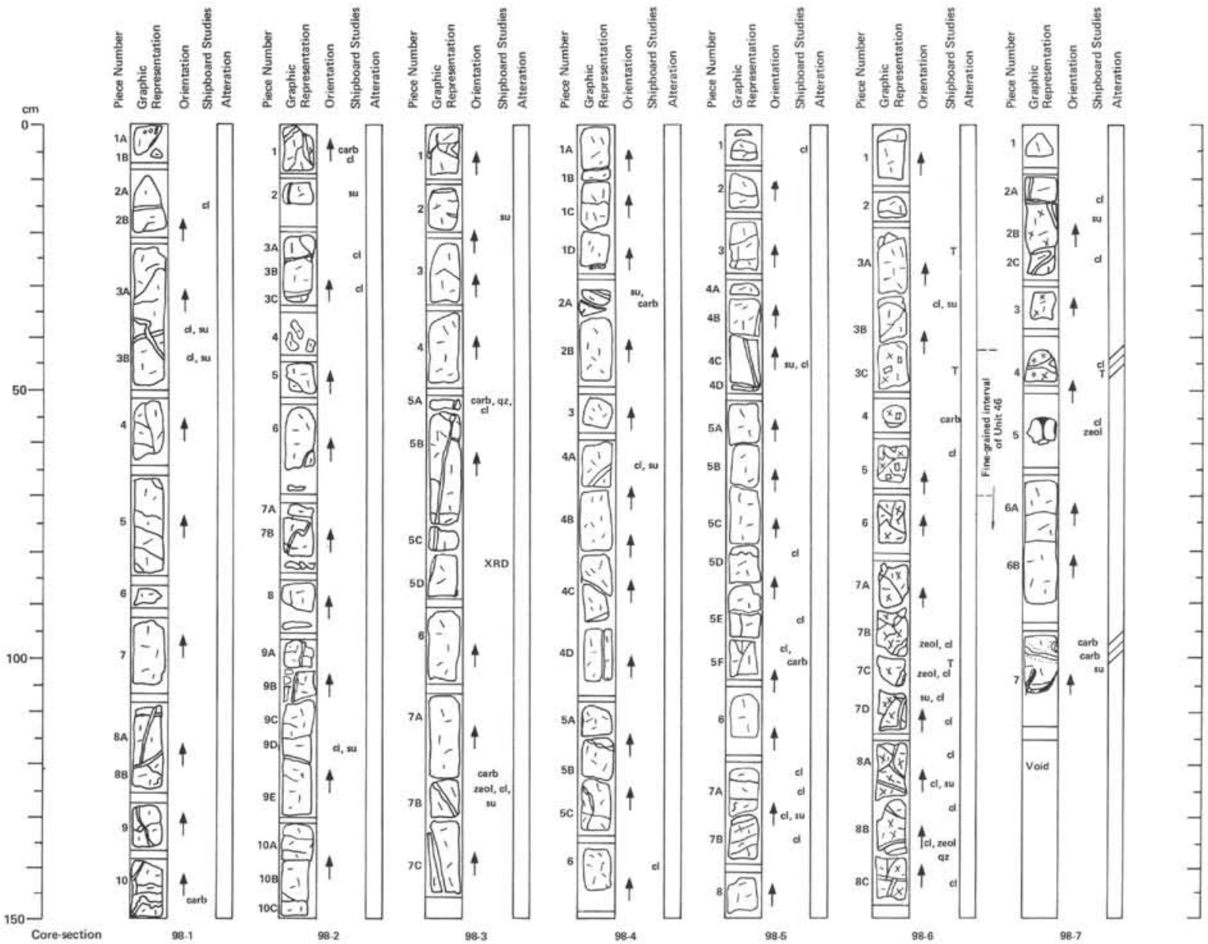

89-462A-98

Depth: 1113.2–1122.3 m

Section 1:

Macroscopic description:

1. Homogeneous bluish gray (5B 6/1) aphyric and sparsely olivine-pyroxene microphyric basalt (Unit 46).
2. Veinlets are (a) saponite ± pyrite or (b) fine-grained silica, sometimes colored green by smectite, with a white carbonate (calcite) on margins and within vein center.

e.g. Piece 10:

Section 2:

Macroscopic description:

As Section 1, Unit 46. Sparsely olivine-pyroxene microphyric basalt. Veinlets again contain calcite.

Section 3:

Macroscopic description:

As Section 1, Unit 46. Sparsely olivine-pyroxene microphyric basalt. Calcite-quartz plus saponite vein in Piece 5, dips 70° relative to the horizontal.

XRD: Calcite plus quartz only, no zeolite. Pyrite sometimes associated in zeolite-bearing veins (e. g. Piece 7B).

Section 4:

Macroscopic description:

As Section 1, Unit 46. Aphyric and sparsely pyroxene-olivine microphyric basalt. Pyrite-saponite veinlets still common, ±carbonate.

Section 5:

Macroscopic description:

As Section 1, Unit 46. Aphyric and sparsely olivine-pyroxene microphyric basalt. Subhorizontal fractures towards base of section.

Section 6:

Macroscopic description:

1. 0–42 cm: Homogeneous bluish gray sparsely olivine-pyroxene microphyric basalt.
2. At about 42 cm interval, decrease in grain-size and incoming of sparse plagioclase phenocrysts – gradual, no junction defined. Dark bluish gray (5B 4/1) fine-grained moderately olivine-pyroxene-plagioclase-phyric basalt (Piece 4 is pyroxene-plagioclase glomerophyric).
3. At 70 cm becomes coarser again and plagioclase phenocrysts disappear; moderately olivine-pyroxene-phyric basalt from 70–150 cm.

All core still Unit 46.

Section 7:

Macroscopic description:

Dominantly, sparsely to moderately olivine-pyroxene microphyric basalt.

30–50 cm: marginally finer grained with altered pyroxene(?) glomerocrysts.

Piece 4: Dark pyroxene/olivine clots to green clay?

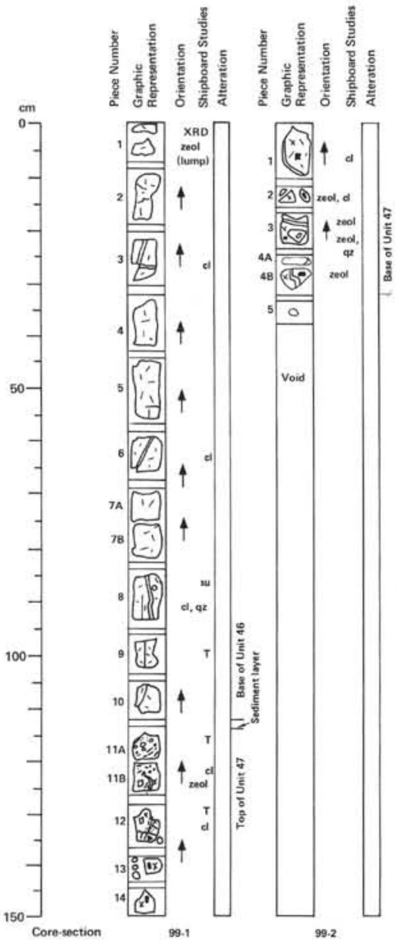

89-462A-99

Depth: 1122.3–1131.5 m

Section 1:

Macroscopic description:

1. 0–110 cm: Homogenaous sparsely olivine-pyroxene microphyric basalt.
2. 113–119 cm: Sediment layer, Piece 11A, composed of purple sedimentary clasts (1–7 mm), silt-sized fragments, pyroxene crystals and smectite-replaced glass shards(?) – represents boundary to Units 46 and 47 (see sediment Visual Core Description).
3. 121–150 cm: Fine-grained moderately pyroxene-plagioclase-olivine(?) phyric basalt (Unit 47). Top of unit represented by black spalled glass shards in green smectite and zeolite matrix (zone 5 mm thick). A fine-grained zone extends to about 140 cm, then coarser again to base. Plagioclase phenocrysts also decrease with depth.

Zeolite is stilbite (XRD) (dark green spheres of acicular crystals within stilbite tablets) = epidote? or pumpellyite?

Section 2:

Macroscopic description:

0–32 cm: Moderately pyroxene-olivine ± plagioclase phyric basalt veined by zeolites with saponite margins.

Piece 5: Purple and pale green laminated fine-grained claystone – smectite and crystal fragments? (alteration zone of flow top, unmetamorphosed)?.

Base of Unit 47 placed above (see sediment Visual Core Description).

SITE 462 HOLE A CORE 99 CORED INTERVAL 1122.3–1131.5 m sub-bottom; 6308.3–6317.5 m below rig floor

TIME – ROCK UNIT	BIOSTRATIGRAPHIC ZONE	FOSSIL CHARACTER: FORAMINIFERS	NANNOFOSSILS	RADIOLARIANS	DIATOMS	SECTION	METERS	GRAPHIC LITHOLOGY	DRILLING DISTURBANCE	SEDIMENTARY STRUCTURES	SAMPLES
Late Jurassic to early Aptian				RP		1	0.5	Basalt			
							1.0				
						2		Basalt			

LITHOLOGIC DESCRIPTION

1, 110–124 cm: silty claystone as detailed in figure below.

2, 36–37 cm: claystone and silty claystone in wispy, burrowed(?) laminae of dark greenish gray (5G 6/1) and grayish blue green (5BG 6/2).

110 cm

SILTY CLAYSTONE, dark greenish gray (5GY 4/1) with olive gray (5Y 4/1) sediment clasts at base with zeolite-filled veins (designated by black)

GLASSY BASALT MARGIN, dark greenish black (5G 2/1)

BASALT, medium dark gray (N4) with pyrite, zeolite, and diagenetic clay-filled veins and fractures

124 cm

SMEAR SLIDE SUMMARY (%):

	1, 116 M	1, 112 M	2, 36 M	2, 36 M	1, 117 M
Texture:					
Silt	1	–	7	30	–
Clay	99	100	93	70	100
Composition:					
Feldspar	Tr	Tr	Tr	Tr	–
Heavy minerals	–	–	–	Tr	–
Clay	98	96	93	69	97
Volcanic glass	1	3	7	30	1
Zeolite	1	1	Tr	1	2
Radiolarians	–	Tr	Tr	Tr	Tr
Fish remains	Tr	Tr	Tr	Tr	Tr

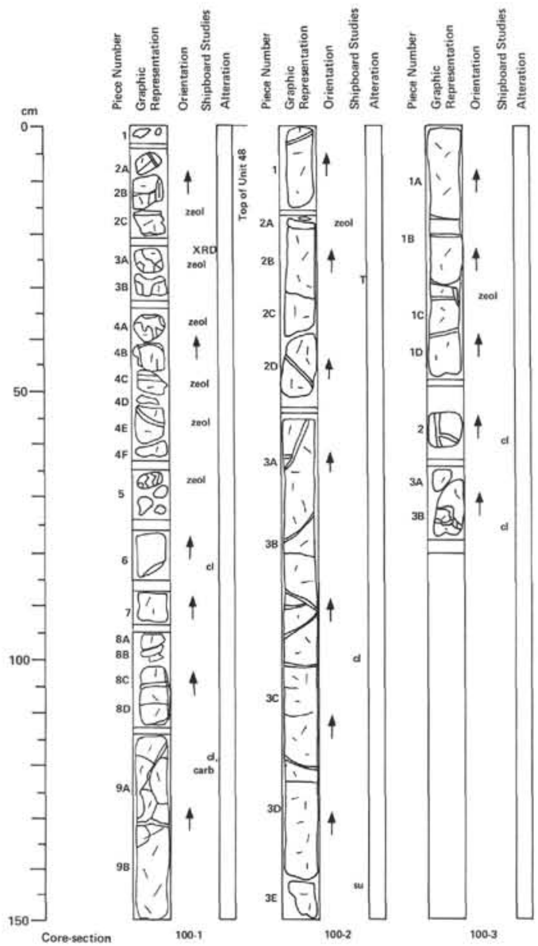

89-462A-100

Depth: 1131.5–1134.5 m

Section 1:

Macroscopic description:

1. Homogeneous bluish gray (5B 6/1) aphyric to sparsely olivine-pyroxene microphyric basalt. Bright green smectite flakes partly replace olivine.
2. Considerable zeolite veining in Pieces 2–5.

XRD: Zeolite is stilbite.

Section 2:

Macroscopic description:

Continuation of Unit 48 — aphyric and sparsely olivine microphyric basalt. Green smectite in matrix and replacing olivine.

Section 3:

Macroscopic description:

Homogeneous aphyric to sparsely pyroxene microphyric basalt (Unit 48). Olivine and smectite have disappeared relative to Section 2; some pyroxene phenocrysts appear to be large subophitic pyroxene pools than true phenocrysts.

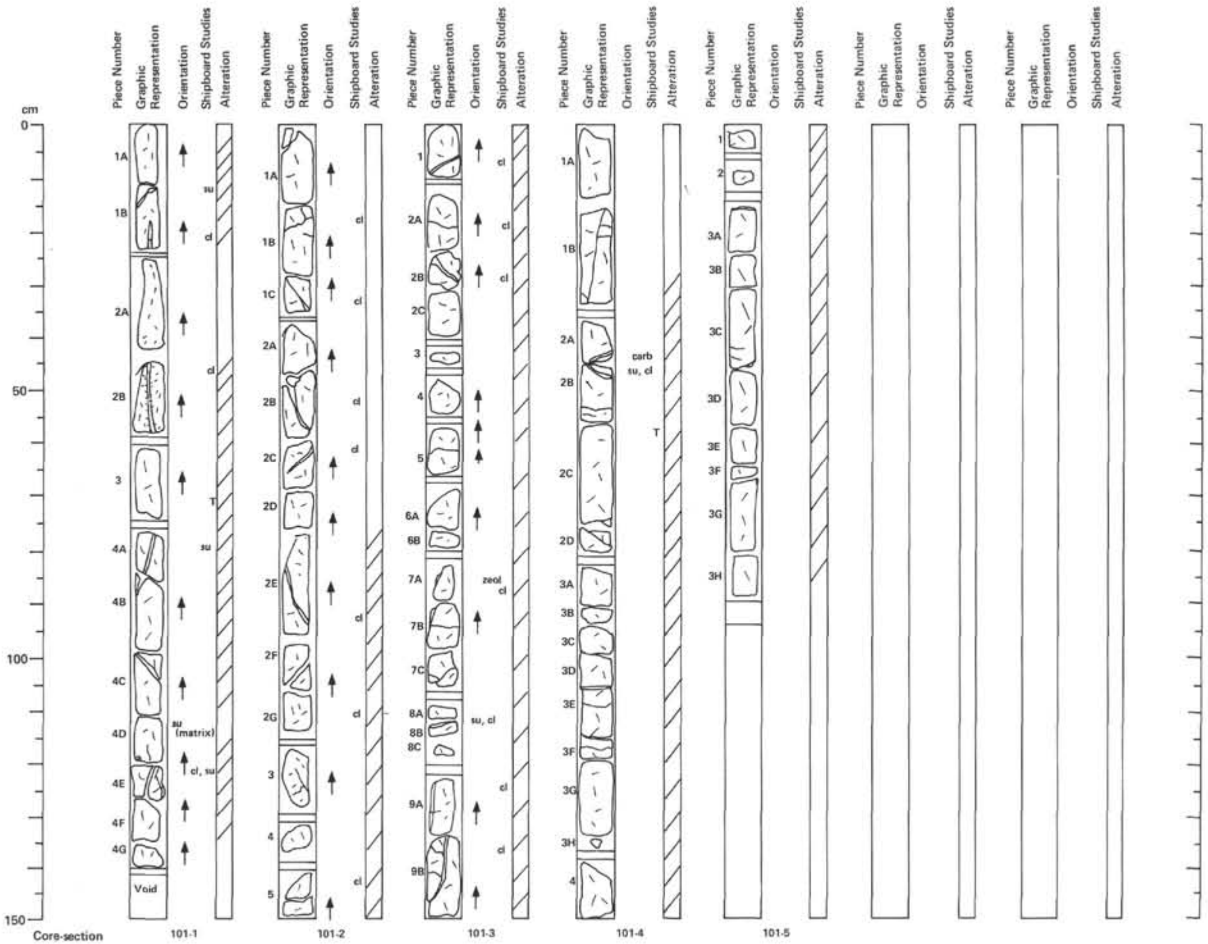

89-462A-101

Depth: 1134.5–1142.9 m

Section 1:

Macroscopic description:

1. Relatively homogeneous bluish gray (5B 6/1) aphyric basalt – relatively coarse-grained for basalt.
2. Considerable development of green smectite patches. Disseminated pyrite in matrix and veins.

Unit 48.

Section 2:

Macroscopic description:

As Section 1, continuation of Unit 48. Aphyric basalt (granular texture). Blue green and dark green smectite common in matrix and veins.

Section 3:

Macroscopic description:

Aphyric basalt (Unit 48).
Granular texture, smectite patches throughout.

Marginally finer-grained than Sections 2 and 4, increasing in grain-size towards base (fine-grained section 12–106 cm).

Section 4:

Macroscopic description:

Aphyric basalt (Unit 48).

Coarser grained again relative to Section 3.

Green smectite patches and veins throughout.

Section 5:

Macroscopic description:

Aphyric basalt (Unit 48).

Patchy smectite alteration throughout.

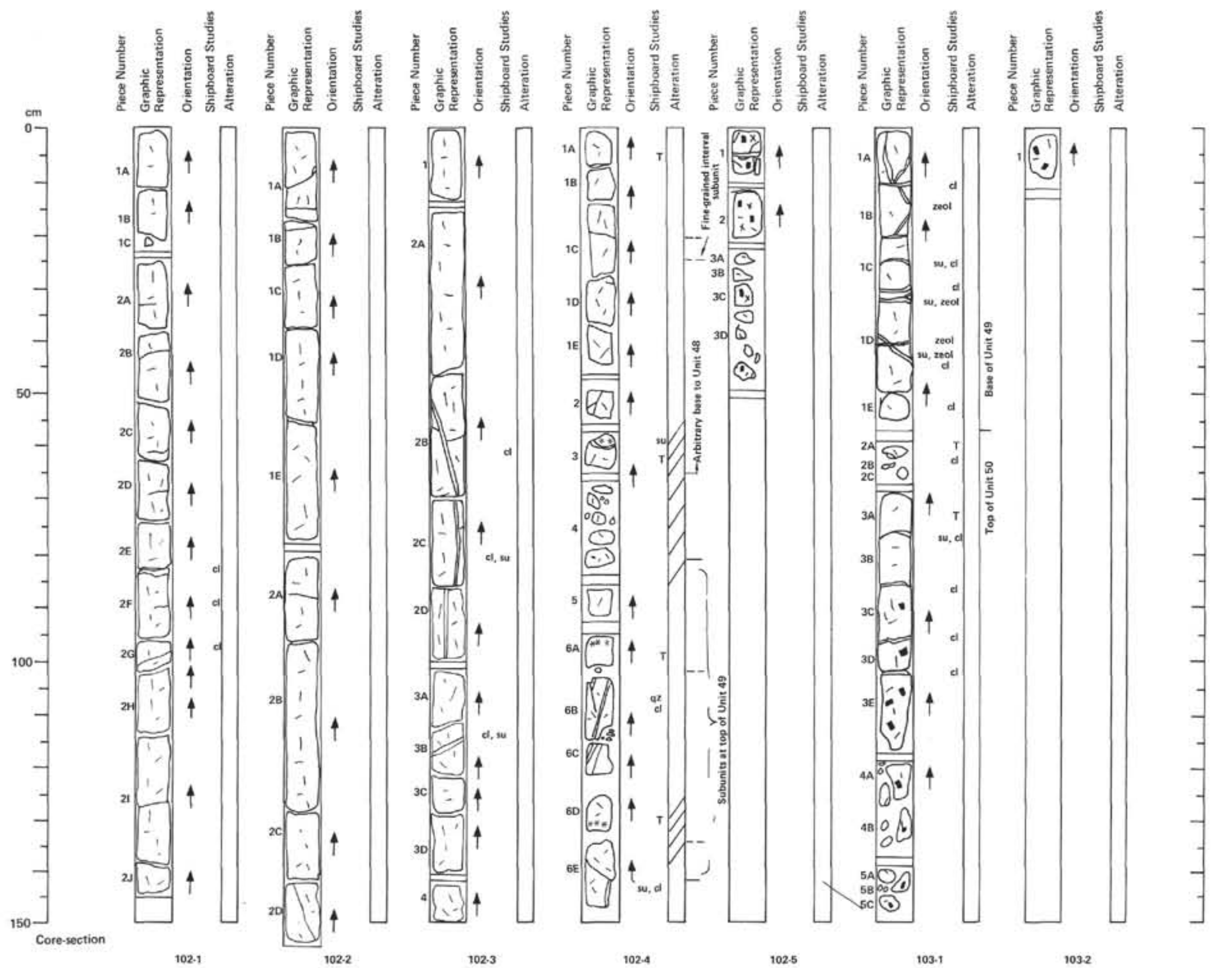

89-462A-102 Depth 1142.9–1152.0 m

Section 1:

Macroscopic description:

Homogeneous medium bluish gray (5B 5/1) sparsely to moderately olivine-pyroxene-plagioclase phyric basalt (Unit 48). Few horizontal smectite-filled fractures.

Section 2:

Macroscopic description:

Homogeneous sparsely olivine(?) or pyroxene phyric basalt (Unit 48). Phenocrysts replaced by green smectite are probably olivine.

Section 3:

Macroscopic description:

Homogeneous sparsely olivine or pyroxene phyric basalt (Unit 48) – similar to Sections 1 and 2 above.

Section 4:

Macroscopic description:

1. 0–43 cm: Homogeneous sparsely olivine and pyroxene phyric basalt, becoming finer towards base. Also a fine-grained interval subunit at 21–23 cm.
2. 43–150 cm: Very fine-grained (quench textured?) pyroxene-plagioclase glomerophyric ± olivine phyric basalt.
3. Within 43–150 cm interval are 3 glass-rich layers (at 58, 96, and 132 cm) – possibly represent bases of 3 subunits.

Arbitrary base to Unit 48 placed at 65 cm below olivine layer – from then on glomerophyric texture decreases and grain-size increases towards base.

Section 5:

Macroscopic description:

Homogeneous fine-grained moderately olivine-pyroxene phyric basalt – possibly top of a new unit(?) Unit 49.

89-462A-103 Depth 1152.0–1161.2 m

Section 1:

Macroscopic description:

1. Homogeneous fine-grained bluish gray (5B 6/1) sparsely olivine-pyroxene glomerophyric basalt. Unit 49 (basal section to about 55 cm).
2. Very fine-grained or glassy basalt at 60 cm (Piece 2) (top of new unit [Unit 50]) becomes olivine phyric with depth.

Section 2:

Macroscopic description:

Moderately olivine phyric (and pyroxene glomerophyric?) basalt (Unit 50) coarser than majority of Section 1.

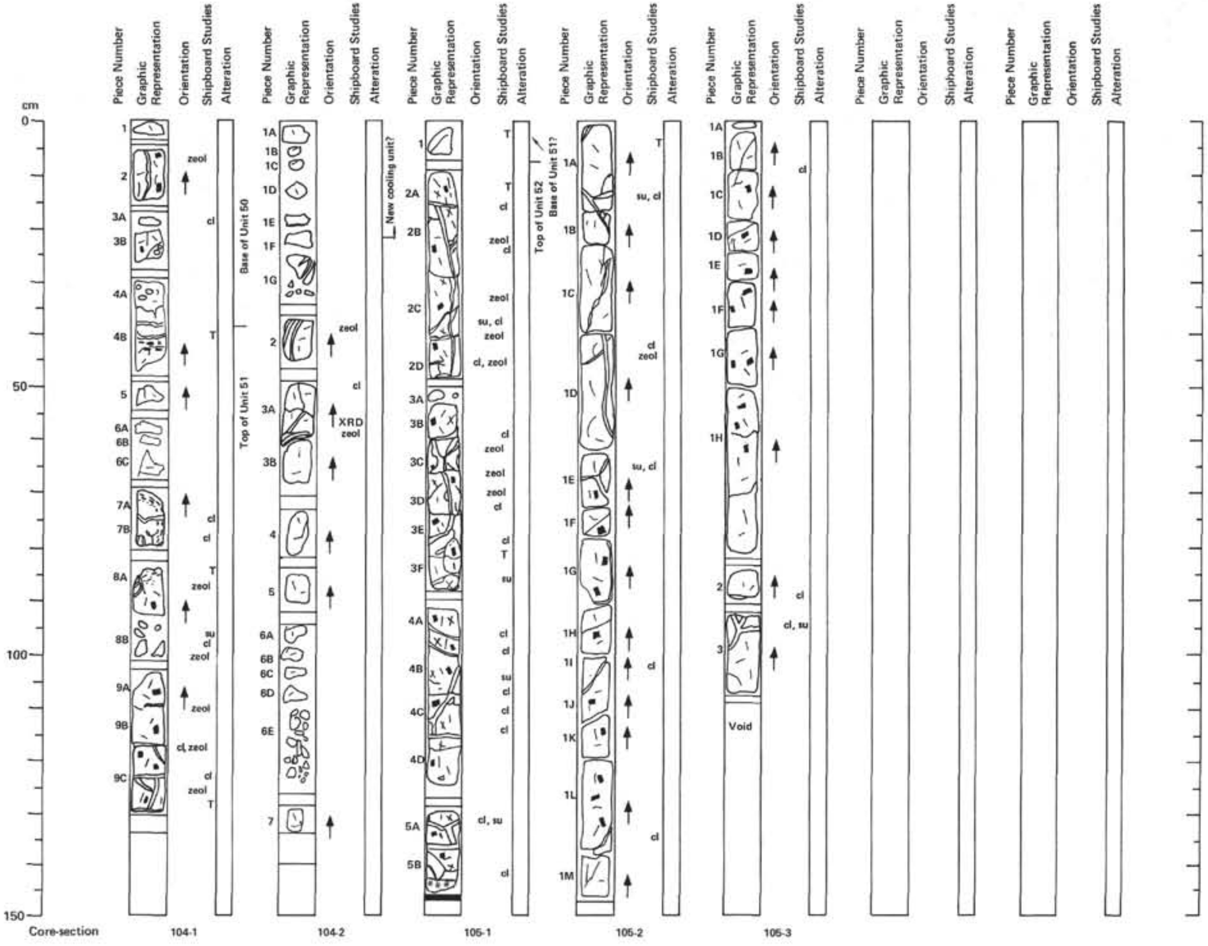

89-462A-104 Depth: 1161.2–1170.3 m

Section 1:

Macroscopic description:

1. 0–41 cm: Homogeneous medium bluish gray (5B 5/1) moderately olivine phyric basalt, vesicular between 24–33 cm *interval (infilled with pale and dark green smectite ± pyrite)* = basal Unit 50.
2. 41–130 cm: Fine-grained pillowed olivine phyric basalt. Only 2 thin cooling units with curved glassy margins seen – unit increases in massiveness and grain size with depth from about 90 cm = top of Unit 51 (olivine now green smectite).

Granular top of unit may be a contact metamorphosed and recrystallized hyalopilitic textured clinopyroxene phyric glassy basalt.


Piece 4B:
curved chilled margin

Piece 7A and B:


curved chilled margin

Piece 8A:


curved chilled margin

Section 2:

Macroscopic description:

Continuation of Unit 51 with possible base to cooling unit (in base of Section 1) at about 20 cm. Sparsely to moderately olivine phyric basalt that varies considerably in grain-size (fine-grained to medium-grained basalt) down section – from piece to piece = pillowed basalt sequence(?) although chilled margins missing, perhaps removed during drilling.

XRD: Zeolite is stilbite.

89-462A-105 Depth: 1170.3–1174.3 m

Section 1:

Macroscopic description:

1. 0–6 cm: Homogeneous coarse-grained aphyric basalt (Unit 51 base)?
2. 8–145 cm: Moderately olivine ± pyroxene phyric (possibly glomerophyric) basalt decreasing marginally in grain size down section (Unit 52). Olivine (now green smectite) rich layer at 143 cm; basalt below is finer-grained (near base of flow unit?).

Piece 4D: Abundant pyrite on working half.

Olivine-rich layer at bottom of Piece 5B.

Section 2:

Macroscopic description:

Continuation of Unit 52? or a subunit. Bluish gray (5B 6/1) sparsely to moderately olivine phyric basalt. Distribution of phenocrysts very variable, concentrated more towards base of section. Increase in grain-size also towards base.

Section 3:

Macroscopic description:

Continuation of Unit 52. Sparsely to moderately olivine phyric basalt. Relatively coarse-grained throughout.

Saw cut at 9 cm.

107 cm: Bottom of section.

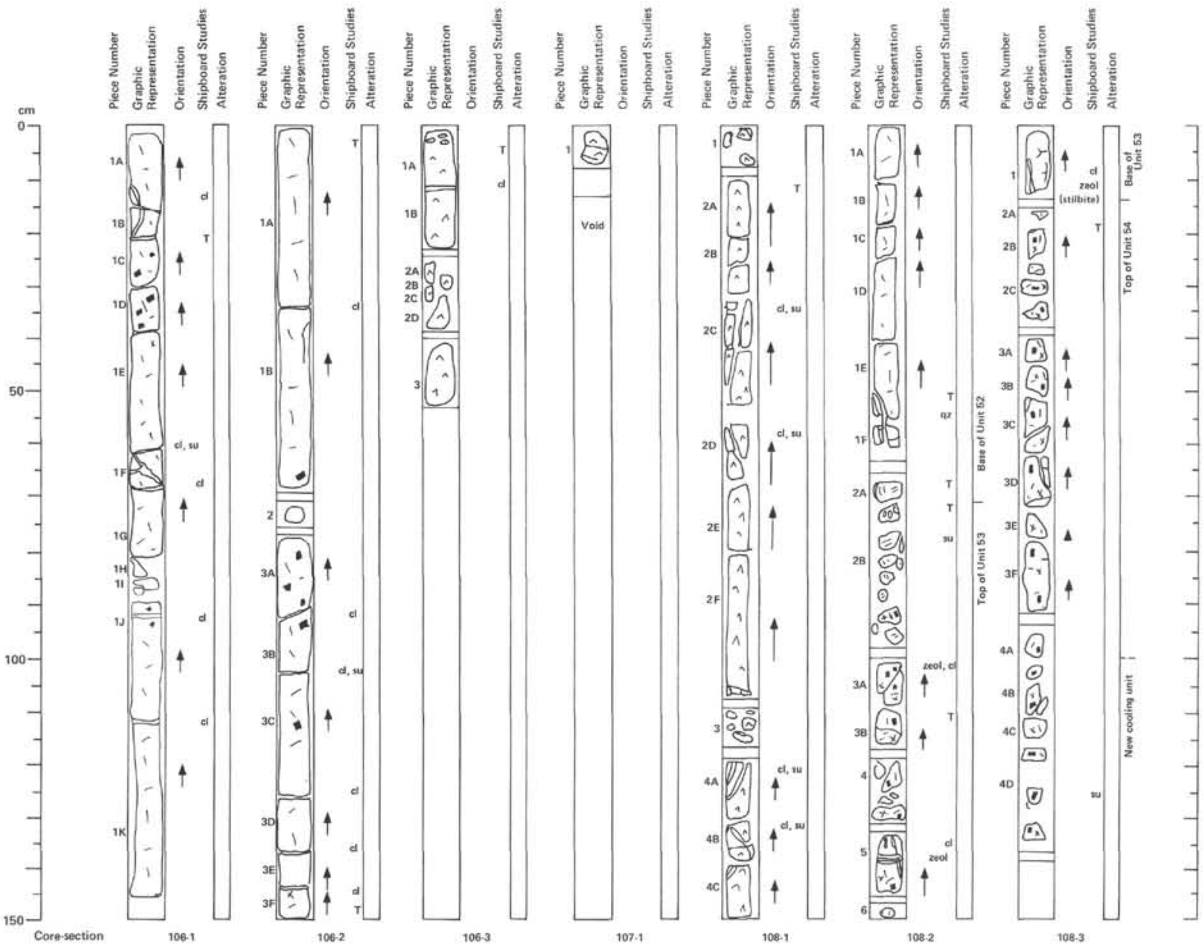

89-462A-106 Depth: 1174.3–1180.4 m

Section 1:

Macroscopic description:

Probably continuation of Unit 52. Homogeneous, relatively coarse-grained, bluish gray (5B 6/1) aphyric to sparsely olivine phyric basalt. (Phenocryst concentration from about 15–40 cm.)

Section 2:

Macroscopic description:

Continuation of Unit 52. Aphyric to sparsely olivine phyric basalt; slight increase in grain-size at base of section. Whole section relatively coarse for a basalt.

Section 3:

Macroscopic description:

1. Aphyric to sparsely olivine phyric fine-grained dolerite. Coarser-grained than previous sections with grains about 1 mm or greater in size.
2. 0–3 cm: Few vugs, some lined with smectite.

89-462A-107 Depth: 1180.4–1189.5 m

Section 1:

Macroscopic description:

Homogeneous fine-grained aphyric olivine dolerite (still Unit 52).

89-462A-108 Depth: 1189.5–1198.7 m

Section 1:

Macroscopic description:

Continuation of Unit 52. Homogeneous, bluish gray (5B 6/1) fine-grained aphyric olivine dolerite.

Marginally finer grained at base of section than at top.

Few scattered olivine phenocrysts and disseminated pyrite. Concentration of olivine at about 38–50 cm interval.

Section 2:

Macroscopic description:

1. 0–62 cm: Aphyric to sparsely olivine phyric coarse-grained basalt, decreasing in grain size downwards.
2. 65–71 cm (Piece 2A): Olivine-pyroxene phyric very fine-grained basalt (= basal chilled margin to Unit 52).
3. 72–75 cm (Piece 2B): Green altered glass with olivine phenocrysts coating very fine-grained (quenched?) olivine phyric basalt (= top of Unit 53). Pillow breccia?
4. 76–150 cm: Olivine-pyroxene phyric fine-grained basalt, increasing in grain-size downwards. Quenched basalt below Piece 2B, becoming holocrystalline with depth (pillow?).

Section 3:

Macroscopic description:

1. 0–12 cm (Piece 1): Moderately olivine-pyroxene phyric basalt (Unit 53).
2. 15–135 cm: Moderately phyric to olivine-pyroxene phyric basalt (clinopyroxene–glomerophyric) – dark chilled zone on Piece 2B, grain-size then increases downwards to 10 cm (Piece 4A); followed by a decrease (Piece 4B) with fine-grained phyric basalt (= Unit 54 composed of a number of cooling units having same phenocryst composition throughout.) Pillow lava sequence? (including Units 53 and 54).

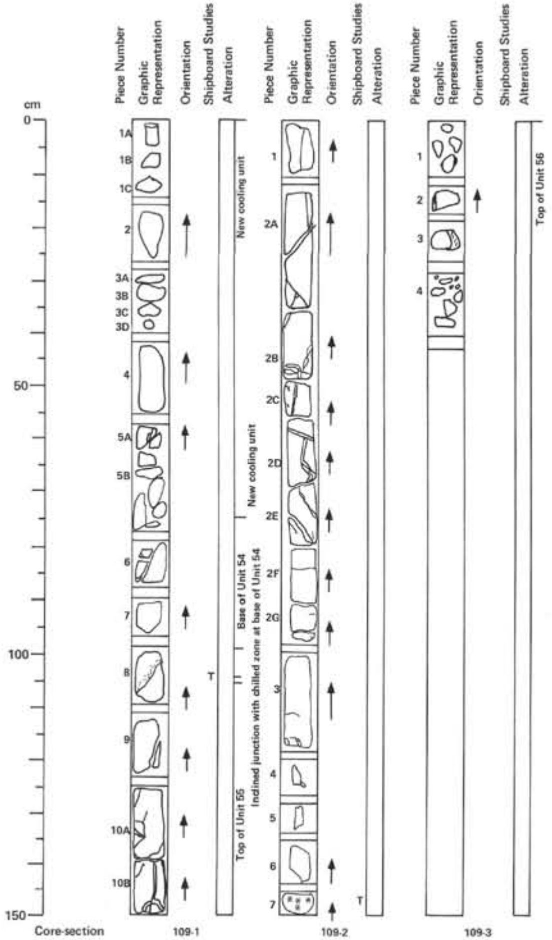

89-462A-109 Depth 1198.7–1209.0 m

Section 1:

Macroscopic description:

1. 0–104 cm (to Piece 8): Olivine-pyroxene phyric basalt – bluish gray (5B 6/1). Varies in grain size from fine to slightly coarser down section (fine-graned portions at 8–12 and 73–76 cm). Probably 2 small cooling units as in Core 108; continuation of Unit 54.
2. At ~101–106 cm (Piece 8): Inclined junction (45° to horizontal) and represents boundary between Units 54 and 55. Junction is microscopically irregular, although Unit 54 chills against Unit 55 below (whitish zone 3 mm wide).
3. From Piece 8 to base Unit 55 (similar to Unit 54) – olivine-pyroxene phyric basalt.

Section 2:

Macroscopic description:

Continuation of Unit 55. Moderately olivine-pyroxene phyric basalt. Accumulation of olivine phenocrysts at base of unit (now altered to green smectite).

Section 3:

Macroscopic description:

Moderately olivine-pyroxene phyric basalt, varying in grain-size from fine to coarse and back again. Phenocryst content and distribution, together with grain size variation similar to Unit 54 – probably a series of thin flows.

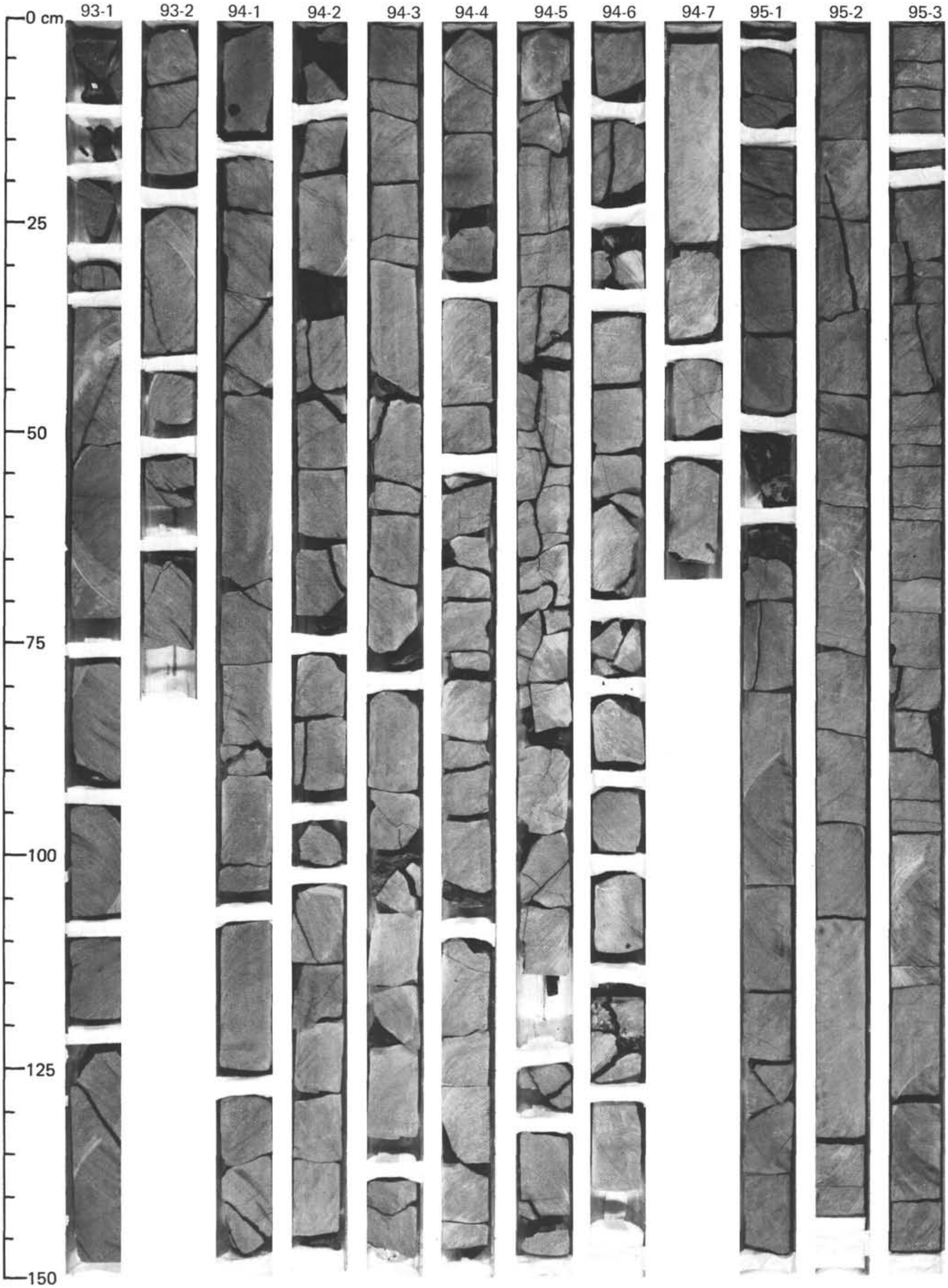
0 cm
25
50
75
100
125
150
93-1
93-2
94-1
94-2
94-3
94-4
94-5
94-6
94-7
95-1
95-2
95-3

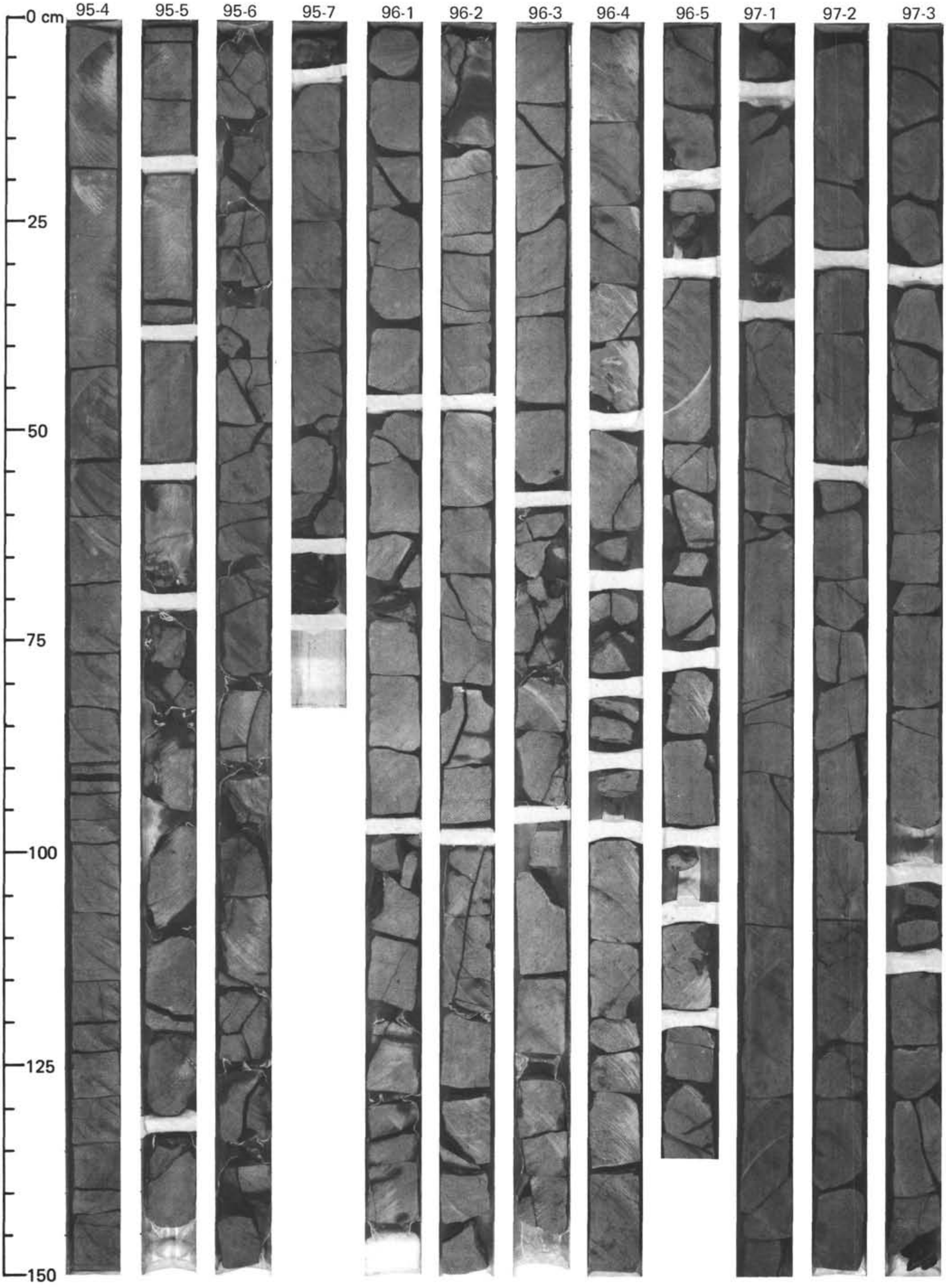
0 cm
25
50
75
100
125
150
95-4
95-5
95-6
95-7
96-1
96-2
96-3
96-4
96-5
97-1
97-2
97-3

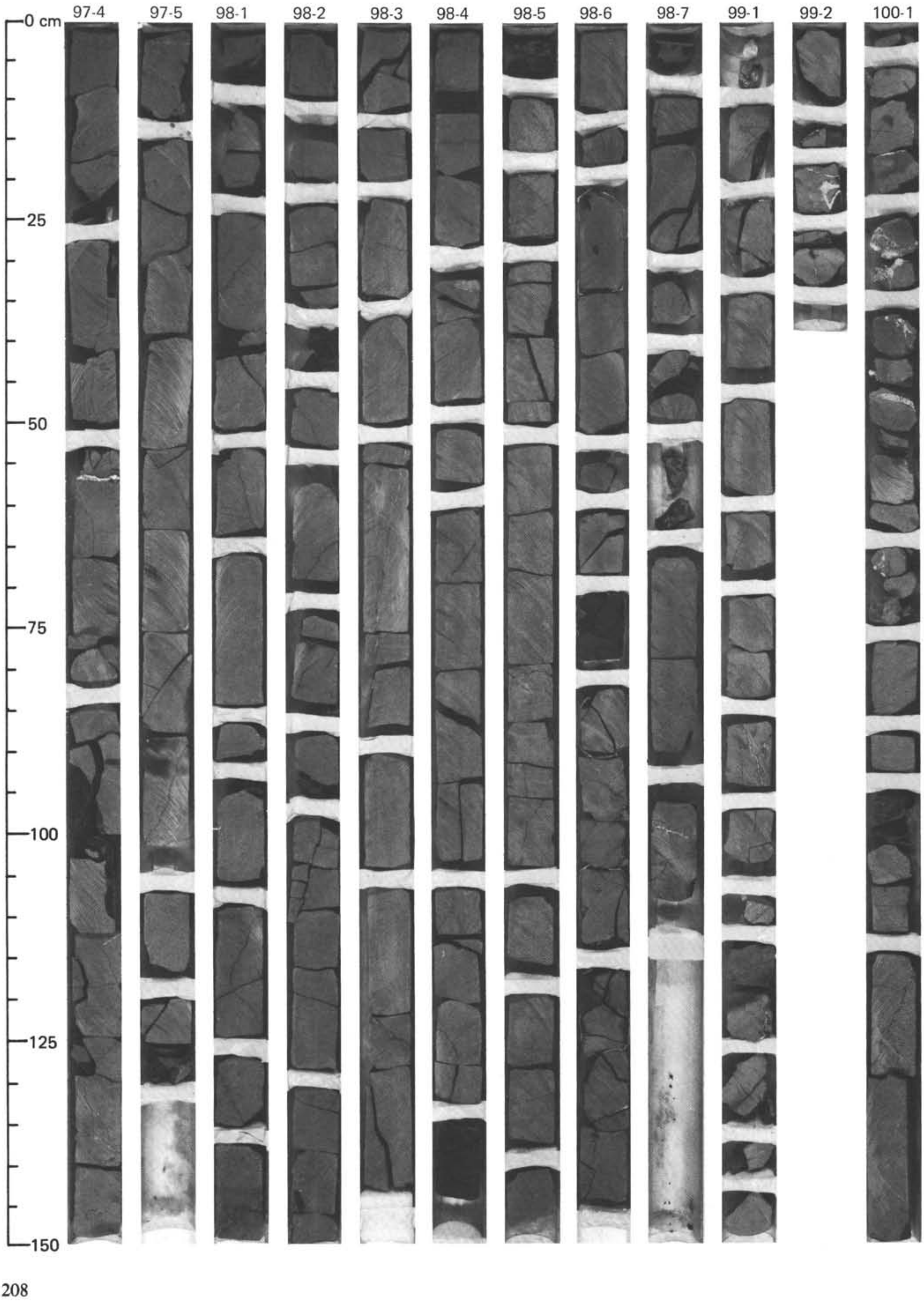

97-4
97-5
98-1
98-2
98-3
98-4
98-5
98-6
98-7
99-1
99-2
100-1
0 cm
25
50
75
100
125
150

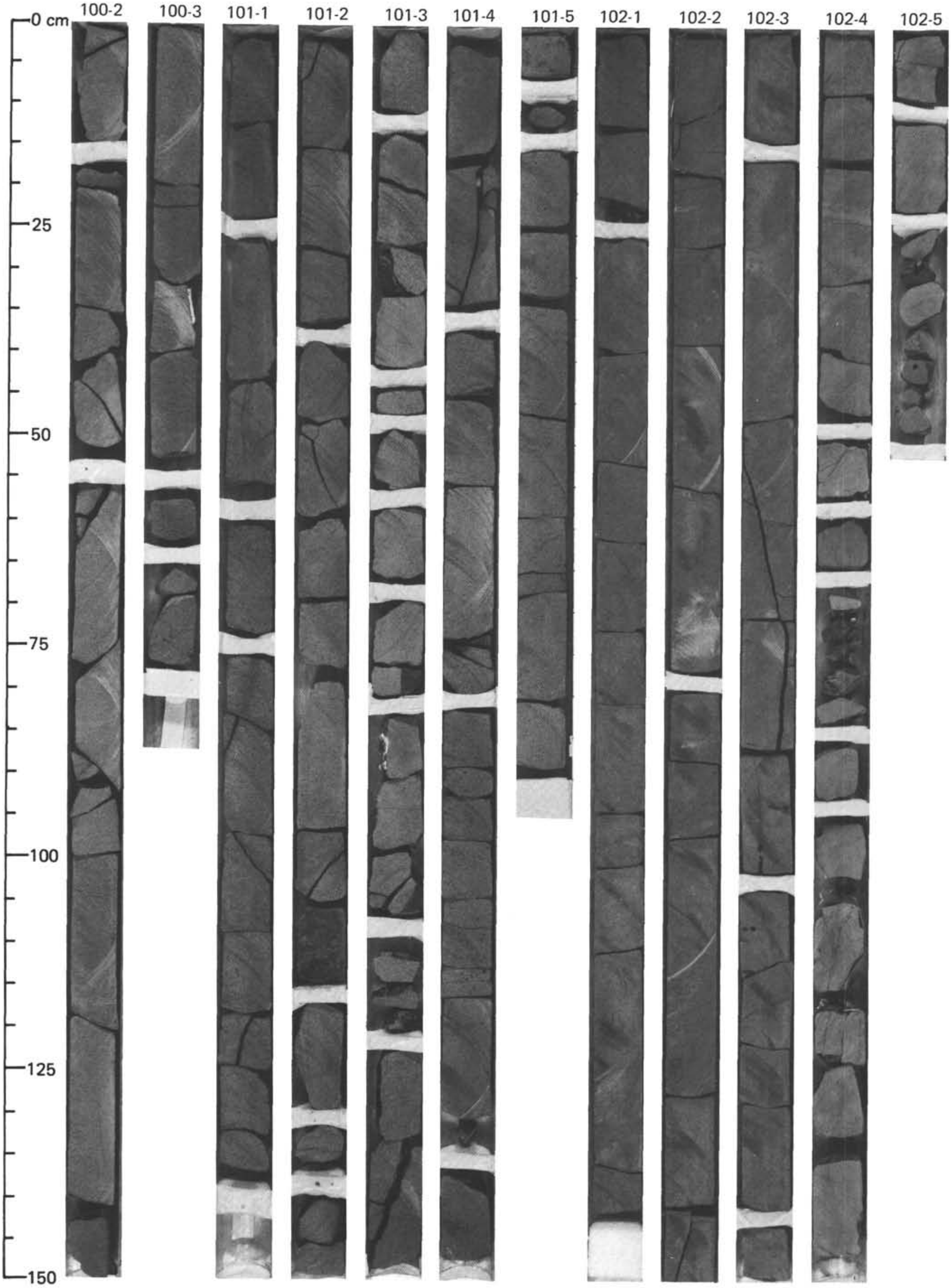
0 cm
25
50
75
100
125
150
100-2
100-3
101-1
101-2
101-3
101-4
101-5
102-1
102-2
102-3
102-4
102-5

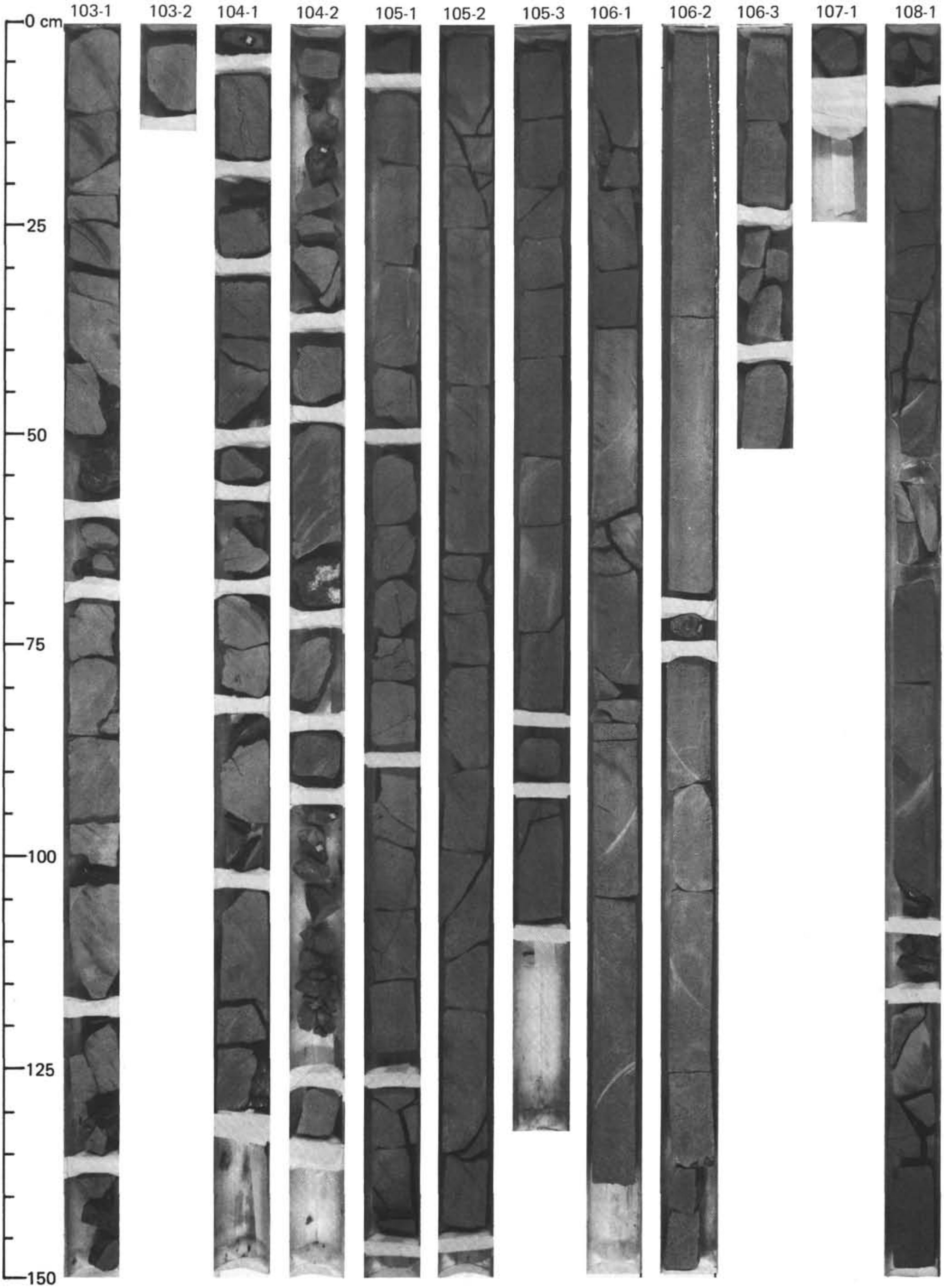
103-1
103-2
104-1
104-2
105-1
105-2
105-3
106-1
106-2
106-3
107-1
108-1
0 cm
25
50
75
100
125
150

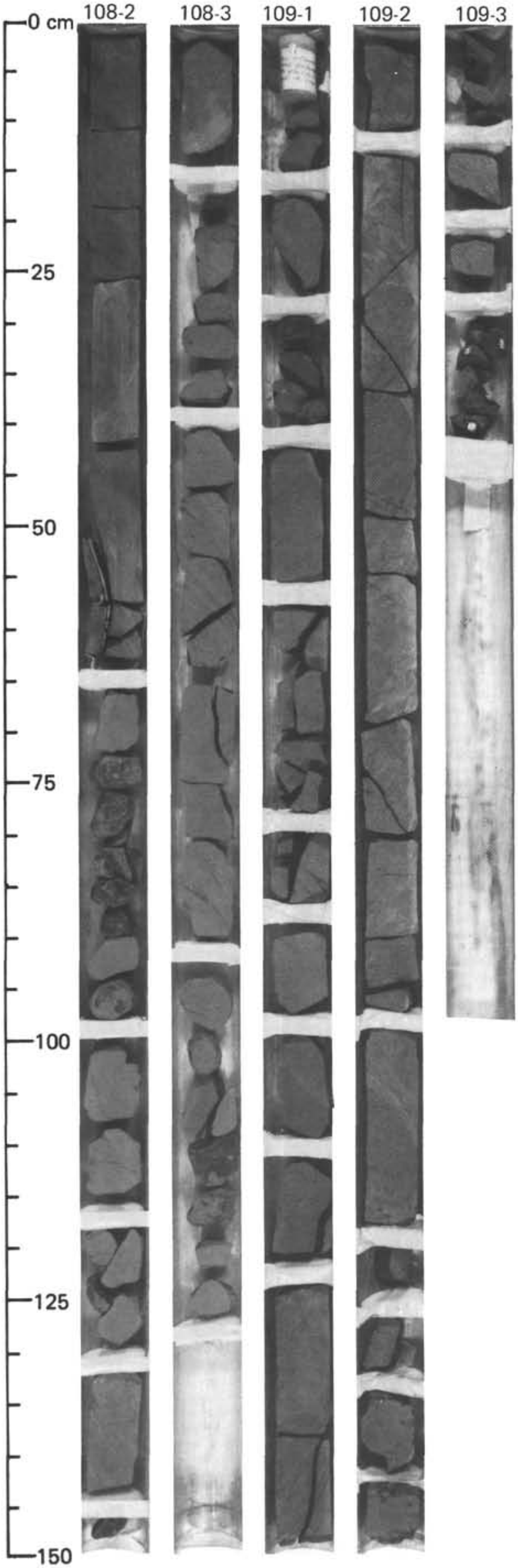
0 cm
25
50
75
100
125
150
108-2
108-3
109-1
109-2
109-3